Synthesis and Characterization of Thermoresponsive Starch Nanoparticles

by

Bowei Zheng

A thesis
presented to the University of Waterloo
in fulfillment of the
thesis requirement for the degree of
Master of Science
in
Chemistry (Nanotechnology)

Waterloo, Ontario, Canada, 2016

AUTHOR'S DECLARATION

I hereby declare that I am the sole author of this thesis. This is a true copy of the thesis, including any required final revisions, as accepted by my examiners.

I understand that my thesis may be made electronically available to the public.

Abstract

Thermoresponsive polymers (TRPs) are polymers that exhibit an abrupt change in their physical properties, such as solubility, with a change in temperature. The vast majority of TRPs produced to date are synthetic and petroleum-based polymers. Commercial applications of these TRPs have been limited to only a few low-volume applications. The main reasons for this are the high costs of production, and environmental and health concerns, such as biodegradability and toxicity. TRPs based on benign natural polymers such as cellulose and starch have garnered some attention recently due to their biodegradability, biocompatibility, low toxicity and potentially low production cost. The modification of starch nanoparticles (SNPs) with 1,2-butene oxide (BO) was studied. This yielded hydroxybutyl SNPs (HBSNPs) that exhibit thermoresponsive behavior. Turbidity measurements showed that an increase in the molar substitution (MS) resulted in a decrease in the cloud point temperature (T_c), and an increase in the concentration of the aqueous HBSNP dispersions also decreased the T_c. The T_c of the HBSNPs were tuned in a range from 33 to 52^oC by adjusting the MS. For HBSNPs to exhibit thermoresponsivity, the MS of the HB groups had to be greater than 1. Dynamic light scattering studies showed that there was a substantial increase in the particle size of HBSNPs when the temperature reached the T_c. Studies of the effect of salts on T_c revealed that as the concentration of the salts increased, kosmotropic salts decreased the T_c, while chaotropic salts increased the T_c. Phenyl hydroxyethyl SNPs (PHESNPs) were prepared by modifying SNPs with styrene oxide (SO). PHESNPs had relatively poor dispersability in

water due to the high hydrophobicity of the substituting phenyl hydroxyl groups, and they do not exhibit thermoresponsive behavior.

Acknowledgements

First, I would like to express my deepest gratitude to my Supervisor, Professor Scott D. Taylor, who is always kind, supportive, knowledgeable and inspiring to his students. As one of his students, I had the honor and joy of working with Professor Taylor on an exciting project that only few people in the world have looked into. His wisdom, hard-work and dedication to the world of science have inspired me for my life as a scientist in the years coming. Without his guidance and persistent help, this thesis would not have been possible.

I would also like to thank my advisory committee, Professor Mario Gauthier and Professor Juewen Liu for their valuable guidance and generous help during my M.Sc. study. I would also like to thank Jan Venne for her help with NMR use, Professor Jean Duhamel and Professor Thorsten Dieckmann for the help with UV-Vis spectrophotometer use, Professor Elizabeth Meiering for the help with DLS use, and Dr. Richard Smith for the training on mass spectrometer. I would like to specially thank Professor Duhamel and Dr. Steven Bloembergen for their fruitful discussions and suggestions.

I would like to acknowledge all my current and former lab mates in the Taylor lab (2014-2016). I had the pleasure of working with many great people in the lab and in the ECO-WIN group. I would like to specially thank Magda Karski, a former student in the Taylor lab for her generous help during my early days in this project. I would also like to thank Lu Li, a

PhD student in the Duhamel lab, for her thoughtful advice, and Braden Kralt for his help and good company in the lab.

Last but not least, I am grateful to my parents who selflessly give me all the love and support in my whole life, and especially during my M.Sc. study. I am equally grateful to my beloved wife, Sandy, who has been constantly supporting me and being by my side to experience happiness and more importantly, to overcome many stressful and challenging moments in life together.

In dedication to my beloved wife, parents & sister;

For their love, endless support, encouragement & sacrifices

Table of Contents

List of Figures

List of Schemes

List of Tables

List of Abbreviations

AGU	Anhydroglucose unit
BE_mS	3-[2-Butoxy(ethoxy)$_m$]-2-hydroxypropyl starch ethers
BGE	Butyl glycidyl ether
BO	1,2-Butene oxide
CMC	Critical micelle concentration
CMT	Critical micelle temperature
CP	2-Chloropropionamide
CSNP	Commercial-grade SNP
D_2O	Deuterium oxide
D_h	Hydrodynamic diameter
DLS	Dynamic light scattering
DMSO-d_6	Dimethyl sulfoxide-d_6
DS	Degree of substitution
ECP	Ethyl 2-chloropropionate
EHEC	Ethylhydroxyethyl cellulose
GPC	Gel permeation chromatography
GX	Glyoxal
GY	Glycerol
HBPS	2-Hydroxy-3-butoxypropyl starch
HBSNP	Hydroxybutyl SNP
HEMC	Hydroxyethyl methyl cellulose
HHSNP	Hydroxyhexyl SNP
HIPS	2-Hydroxy-3-isopropoxypropyl starch
HPC	Hydroxypropyl cellulose
HPeSNP	Hydroxypentyl SNP

HPLC	High performance liquid chromatography
HPMC	Hydroxypropyl methyl cellulose
HPSNP	Hydroxypropyl SNP
HR+ESIMS	High resolution positive electrospray ionization mass spectrometry
IPGE	Isopropyl glycidyl ether
i-PrCP	*N*-Isopropyl-2-chloropropionamide
LCST	Lower critical solution temperature
MC	Methyl cellulose
MCP	Methyl 2-chloropropionate
MS	Molar substitution
MSDS	Material safety data sheet
MW_{cutoff}	Molecular weight cut-off
PAPR	Poly(*N*-acryloylpyrrolidine)
PDEAM	Poly(*N*,*N*-diethylacrylamide)
PDI	Polydispersity index
PDMAEMA	Poly(2-(dimethylamino)ethyl methacrylate)
$PEEO_nMA$	Poly(ethyl ethoxymethacrylate)
PEG	Poly(ethylene glycol)
PEI	Poly(ethyleneimine)
PEI-PNIPAAm	Poly(ethyleneimine)-PNIPAAm
PEO-PPO-PEO	Poly(ethylene oxide)-poly(propylene oxide)-poly(ethylene oxide) block copolymer
PhCP	*N*-Phenyl-2-chloropropionamide
PHESNP	Phenyl hydroxyethyl SNP
$PMEO_2MA$	Poly(2-(2-methoxyethoxy) ethyl methacrylate)

P(MEO_2MA-*co*-OEGMA)	Poly(2-(2'-methoxyethoxy)ethyl methacrylate-*co*-oligo(ethylene glycol) methacrylate)
PMMA	Poly(methyl methacrylate)
PNIPAAm	Poly(*N*-isopropylacrylamide)
PNIPAAm-DEGMA	PNIPAAm-diethyleneglycol methacrylate
PNIPAAm-PBMA	Poly(*N*-isopropylacrylamide-*b*-butylmethacrylate)
PO	Propylene oxide
P(S-*b*-NIPAAm)	Poly(styrene-*b*-(*N*-isopropyl acrylamide))
PSNP	Purified CSNP
PSO	Poly(styrene oxide)
PTFE	Poly(tetrafluoroethylene)
PVCL	Poly(*N*-vinyl caprolactam)
PVME	Poly(vinyl methyl ether)
R_g	Radius of gyration
R_h	Hydrodynamic radius
rt	Room temperature
SNP	EcoSphere™ starch nanoparticle
SO	Styrene oxide
SRP	Stimuli-responsive polymer
T_c	Cloud point temperature
TFA-*d*	Trifluoroacetic acid-*d*
TMSP-d_4	3-(Trimethylsilyl)-2,2',3,3'-tetradeuteropropionic acid
TRP	Thermoresponsive polymer
TRS	Thermoresponsive starch
TRSNP	Thermoresponsive SNP
UCST	Upper critical solution temperature

Chapter 1

Introduction

1.1 Introduction to Stimuli-responsive Polymers

"Smart polymers", also known as stimuli-responsive polymers (SRPs), are polymers that undergo drastic changes in their physical properties in response to external stimuli. The various external stimuli include pH, temperature, ionic strength, humidity and other changes in the environment. These stimuli often affect the interactions between polymer chains or between polymer chains and solvents at the molecular level.[1] Because of the unique properties of these polymer systems they have gathered significant attention in the past decade, and their potential applications in the biomedical fields and non-biologically related fields are currently being explored. Potential applications include drug delivery[2] and gene delivery[3] vehicles, tissue engineering and cell culturing materials[4], smart building coatings[5], extraction[6] and concentration processes[7], etc.

Manipulating the temperature is relatively easy when compared to other types of stimuli. Hence, thermoresponsive polymers (TRPs) are one of the most intensively studied SRPs. TRPs undergo an abrupt change in their physical properties, in most cases, a change in their dispersability in water, with a change in temperature. The majority of studies on TRPs have been done using synthetic polymers. The most popular example is poly(*N*-isopropylacrylamide) or PNIPAAm, which exhibits a drastic change in dispersability at a critical

temperature of approximately 32°C.[8] Other well-known thermoresponsive polymers include poly(ethylene oxide) and poly(propylene oxide) block copolymer systems (PEO-PPO-PEO), poly(*N*-vinyl caprolactam) (PVCL), and poly(vinyl methyl ether) (PVME) to name a few.[9,10] Unfortunately, PNIPAAm as well as many other thermoresponsive synthetic polymers share the same disadvantages: questionable toxicity, biodegradability and biocompatibility. Hence, these serious drawbacks have limited their use in real-world applications. Because of that, TRPs based on natural polymers such as cellulose, chitosan, and starch have emerged as alternatives in recent years due to their nontoxicity, biodegradability, biocompatibility as well as other attractive properties such as natural abundance and potentially low production costs.[11]

1.2 Introduction to Thermoresponsive Polymers (TRPs)

Thermoresponsive polymers (TRPs) can be classified into two main types based on their behaviors in a solvent: upper critical solution temperature (UCST) and lower critical solution temperature (LCST).[1] Both UCST and LCST are the critical temperature points at which the polymer and the solvent become completely miscible or immiscible (**Fig. 1.1**).

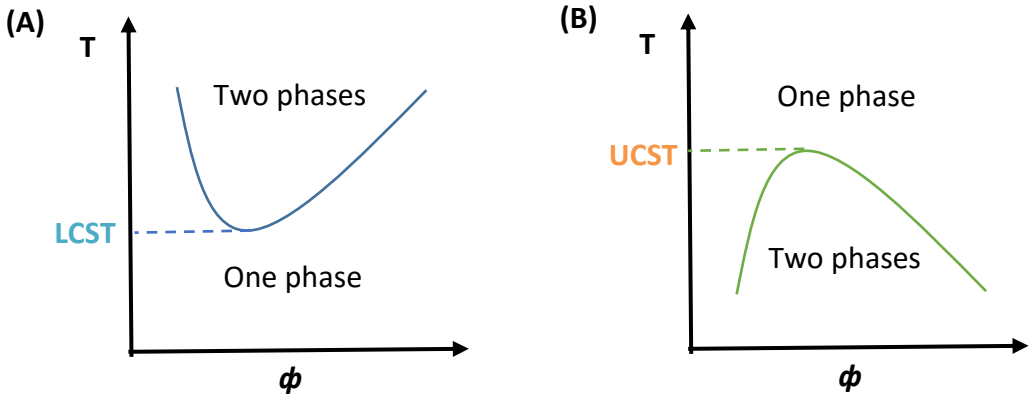

Figure 1.1. Schematic illustration of phase diagrams giving the critical temperature as a function of polymer volume fraction, ϕ, for (**A**) lower critical solution temperature (LCST) and (**B**) upper critical solution temperature (UCST).

The LCST is generally considered as an entropy-driven phenomenon. When the temperature of a TRP dispersion is higher than the LCST, the polymer dispersion undergoes phase separation. The polymer separates from its surrounding water molecules, resulting in an increase in entropy for the water molecules. On the other hand, the UCST is enthalpically driven. The main driving force is the increase in enthalpy when dispersing the polymer, which is governed by solvation effects as well as inter- and intramolecular interactions. In comparison to TRPs with UCSTs, TRPs with LCSTs have more potential applications, such as drug delivery, gene delivery and engineering.[12-16] Thus, the majority of the studies on TRPs has been focused on the ones with LCST-type thermotransitions, which is also the main focus of this thesis. The term, LCST, is used interchangeably with the cloud point temperature (T_c) throughout the thesis.

1.3 Thermodynamics of Thermotransitions

A polymer dispersion with an LCST-type thermotransition appears to be clear and homogeneous below LCST, while it turns turbid and immiscible above the LCST. Phase separation is energetically more favorable, as the entropy of the system increases when the temperature reaches LCST.[1] To elaborate, in a polymer-water system, the polymer stays solvated below the LCST due to the presence of hydrogen bonding between the hydrophilic regions of the polymer and water molecules. Moreover, the hydrophobic regions of the polymer are surrounded by an ordered arrangement of water molecules. The behavior of these hydrophobic regions in water is comparable to the one of nonpolar substances in water.[17-19] Thermodynamically, considering the Gibbs equation $\Delta G = \Delta H - T\Delta S$ (where G is the Gibbs free energy, H is the enthalpy and S is the entropy), the presence of a vast number of polymer-water hydrogen bonds results in a large negative enthalpy.[18] Although the ordered arrangement of water molecules contributes to a decrease in entropy, the free energy of the system remains negative (energetically favorable for homogenous solution) below the LCST.[18,20] On the other hand, as temperature increases, the enthalpy of the system becomes less negative as a result of disruption or weakening of the polymer-water hydrogen bonds.[20] Additionally, the dissociation of water molecules from the polymer increases the entropy.[21] As the entropy dominates the contribution to the negative free energy of the system, it becomes the main driving force for the phase separation above the LCST.

1.4 Phase Transition Behaviors

Depending on the nature of the TRPs (with an LCST-type thermotransition), they can exhibit two distinctive phase transition behaviors: a coil-to-globule transition (intramolecular aggregation) and/or intermolecular aggregation.[1] A coil-to-globule transition describes a process by which a linear flexible polymer chain adopts other thermodynamically stable conformations due to a change in temperature (**Fig. 1.2A**).[8] The polymer chain completely dispersed in water adopts a random coil conformation below the LCST via the formation of extensive hydrogen bonding between the polymer and water molecules. Above the LCST, the disruption of polymer-water hydrogen bonding results in intramolecular aggregation (the polymer collapses into a globular conformation). One example of such TRPs is PNIPAAm, which typically undergoes a coil-to-globule transition at 32°C. The coil-to-globule transition of PNIPAAm is supported by the experimental observation that the hydrodynamic radius (R_h) of the polymer in a very diluted dispersion decreases as the temperature reaches the LCST (**Fig. 1.2B**). In a relatively concentrated dispersion, the polymer chains form large aggregates (intermolecular interactions) after the coil-to-globule transition. Two other TRPs that exhibit this type of transition behavior are poly(*N*,*N*-diethylacrylamide) (PDEAM) and poly(2-(dimethylamino)ethyl methacrylate) (PDMAEMA).[1]

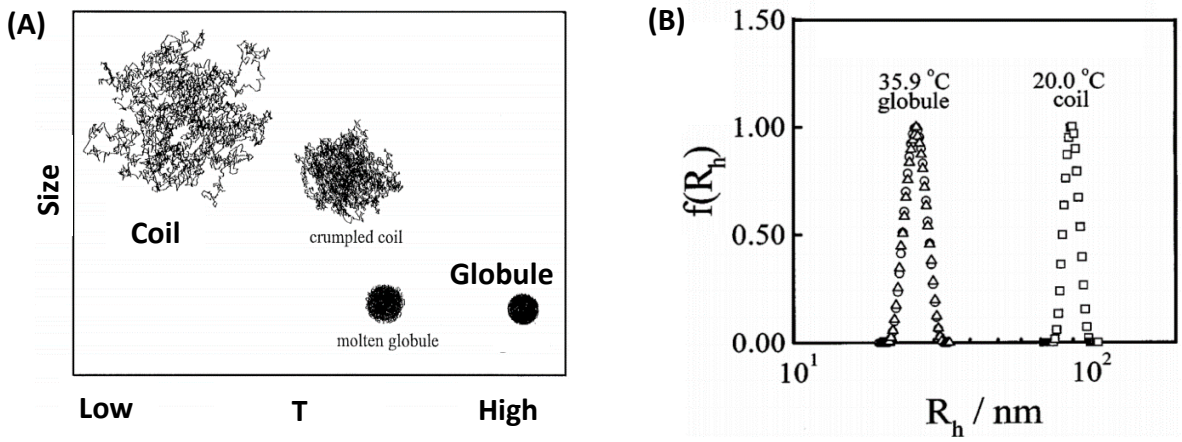

Figure 1.2. Schemetic representation of a coil-to-globule transition and typical hydrodynamic radius distribution, $f(R_h)$, of PNIPAAm. (**A**) illutrates four thermodynamically stable states of PNIPAAm in solution. (**B**) shows $f(R_h)$ of PNIPAAm in aqueous solution with an extremely low concentration at 35.9°C and 20.0°C. Both diagrams were adapted from Wu et al.[8]

TRPs with a phase transition involving intermolecular aggregation, but without experiencing the coil-to-globule transition, are typically amphiphilic block copolymers that consist of hydrophilic and hydrophobic regions.[1] The hydrophilic-hydrophobic balance of this type of TRPs enables the self-assembly of single polymers into micelles and/or the formation of other intermolecular aggregates such as gels. Below the critical temperature (critical micelle temperature or CMT in the case of micelle formation), the polymer chains are typically in a random coil conformation in an aqueous dispersion (**Fig.1.3**).[22] As the critical temperature is reached the coil conformation is no longer thermodynamically stable, which results in intermolecular association of the polymer chains into large aggregates (**Fig.1.3**). One of the most well-known TRPs of this type is the PEO-PPO-PEO triblock copolymer system (also known as Pluronics™). This triblock copolymer in a less concentrated dispersion would

exhibit thermoresponsive micellization behavior, but exhibit a thermoresponsive solution-to-gel (sol-gel) transition at higher concentrations.[23]

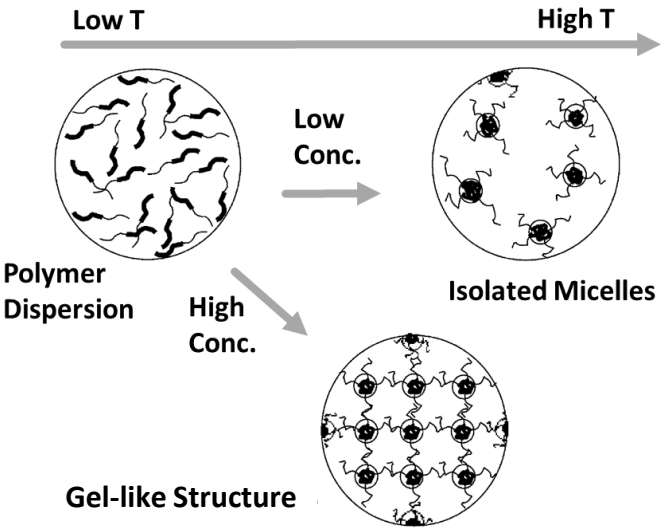

Figure 1.3. A schematic representation of conformational changes of amphiphilic block copolymers in aqueous dispersion. At low concentration, polymer chains assemble into isolated micelles when the LCST is reached; at high concentration, these polymeric micelles further assemble into an ordered gel-like structure. Pictures were adapted from Gil et al.[1]

The thermotransition behaviors can often be controlled by the structure of a thoughtfully designed block copolymer. When a hydrophilic polymer is grafted onto a TRP such as PNIPAAm, it may be possible to control the formation of micelles for the resulting block copolymer in aqueous dispersions by manipulating the temperature. On the contrary, when a hydrophobic polymer is grafted, such a block copolymer may gain the ability to switch on and off the formation of the micelles. Block copolymers consisting of a hydrophobic substrate and a thermoresponsive segment form micelles with a hydrophobic core and a hydrophilic outer corona in water below the LCST (and above the critical micelle

concentration or CMC); when the LCST is reached, they collapse and precipitate out of the solution (**Fig. 1.4A**).[1] On the contrary, block copolymers containing hydrophilic blocks and thermoresponsive blocks form micelles triggered by the change in temperature (**Fig. 1.4B**).[1]

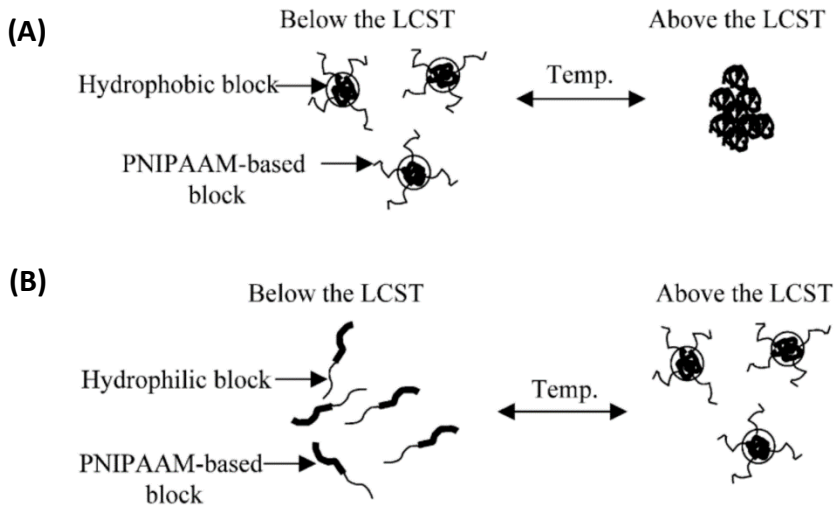

Figure 1.4. Schematic representation of two types of micellar structures of a PNIPAAm grafted block copolymer in aqueous dispersion. (**A**) shows a block copolymer consisting of hydrophobic blocks and thermoresponsive blocks; (**B**) shows a block copolymer containing hydrophilic blocks and thermoresponsive blocks. Both diagrams were adapted from Gil et al.[1]

1.5 Types of Phase Separation Behaviors

TRPs in aqueous dispersions are homogeneous below the LCST and undergo phase separation above the LCST. This transition is highly reversible. Phase separation of the TRP dispersion and the reversible process can often be monitored with a UV/Visible spectrometer equipped with a temperature controller. The absorbance of the dispersion is measured and recorded during a steady increase or decrease in temperature. Transmittance curves can then

be obtained. Based on how fast the phase separation and the reversible process respond to the change in temperature, there are generally three types of transmittance curves that have been reported in the literature.[24] First, phase separation occurs very suddenly at a critical temperature, and the transmittance curves for the heating and cooling process almost overlap (**Fig. 1.5A**). Second, phase separation also occurs abruptly at a critical temperature, but the transmittance curve for the cooling process does not overlap with the heating curve and a noticeable hysteresis can be observed (**Fig. 1.5B**). Third, phase separation occurs slowly over a wide temperature range (**Fig. 1.5C**).

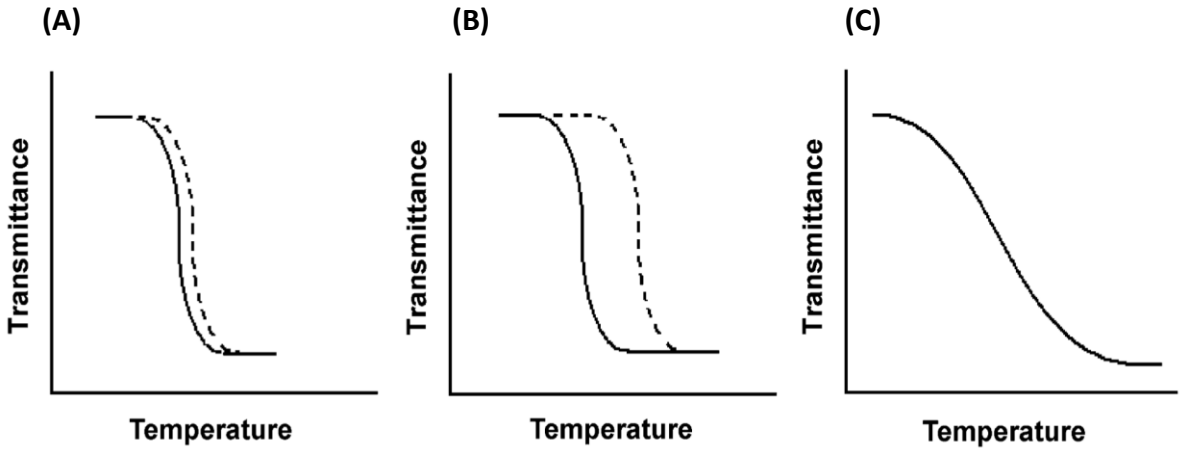

Figure 1.5. Transmittance curves for heating and cooling cycles showing **(A)** overlapping curves, **(B)** curves with a hysteresis, and **(C)** slow phase transition. Pictures were adapted from Dimitrov et al.[24]

The first type of thermotransition behavior, where the heating and cooling cycles almost overlap, are primarily caused by a disruption of the hydrophobic-hydrophilic balance of the TRP in water through a change in temperature. It often occurs for copolymers that have both hydrophobic and hydrophilic segments. When the hydrophobic-hydrophilic

balance of the copolymer is right, the copolymer is solvated in an aqueous dispersion below the LCST. When the temperature reaches the LCST, the copolymer becomes more hydrophobic and the hydrophobic-hydrophilic balance is disrupted. This triggers the aggregation or possibly self-assembly of the individual copolymer chains into large aggregates via hydrophobic interactions, which eventually leads to a phase separation. TRPs consisting of poly(vinylether)s, poly(phosphoester)s as well as acrylate- and methacrylate-based polymers, such as the copolymer poly(2-(2'-methoxyethoxy)ethyl methacrylate-*co*-oligo(ethylene glycol) methacrylate) (P(MEO_2MA-*co*-OEGMA)), usually exhibit this type of thermotransition.[10,24,25]

The second type of behavior, where large hysteresis can be found, are mainly caused by intramolecular interactions. When the temperature is higher than the LCST, the polymer chains undergo a coil-to-globule transition and eventually precipitate out as large aggregates.[24] Typically, PNIPAAm or PNIPAAm copolymers exhibit this type of behavior.[26] The hysteresis in heating and cooling cycles can be attributed to the hindered diffusion of water molecules into the dense hydrophobic aggregates formed above the LCST.[10] The hindered diffusion effectively slows the dissociation of the aggregates and the solvation of the individual polymer chains. At slower heating and cooling rates, a less concentrated dispersion and the formation of macroporous aggregates below the LCST would generally result in smaller hysteresis.[10,26,27]

The shape of the transmittance curve is usually quite informative. A sharp transmittance curve indicates a fast thermotransition. Depending on the need of a potential application, a fast thermotransition may be preferable as it ensures that there is a maximum amount of interactions between the polymer and water below a critical temperature, but once the critical temperature is reached, such interactions are minimized.[24] A fast thermotransition is thought to contribute to the formation of well-defined monodispersed aggregates above the LCST.[24] On the other hand, a shallow transmittance curve means that the thermotransition is slow. This type of transmittance curve often involves the collapse of micelles to form insoluble aggregates above LCST. A common example is poly(styrene-*b*-(*N*-isopropyl acrylamide)) diblock copolymers or P(S-*b*-NIPAAm), for which the transmittance curve is shown in **Fig. 1.6**.[28] Below the LCST, P(S-*b*-NIPAAm) forms micelles in a aqueous dispersion when the critical micelle concentration (CMC) is reached. Above the LCST, the micelles collapse and form aggregates of the collapsed micelles as the temperature continues to increase. Hence, the transmittance of the dispersion decreases as the number of aggregates present increases. The size distribution of the aggregates in this case could be very polydisperse.

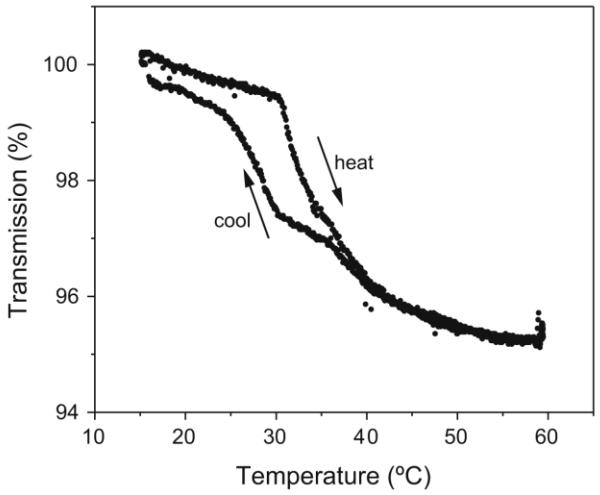

Figure 1.6. Transmittance curve for a 0.2 mg/mL aqueous dispersion of poly(styrene-*b*-(*N*-isopropyl acrylamide)). The figure was adapted from Troll et al.[28]

1.6 Potential Applications of Thermoresponsive Polymers

1.6.1 Drug Delivery Vehicles

Drug delivery vehicles are often employed to facilitate the administration of therapeutics in a temporally and spatially controlled manner.[29] The key features of a drug delivery vehicle are to transport drugs to a targeted area in the human body, and to release the drug at a controlled rate. Traditional drug delivery systems often suffer from that there is little control over the drug-releasing location, rate and concentration once the drug-loaded vehicles are administrated into the human body. Hence, the use of TRPs as drug delivery vehicles is advantageous due to their inherited switchable thermoresponsive properties. The site-specific and sustained release of drugs can be controlled by changing the temperature of

the target site. As an example, the block copolymer poly(*N*-isopropylacrylamide-*b*-butyl methacrylate) (PNIPAAm-PBMA) exhibits an LCST of 32.5^{o}C, and was used in a TRP-assisted drug release study conducted by Chung et al.[2] Below the LCST, the hydrophobic PBMA blocks aggregate to form the hydrophobic inner core of a micelle, which enables the loading of hydrophobic drugs inside the micelles. At the same time, the thermoresponsive PNIPAAm blocks become the hydrophilic outer corona of the micelle, which prevent their interaction with surrounding micelles and with other bio-components below the LCST (**Fig. 1.7A**). Upon the administration of the drug-loaded TRP micelles, the micelles travel through the body without non-specific interactions until they reach the target site. At the target site, the local temperature can be adjusted to reach the LCST of the TRPs, potentially by hyperthermia treatment or thermotherapy, triggering the thermotransition. As a result, the hydrophilic outer corona become more hydrophobic, which leads to enhanced attachment of the drug carriers to the cells at the target site (**Fig. 1.7B**). At the same time, deformation of the micelles induces an initially rapid, but then sustained release of the loaded drugs at the target site. This represents one type of the controlled drug release systems that are based on thermoresponsive micelle formation and deformation. Another type of this system involves the use of injectable thermoresponsive hydrogels. The drug-loaded hydrogels can be injected as a low viscosity solution at room temperature, but quickly undergo rapid gelation at body temperature to achieve sustained release of the drugs at the injection site.[30]

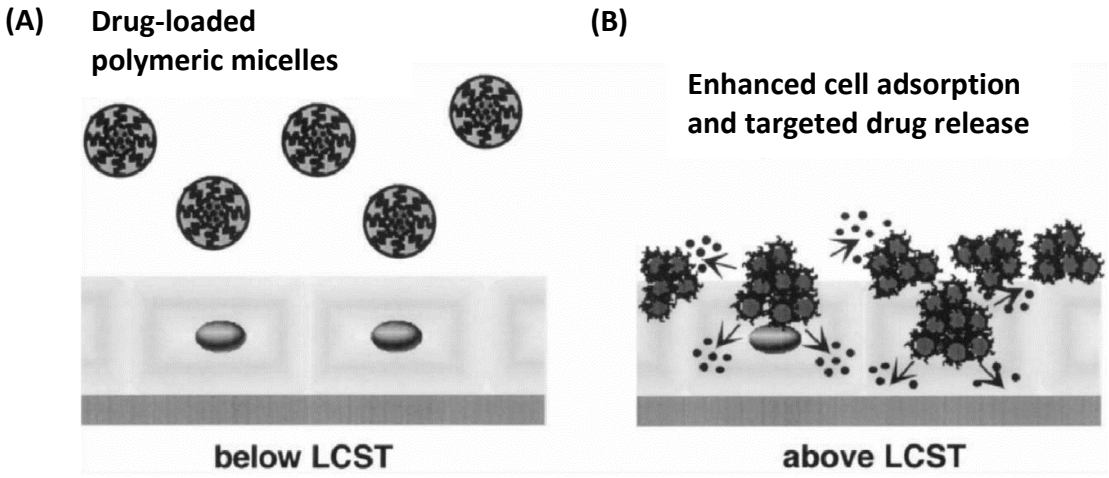

Figure 1.7. Schematic representation of thermoresponsive micelles for site-targeted drug delivery. (**A**) Below the LCST, the polymeric micelles have a low affinity for cells; (**B**) at the target site and above the LCST, the micelles become hydrophobic and their adhesion to cells is enhanced. Both diagrams were adapted from Chung et al.[2]

1.6.2 Gene Delivery Vectors

TRPs have been examined as delivery vectors for gene therapy. Generally, gene therapy involves transfecting therapeutic genes into cells, in order to replace or repair defective genes to cure genetic disorders.[29] Successful gene transfection requires the overcoming many obstacles such as the transportation of negatively charged, hydrophilic DNA strands across the negatively charged, hydrophobic cell membrane. Utilizing gene delivery vectors has made gene therapy feasible, as ideally the vectors are able to efficiently complex with the therapeutic genes and then translocate them across the cell membrane, followed by release of the gene cargo in the cell (**Fig. 1.8**).

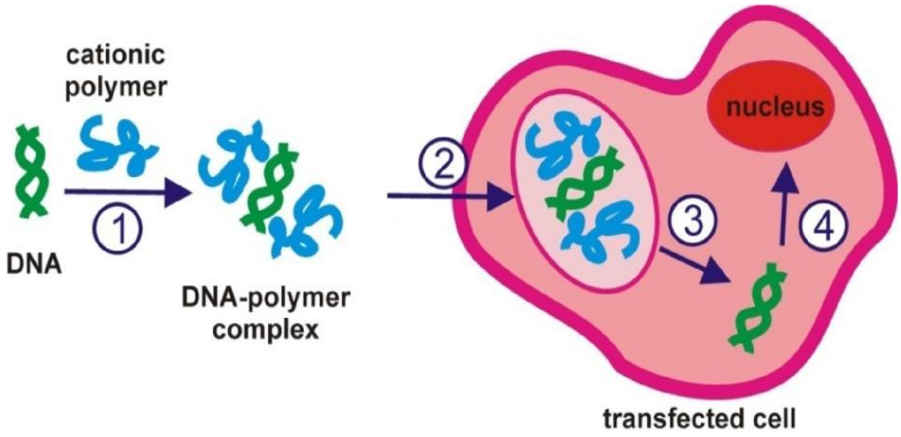

Figure 1.8. Schematic representation of gene delivery using a polymeric vector. **(1)** DNA complexes with the polymeric vector; **(2)** translocation of the DNA-polymer complex across the cell membrane; **(3)** release of DNA from the complex; **(4)** transfection of the DNA into the nucleus. The picture was adapted from Ward et al.[29]

For polymeric vectors, the biggest challenge could be to trigger the release of the gene from the gene-vector complex after the transfection.[29] For TPR-based gene delivery vectors, their themoresponsive properties could make such a process much more efficient. For example, poly(ethyleneimine) grafted PNIPAAm (PEI-PNIPAAm) vectors have shown an improvement in transfection efficiency over the poly(ethyleneimine) (PEI) vector alone (PEI is generally considered as one of the most efficient polymeric vectors).[3] Lavigne et al. proposed that the enhancement in gene transfection efficiency may arise from: first, enhanced cellular uptake as a result of the more compact and better protected DNA during translocation; second, the ability to trigger the release of the DNA from the complex, which could be mediated by conformational changes of the polymeric vectors upon

thermotransition.[3] Thus, targeted delivery of the therapeutic genes can be achieved by inducing a temperature elevation in the target cells.

1.6.3 Tissue Engineering

Tissue engineering generally describes a set of methods towards the regeneration of biological tissues or organs from host cells grown in a biocompatible scaffold, in order to replace the damaged tissues or organs in a host.[29] Finding suitable materials for the cells to grow on is crucially important to tissue engineering, as the survival of the cells greatly depends on the mechanical support, nutrients and growth factors that are provided by the scaffold materials. Generally, there are two main areas that could employ TRPs in tissue engineering: cell culture bioadhesives and *in situ* scaffold materials.

TRPs can be used as bioadhesives to regulate the attachment and detachment of cells or proteins from cell culture plates.[4,29,31,32] This regulation is mediated by the temperature-induced transition between hydrophobic and hydrophilic states of the TRP-coated surface.[29] PNIPAAm-based copolymer-coated thermoresponsive surfaces have the potential to effectively absorb a number of proteins (such as bovine serum albumin, cytochrome C) and to attach both gram negative (such as *Salmonella typhimurium*) and gram positive (such as *Bacillus cereus*) bacteria above the LCST.[32] Nitschke et al. have described a process that involves the use of a reusable thermoresponsive film that is made of PNIPAAm-grafted

diethyleneglycol methacrylate (PNIPAAm-DEGMA) to harvest human corneal endothelial cell sheets.[4] In fact, the TRP-based cell culture coating developed by Nakayama et al. is one of the rare examples of TRP applications that have been successfully commercialized.[33]

Another main application for TRPs in the field of tissue engineering is as a scaffold for *in situ* tissue regeneration. The basic concept is that first, a solution containing TRPs, cells, nutrients and growth factors is injected where the defective cell tissues are located in the human body; second, a gelation process takes place to form a scaffold in response to the body temperature.[29,30] As a result, the scaffold encapsulates the cells and nutrients in that location, hence providing a suitable environment for cell growth.[29,30] To date, many thermoresponsive polymer systems have been reported to have the ability to form a stable physical gel in response to the change in temperature and have shown potential as scaffold materials for tissue engineering.[34-38]

1.6.4 Non-biomedical Applications

While biomedical applications remain the main focus of the research on TRPs, potential non-biomedical applications are also being investigated. For example, studies have been conducted on using a TRP-modified stationary phase to separate biomolecules in aqueous chromatography.[39-42] In these studies, it has been demonstrated that when compared to conventional chromatography methods, better separation of biological compounds can be achieved by using the modified chromatography method with a TRP-

based stationary phase. The ability to separate is provided by simply adjusting the column temperature, which would lead to a change in the physical properties (mainly the hydrophobicity) of the thermoresponsive stationary phase.

Another potential non-biomedical application of TRPs is that they can be used to pre-concentrate heavy metal ions such as copper(II), nickel(II), cobalt(II) and lead(II) for analytical detection of these heavy metal ions.[7,43] This type of TRPs are usually functionalized with chelating agents. Examples of such TRPs include PNIPAAm-imidazole, PNIPAAm-carboxylic acid and PNIPAAm-iminodiacetic acid, etc.[7] Specifically, the thermoresponsive chelating polymers are added to the heavy metal ion-containing aqueous analyte solution, which is then agitated below LCST to promote the attachment of the heavy metal ions onto the chelating polymers.[7] Subsequently, the metal ion-chelated polymers can be isolated by raising the temperature to above the LCST and then re-dispersed in a desirable amount of solvent to release the metal ions for analytical detection.

TRPs often inspire green and innovative ideas to solve environmental problems. One interesting example is the thermoresponsive hydrogel-based rooftop coating, which was invented by Rotzetter et al.[5] This rooftop coating contains a PNIPAAm-based hydrogel that is thermoresponsive. When the roof of a building is coated with this type of hydrogel, it has been demonstrated that the coating can effectively and efficiently cool the building off on a hot day. More specifically, the TRP-coated surface absorbs water on a cold and rainy day

when the temperature is below the LCST, but then releases the absorbed water on a hot day to help passively cool the building, similar to the process of sweating in the human body. This technology could lead to more sustainable urban energy management if it is successfully commercialized and implemented.

Another particularly ingenious example of potential TRP applications aims to extract crude oil from oil sands. Recently, Duhamel et al. reported that several thermoresponsive block copolymers consisting of poly(ethylene glycol) (PEG) and poly(2-(2-methoxyethoxy) ethyl methacrylate) ($PMEO_2MA$) can recover oil from oil sands with relatively high efficiency.[6] The block copolymer PEG-*b*-$PMEO_2MA$ has an LCST of 26°C. The extraction protocol described by Duhamel et al. is depicted in **Fig. 1.9**.[6] First, the oil sands were added to a dispersion of PEG-*b*-$PMEO_2MA$; second, the mixture was shaken overnight at a temperature higher than the LCST for a period of time, which resulted in the association of the oil molecules with the hydrophobic $PMEO_2MA$ segment of the block copolymer; third, the mixture was cooled to below the LCST, which resulted in the release of the oil molecules as the $PMEO_2MA$ segment became hydrophilic; fourth, the pristine sand was removed by filtering and the oil was skimmed off. The recovered TRP dispersion was reused in the next cycle of oil recovery. Near 100% recovery of oil sands using PEG-*b*-$PMEO_2MA$ was demonstrated, and about 80% of the polymer was recycled after each extraction.[6] Although the use of PEG-*b*-$PMEO_2MA$ is highly

unlikely to be adopted on a large scale by the oil extraction industry, this study has provided the industry with a new and promising research direction.

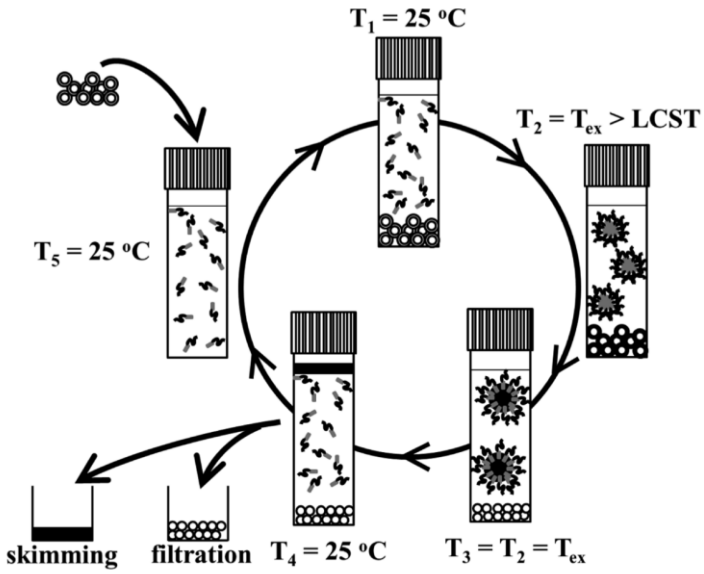

Figure 1.9. Schematics representation of oil recovery procedures using the thermoresponsive block copolymer PEG-*b*-PMEO$_2$MA. Pictures were adapted from Duhamel et al.[6]

1.7 Factors Affecting the LCST

Different applications may require thermoresponsive polymers with different LCSTs. Hence, it is very important to have the ability to conveniently adjust the LCST to satisfy different requirements. As mentioned earlier, PNIPAAm is one of the most intensely studied TRPs and has an LCST of 32^{o}C. However, this LCST often does not meet the temperature that is required for an application. Therefore, for TRPs, having the ability to tune the LCST to meet the requirements for various applications will be the key to the success of this type of smart polymer in real life applications, and the most important area to be investigated.

1.7.1 Effect of the Molecular Structure of TRPs on the LCST

TRPs can be structurally very different as, for example, for PNIPAAm and the triblock copolymer PEO-PPO-PEO. However, a similarity that can be found in these TRPs in that they all contain both hydrophobic and hydrophilic groups or segments. In some way, thermoresponsivity can be obtained when the balance of the hydrophobic and hydrophilic groups on a polymer is right. Hence, changing the hydrophobicity or hydrophilicity of the TRPs should intuitively change their LCSTs. Based on the molecular structure of these TRPs, they can be categorized into two main groups: one is that the polymer is thermoresponsive by itself, and the other type is that the polymer itself is not thermoresponsive but can become thermoresponsive when grafted with other polymers.

For the first type of TRPs (where the polymer is thermoresponsive by itself), the LCST can be tuned by changing the type of alkyl groups on the TRPs. A typical example is poly(*N*-alkylacrylamide). By changing the substituting alkyl groups, the LCST of poly(*N*-alkylacrylamide)s can be adjusted. For example, poly(*N*-alkylacrylamide)s with n-propyl, isopropyl, cyclopropyl or ethyl groups are reported to have LCST values of 23^{o}C, 32^{o}C, 58^{o}C, and 74^{o}C, respectively (**Table 1.1**, entries **1**, **2**, **8** and **9**).[21,44-46] The LCST decreases with increased hydrophobicity of the alkyl groups, due to stronger hydrophobic effects during phase separation (**Table 1.1**). On the other hand, the LCST increases when a relatively hydrophilic group is attached (**Table 1.1**, compare entries **1** and **4**). The increase in LCST is

because of the extra amount of energy needed to break the additional hydrogen bonding between the water molecules and the hydrophilic groups during phase transition.

Table 1.1. Poly(*N*-alkylacrylamide) with different monosubstituting alkyl groups and their LCSTs.

Entry	Poly(*N*-alkylacrylamide)	LCST (°C)
1	poly(*N*-n-propylacrylamide)	23[46]
2	poly(*N*-isopropylacrylamide)	32[45]
3	poly(ethoxypropylacrylamide)	33[47]
4	poly(*N*-(1-hydroxymethyl)propylmethacrylamide	34[48]
5	poly(*N*-(2-ethoxyethyl)acrylamide)	38[49]
6	poly(aminomethoxypropylacrylamide)	43[50]
7	poly(*N*-(2-ethoxyethyl)methacrylamide)	50[49]
8	poly(*N*-cyclopropylacrylamide)	58[44]
9	poly(*N*-ethylacrylamide)	74[21]

Table 1.2. Poly(*N*,*N*-dialkylacrylamide) with different disubstituting alkyl groups and their LCSTs.

Entry	Poly(*N*,*N*-alkylacrylamide)	LCST (°C)
1	poly(*N*,*N*-methylpropylacrylamide)	15[51]
2	poly(*N*,*N*-diethylacrylamide)	32[52]
3	poly(*N*,*N*-ethylmethylacrylamide)	60[53]
4	poly(*N*,*N*-dimethylacrylamide)	216[51]

Poly(*N*,*N*-dialkylacrylamides) have two substituting alkyl groups on their amide nitrogen atoms. Their LCST depends on the hydrophobicity of both alkyl groups. For example, poly(*N*,*N*-diethylacrylamide) and poly(*N*,*N*-ethylmethylacrylamide) have significantly

different LCSTs (**Table 1.2**, compare entry **2** and **3**).[52,53] Another example is poly(*N*,*N*-dimethylacrylamide), which is estimated to have an LCST of 216°C.[51] The methyl groups are not highly hydrophobic, and so poly(*N*,*N*-dimethylacrylamide) exhibits a very high LCST.

As discussed above, the LCST decreases as the hydrophobicity of the TRP increases. However, there are exceptions to this. For example, poly(*N*-isopropylacrylamide) (**Fig. 1.10A**) and poly(*N*-isopropylmethacrylamide) (**Fig. 1.10B**) have LCSTs of 32°C and 46°C, respectively.[45,54] Djokpe et al. speculated that this phenomenon could be a result of steric hindrance.[55] The additional methyl group prevents the other hydrophobic groups coming together during the phase transition. Hence, this interferes with the hydrophobic effect and causes a delay in phase separation.

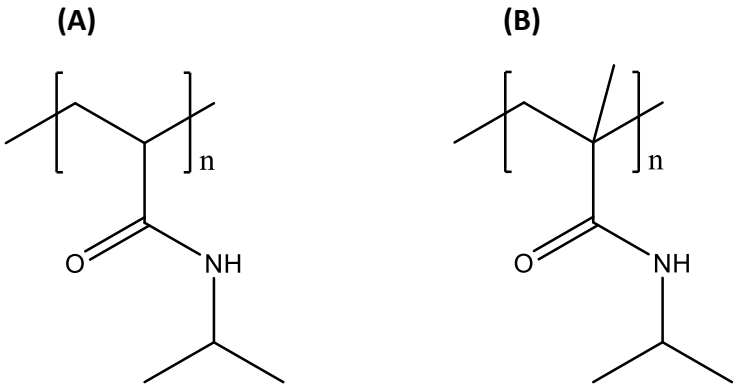

Figure 1.10. Chemical structure of **(A)** poly(*N*-isopropylacrylamide) and **(B)** poly(*N*-isopropyl methacrylamide).

The other type of TRPs (where the polymer itself is not thermoresponsive, but can become thermoresponsive when grafted with other polymers), are copolymers that are made of non-thermoresponsive homopolymers. Thermoresponsivity can be obtained by adjusting

the ratio of the hydrophobic and hydrophilic segments to the right hydrophobic-hydrophilic balance. Usually a hydrophilic polymer, such as PEG, is introduced into a hydrophobic polymer and the LCST can be adjusted by varying the length of the PEG units. For example, poly(methyl methacrylate) (PMMA) is hydrophobic and not thermoresponsive. When a certain number of PEG units are placed in between the methyl and methacrylate groups (**Fig. 1.11A**), the resulting poly(methyl ethoxymethacrylate)s ($PMEO_nMAs$) are thermoresponsive. When the number of PEG units increases from 2, 3 to 4 (n=2, 3 or 4), the LCSTs of these $PMEO_nMAs$ are 26°C[56], 52°C[56], and 68°C[57], respectively. Similarly, adding PEG to poly(ethyl methacrylate) also yields thermoresponsive poly(ethyl ethoxymethacrylate)s ($PEEO_nMAs$), and their LCSTs are much lower when compared to those of $PMEO_nMAs$ with a similar number of PEG units.[57] This is because of the more hydrophobic ethyl terminal groups on the $PEEO_nMAs$ (**Fig. 1.11B**).

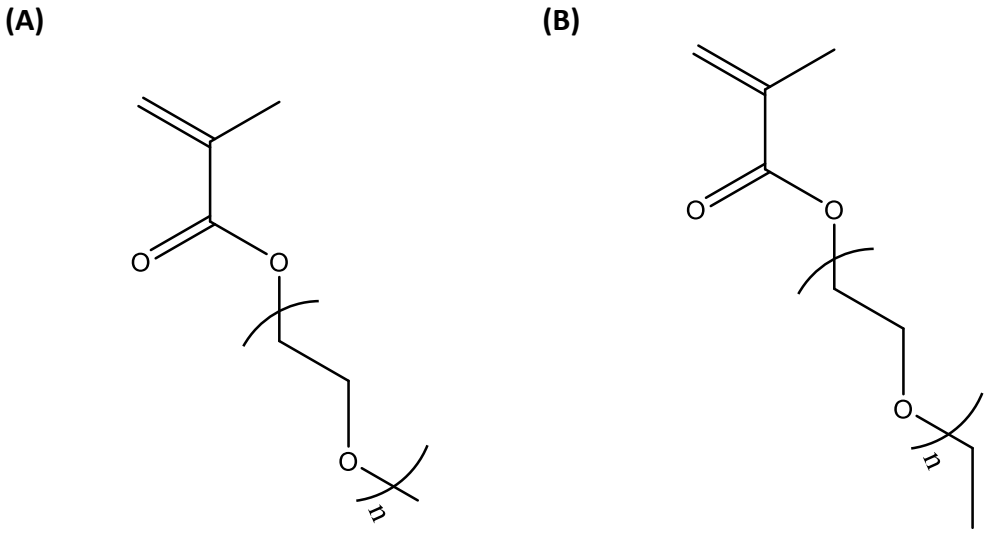

Figure 1.11. Chemical structure of methyl **(A)** methacrylate and **(B)** ethyl methacrylate with n units of PEG.

1.7.2 The Effect of Molecular Weight on the LCST

Generally, the molecular weight of a TRP is negatively correlated with its LCST. The effect of molecular weight on the LCST is more pronounced when the molecular weight is relatively small.[58] On the contrary, the LCST is independent of the molecular weight when the molecular weight is large. The effect of molecular weight is attributed to the effect of the hydrophobic terminal groups on the LCST of a TRP.[59] The terminal groups of a polymer are usually determined by the type of initiator used in the polymerization reaction. For example, PNIPAAm samples prepared using different initiators show different LCSTs when comparing similar molecular weights (**Fig. 1.12**).[60] The effect of the terminal groups becomes smaller as the molecular weight of the TRP increases. Thus, the LCST becomes less dependent on the molecular weight. At low molecular weight, the LCSTs of PNIPAAms with different terminal groups decrease more significantly than those at high molecular weight (**Fig. 1.12**).[60]

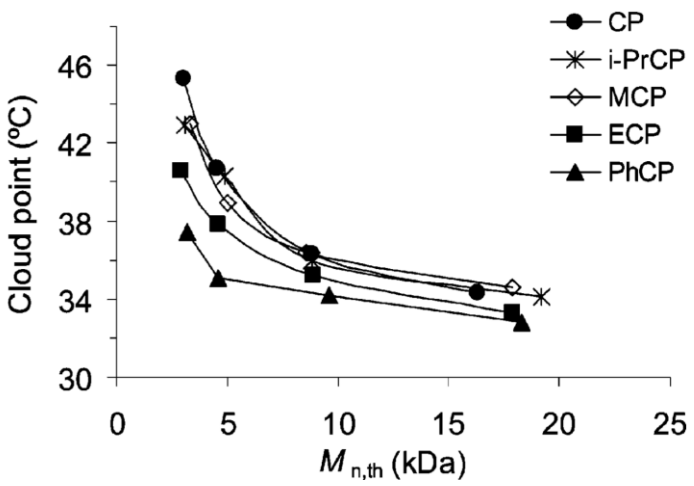

Figure 1.12. Correlation of T_c with the molecular weight of PNIPAAm with different terminal groups. Different initiators were used in the polymerization reactions, including 2-chloropropionamide (CP), *N*-isopropyl-2-chloropropionamide (i-PrCP), methyl 2-chloropropionate (MCP), ethyl 2-chloropropionate (ECP), and *N*-phenyl-2-chloropropionamide (PhCP). The figure was adapted from Xia et al.[60]

1.7.3 The Effect of the Dispersion Concentration on the LCST

In general, the LCST increases as the concentration of a TRP dispersion decreases. This is because a dilute dispersion decreases the chance that polymer chains collide and interact with each other to form large aggregates when the temperature is higher than the LCST. Thus, it would require more energy and a higher temperature to accelerate the formation of the large aggregates eventually leading to phase separation. In fact, the study of the concentration effect is very important, especially when a TRP is developed for biomedical applications. Serious dilution of the TRP dispersion would result in an increase in LCST, and ultimately would lead to the loss of thermoresponsivity.

1.7.4 The Effect of Salts and Salt Concentration on the LCST

Generally, the thermoresponsive behavior of a TRP changes with the addition of small molecules which affect the polymer-water interactions. Salts are known to have a large effect on the LCST and they can be classified into two categories: kosmotropic and chaotropic salts. Kosmotropic salts typically decrease the LCST of a TRP by forming stronger interactions with water and weakening the polymer-water interactions. This makes the TRP less stable in water, which becomes phase separated at a lower temperature. Examples of kosmotropic salts are $CH_3CO_2^-$, HCO_2^-, F^-, OH^-, HPO_4^-, CO_3^{2-}, and SO_4^{2-}. They are typically small and/or have a high charge density. On the other hand, chaotropic salts are less effective in terms of decreasing the LCST. In fact, they sometimes stabilize the hydrophobic segments of a TRP and require more energy for a phase separation. Examples of chaotropic salts include ClO_4^-, SCN^-, I^-, Br^- and Cl^-. These salts are typically large and/or monovalent. **Fig. 1.13** shows that kosmotropic salts are more effective in decreasing the LCST of a PNIPAAm dispersion than chaotropic salts.[61]

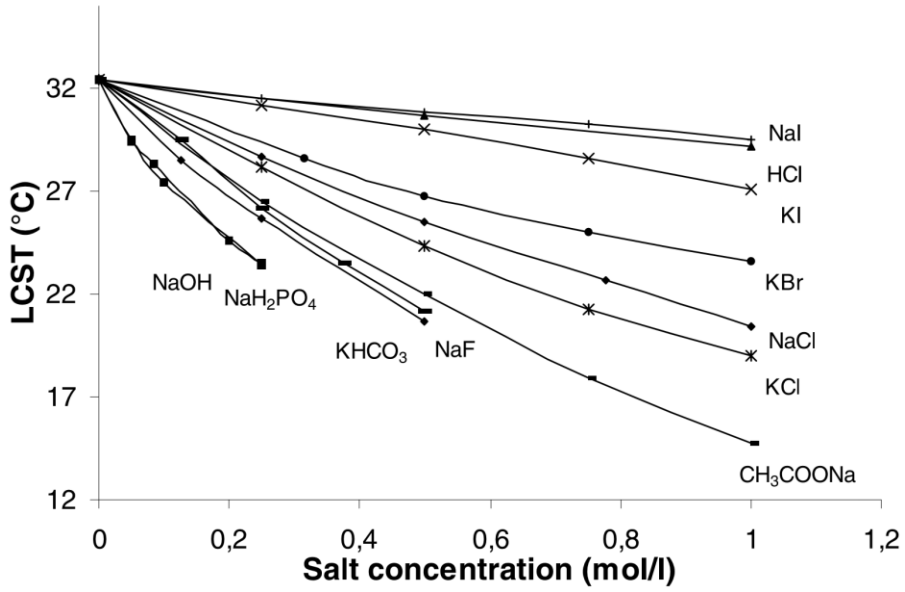

Figure 1.13. Effect of the concentration of different types of salts on the LCST of a PNIPAAm dispersion. The figure was adapted from Eeckman et al.[61]

1.8 Thermoreponsive Polysaccharides

As mentioned earlier in this chapter, thermoresponsive natural polymers are inherently advantageous over synthetic polymers because of their natural abundance, biodegradability, biocompatibility, nontoxicity and potentially low production costs.

1.8.1 Thermoresponsive Cellulose

Cellulose, the most abundant organic polymer on Earth, is a type of polysaccharide consisting of D-anhydroglucose units joined together by β-1,4-glycosidic linkages (**Fig. 1.14A**). A number of cellulose derivatives have been reported to exhibit thermoresponsive behaviors and some examples are shown in **Table 1.3**.[62-67] These cellulose derivatives are prepared by either alkylation or etherification of the hydroxyl groups (OH) at the C-2, C-3 and C-6 positions

on the anhydroglucose units (AGUs) of a cellulose chain (**Fig. 1.14B**).[68] It is noteworthy that different substituents have different effects on the LCST. For example, methyl cellulose (MC) has an LCST of around 68°C,[63] whereas the LCST of hydroxypropyl cellulose (HPC) is approximately 46°C.[62] In addition to different types of substituents, the LCST of cellulose derivatives is also determined by the degree of substitution (DS) and molar substitution (MS). The DS is defined as the average number of substituted OH groups on the AGU, and the MS is referring to the number of moles of substituents per mole of AGU.[68] For instance, hydroxypropyl methyl cellulose (HPMC) with a DS of the methyl group (DS_{Me}) of 1.9 and a MS of the hydroxypropyl group (MS_{HP}) of 0.25 has a lower LCST, at around 65°C,[64] compared to another HPMC sample with a DS_{Me} of 1.45 and a MS_{HP} of 0.11, which has a LCST of 75°C.[65] Interestingly, hydroxyethyl methyl cellulose (HEMC), MC and HPMC have been commercialized by Shin-Etsu Chemical in 1962 under the trade name Metolose™.[63] According to the manufacturer, Metolose™ is mainly used as a binder for solid pharmaceutical drugs such as tablets and granules. Metolose™ is also used as a non-digestive fiber for dietary supplements.

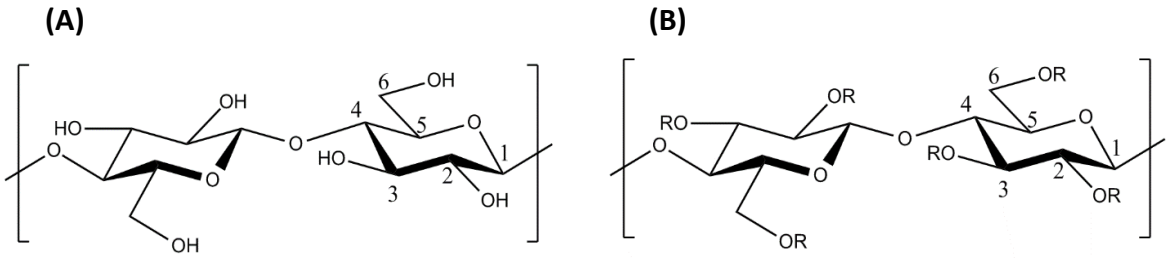

Figure 1.14. Chemical structure of cellulose and cellulose derivatives. (**A**) Two D-anhydroglucose units are joined by β-1,4-glycosidic linkages. (**B**) A cellulose derivative with substituents at C-2, C-3 and C-6 positions.

Table 1.3. Cellulose derivatives with different substituents and LCSTs.

Entry	Cellulose Derivatives	Substituents	LCST (°C)
1	Methyl cellulose (MC)	$-CH_3$	68[63]
2	Hydroxypropyl cellulose (HPC)	$-CH_2CH(OH)CH_3$	46[66]
3	Hydroxyethyl methyl cellulose (HEMC)	$-CH_3$ or $-CH_2CH_2OH$	74[67]
4	Hydroxypropyl methyl cellulose (HPMC)	$-CH_3$ or $-CH_2CH(OH)CH_3$	65[64]
5	Ethylhydroxyethyl cellulose (EHEC)	$-CH_2CH_3$ or $-CH_2CH_2OH$	39[62]

1.8.2 Thermoresponsive Starch

Starch is a naturally occurring polysaccharide produced by most plants for energy storage and consists of two major components: amylose and amylopectin.[69,70] Normal starch such as normal maize, rice and potato contains approximately 70-80% amylopectin and 20-30% amylose.[69] Amylose is primarily a linear polysaccharide that is made of D-anhydroglucose units linked together by α-1,4-glycosidic linkages (**Fig. 1.15A**). Amylopectin is a highly

branched polysaccharide with an α-1,4-linked D-anhydroglucose main chain and many α-1,6-linked branches (**Fig. 1.15B**). The starch produced by most plants has a characteristic granular morphology.[70] Starch granules are made up of alternating crystalline and amorphous layers. The size of starch granules varies from submicron to over 100 microns in diameter, depending on the source.

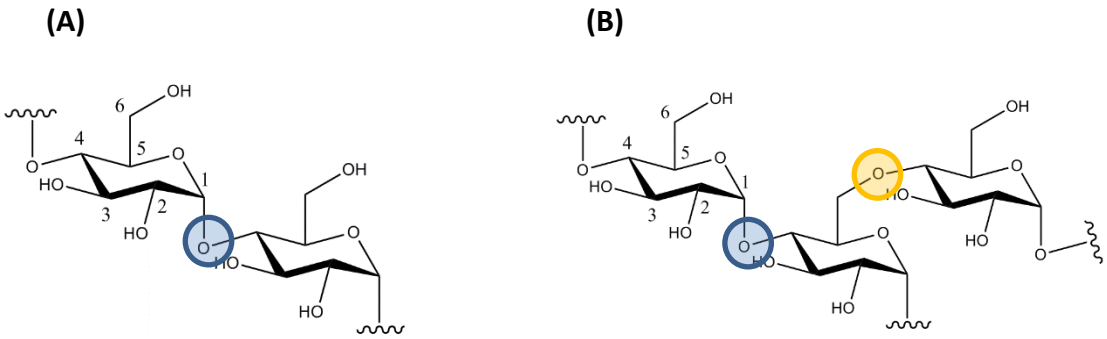

Figure 1.15. Chemical structures of (**A**) amylose and (**B**) amylopectin. The blue shaded area highlights α-1,4-glycosidic linkages and yellow shaded area highlights α-1,6-linked branch points.

Thermoresponsive starch (TRS) was first documented by Ju et al. in 2012. They described a way to prepare thermoresponsive 2-hydroxy-3-butoxypropyl starch (HBPS) by hydrophobically modifying degraded corn starch with butyl glycidyl ether (BGE) (**Scheme 1.1**).[71] Thermoresponsive HBPS with a range of MS from 0.32 to 0.63 were reported along with their LCSTs, which were determined to be from 32.5 to 4.5°C by turbidity measurements. Ju et al. also suggested that the HBPS in an aqueous dispersion has the ability to assemble into micelles below LCST if the critical micelle concentration is reached. When the temperature reaches the LCST, the micelles undergo deformation due to an increase in

hydrophobicity of the polymer. The formation and deformation of the HBPS micelles were monitored using fluorescence spectroscopy and pyrene as a probe. Additionally, an *in vitro* drug release experiment was conducted and the drug-loaded HBPS micelles were demonstrated to display accelerated drug release triggered by a change in temperature.[71]

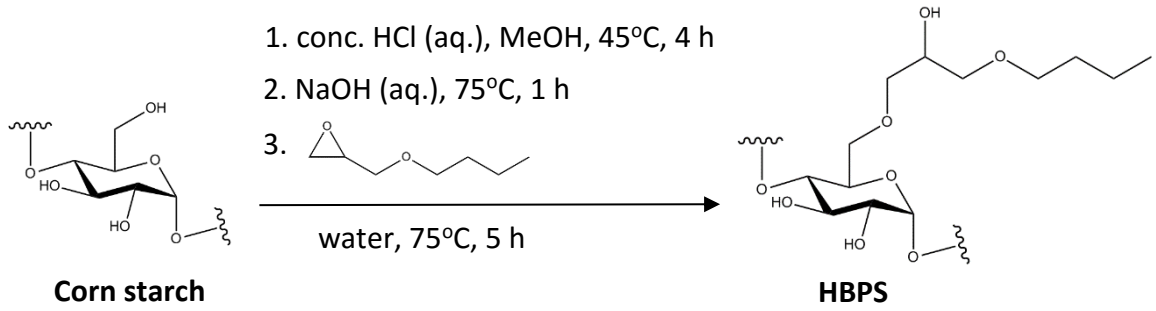

Scheme 1.1. Reaction scheme for the synthesis of HBPS. Corn starch was first subjected to methanol/HCl degradation. NaOH was added to an aqueous dispersion of the degraded starch followed by a pre-heating step in a 75°C water bath for 1 h. Lastly, butyl glycidyl ether (BGE) was added to the mixture and reacted for 5 h at 75°C to yield HBPS. The C-6 substituting HBPS is shown but other substituting positions are also possible. The reaction scheme was adapted from Ju et al.[71]

Shortly thereafter, Ju et al. reported another TRS, 2-hydroxy-3-isopropoxypropyl starch (HIPS). The HIPS was obtained by modifying corn starch with isopropyl glycidyl ether (IPGE) (**Scheme 1.2**).[72] Their LCSTs were adjusted from 69 to 28°C by varying the MS of the HIPS. It was found that the addition of a small amount of certain types of salts or alcohols substantially decreased the LCST of the HIPS.

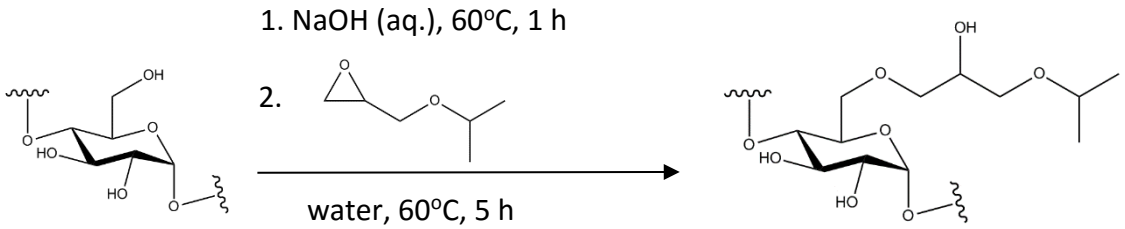

Scheme 1.2. Reaction scheme for the synthesis of HIPS. NaOH was added to an aqueous dispersion of starch and pre-heated in a 60°C water bath for 1 h. Then, isopropyl glycidyl ether (IPGE) was added to react for 5 h at 60°C to yield HIPS. Substitution may occur at the other two hydroxyl groups on the AGU as well. The reaction scheme was adapted from Ju et al.[72]

A number of thermoresponsive starch ethers were synthesized by Ju et al., and the effect of their structure on thermoresponsive behavior was investigated.[73] In particular, 3-[2-butoxy(ethoxy)$_m$]-2-hydroxypropyl starch ethers (BE$_m$S) with oligo(ethylene glycol) spacers of various lengths (m = 0, 1 or 2) were prepared by reacting degraded waxy maize starch with several hydrophobic reagents that differed in the length of the oligo(ethylene glycol) spacers (**Scheme 1.3**).[73] A positive correlation was found between the LCST of the BE$_m$S with a similar MS and the length of the oligo(ethylene glycol) spacers. Additionally, salt additives and the concentration of the BE$_m$S dispersions were reported to have a reduced effect on the LCSTs when the length of the oligo(ethylene glycol) spacers increased.

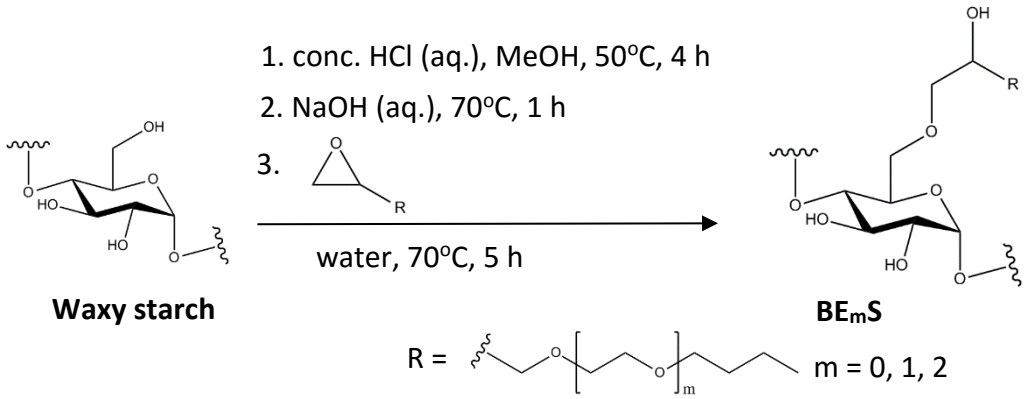

Scheme 1.3. The reaction scheme for the synthesis of BE_mS. Waxy starch was first subjected to methanol/HCl degradation. NaOH was then added to an aqueous dispersion of the degraded starch and pre-heated in a 70°C water bath for 1 h. Lastly, the corresponding epoxides were added to react for 5 h at 70°C to yield BE_mS. Substitution may occur at the other two hydroxyl groups on AGU as well. The reaction scheme was adapted from Ju et al.[73]

1.9 Starch Nanoparticles

Nanoparticles are particles with a diameter of 10 to 1000 nanometers.[74] Starch nanoparticles can be prepared from starch using a number of different methods such as acid hydrolysis,[75] precipitation,[76] and reactive extrusion[77].

EcoSphere™ starch nanoparticles are produced by EcoSynthetix Inc. (Burlington, ON) via a proprietary reactive extrusion process on an industrial scale.[77] Specifically, starch granules are fed continuously into a twin-screw extruder, which creates a high temperature and high shear environment for degrading the starch granules. Various additives are also fed into the extruder including water, glycerol (GY) and glyoxal (GX). Glycerol is a well-known plasticizer which disrupts hydrogen bonding in starch granules. The addition of glycerol and water decreases the glass transition temperature of starch granules and facilitates their

transformation into a thermoplastic melt. High shear provided by the extruder mechanically disrupts the crystalline structure of starch granules and breaks down the starch. Glyoxal is added to cross-link starch fragments via the formation of full acetal or hemiacetal bonds with the hydroxyl groups on starch. The final products that leave the extruder are dry starch nanoparticle agglomerates that are approximately 300 microns in size. Throughout this thesis, the EcoSphere^{TM} starch nanoparticles will be referred to as just starch nanoparticles (SNPs).

Chakraborty et al. have studied the solution properties of aqueous dispersions of these SNPs by dynamic light scattering (DLS).[78] The hydrodynamic diameter (D_h) of the SNPs was reported to be approximately 40 nm and 300 nm, which corresponds to isolated particles and SNP aggregates in the dispersion, respectively. The molecular weight of the isolated particles was estimated to be 2.2-2.6 x 10^6 g/mol. Moreover, an increase in the temperature of the SNP dispersion from 25 to 65^{o}C had no effect on the D_h, suggesting that the unmodified SNPs were not thermoresponsive.

1.10 Hydroxyalkylation of SNPs

Initial studies on the hydroxyalkylation of SNPs in aqueous dispersions were conducted by M. Karski in the Taylor group.[79] The hydroxyalkylation of SNPs involves a hydroxyl group on an anhydroglucose unit (AGU) reacting with an epoxide in aqueous NaOH (**Scheme 1.4**). The reaction proceeds via an S_N2-type attack of the deprotonated hydroxyl

group on the least sterically hindered carbon of the epoxide. Two major side reactions may occur: first, the ring-opening reaction of the epoxide by water or hydroxide to yield a glycol derivative and second, the polymerization of the glycol into polyglycols. Side reaction-minimizing strategies can be employed, which include reducing the water content in the reaction, keeping the reaction temperature below 50°C, and maintaining a pH under 13.

Stability studies of SNPs in aqueous NaOH revealed that the extent of SNP degradation was insignificant when the SNPs were subjected to aqueous NaOH (pH 12-13) at 30-40°C for 24 h.[79] Hence, the hydroxyalkylation reactions were carried out under these conditions to avoid significant SNP degradation.

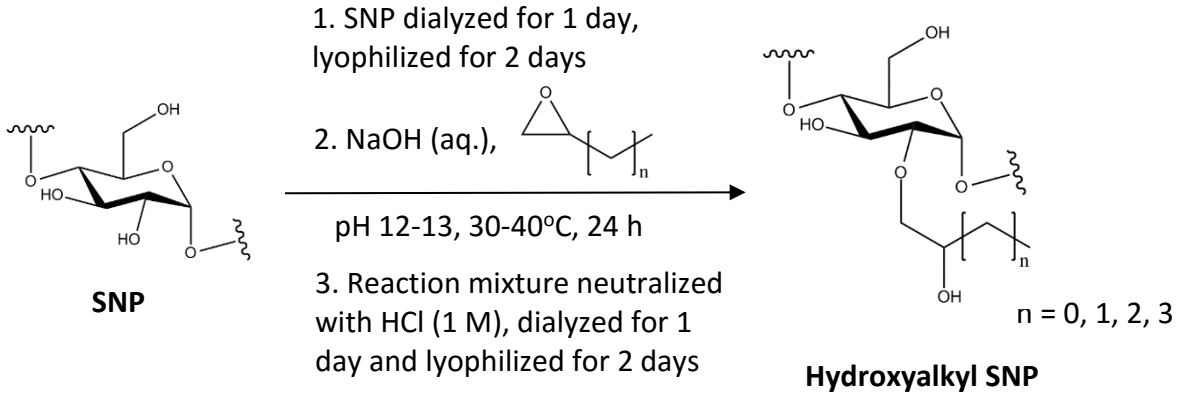

Scheme 1.4. General protocol for the hydroxyalkylation reactions. Hydroxyalkyl SNPs with n = 0, 1, 2, 3 correspond to the products obtained from hydroxypropylation, hydroxybutylation, hydroxypentylation and hydroxyhexylation, respectively. The reaction scheme was adapted from M. Karski's M.Sc. thesis.[79]

A series of hydroxyalkylation reactions including hydroxypropylation, hydroxybutylation, hydroxypentylation and hydroxyhexylation of SNPs were investigated

(**Scheme 1.4**).[79] The hydroxypropylation reaction yielded hydroxypropyl SNPs (HPSNPs) with MS values from 0.08 to 2.06 depending on the molar equivalents (mol equiv) of propylene oxide (PO) used. Unlike the HPC, which exhibits a LCST of 46°C as mentioned in **Section 1.8.1**, HPSNPs were not thermoresponsive across the aforementioned MS range. The reaction of SNPs with 1,2-butene oxide (BO) produced hydroxybutyl SNPs (HBSNPs), some of which were thermoresponsive SNPs (TRSNPs). HBSNPs with a MS of 1.16 or greater exhibited thermoresponsive behavior with relatively sharp transmittance curves and fast thermotransitions. The LCST decreased linearly as the MS of the HBSNPs increased from 1.16 to 1.66, the lowest LCST being 37.8°C. Preliminary results for hydroxypentylation and hydroxyhexylation of SNPs were also reported in Karski's M.Sc. thesis.[79] For example, $HPe_{0.54}$SNP (hydroxypentyl SNP with a MS of 0.54) exhibited a LCST of 52.8°C, but $HH_{0.14}$SNP (hydroxyhexyl SNP with a MS of 0.14) was not thermoresponsive. The reaction efficiencies for both hydroxypentylation and hydroxyhexylation reactions were very low since these reactions typically required relatively harsh reaction conditions (140°C, 1 h, 0.4 M KOH/*n*AGU).[80] Overall, Karski's result suggested that a lower LCST could be achieved when the SNPs were reacted with a more hydrophobic epoxide.

1.11 Research Objectives

The goal of this research was to prepare and characterize thermoresponsive starch nanoparticles. This goal was pursued by hydrophobically modifying SNPs with butene oxide or styrene oxide, followed by detailed characterization of the resulting modified SNPs. The

characterization of these TRSNPs aims to provide fundamental and in-depth understanding of these novel thermoresponsive polymer systems.

Chapter 2

Synthesis and Characterization of Hydroxybutylated Starch Nanoparticles

2.1 Determination of Anhydroglucose Units (AGUs) in the SNPs

Prior to SNP modification, the mols of anhydroglucose units (AGUs) per unit mass of the SNPs had to be determined. The mols of AGUs in the SNPs cannot be accurately determined simply by dividing the weight of the SNPs by 162 g/mol, which is the molecular weight of an AGU, because the commercial grade SNPs (CSNPs) contain a considerable amount of water, GY and GX. Hence, ^{1}H-NMR was used to determine how many grams of AGUs were actually present in the SNPs. This was done as follows. An accurately weighed quantity of the CSNPs was dispersed in D_2O and transferred into an NMR tube. An accurately weighed quantity of an internal standard, 3-(trimethylsilyl)-2,2',3,3'-tetradeuteropropionic acid (TMSP-d_4), was added, and the ^{1}H NMR spectrum was obtained. The ^{1}H-NMR spectrum of the CSNPs in D_2O is shown in **Fig. 2.1**.

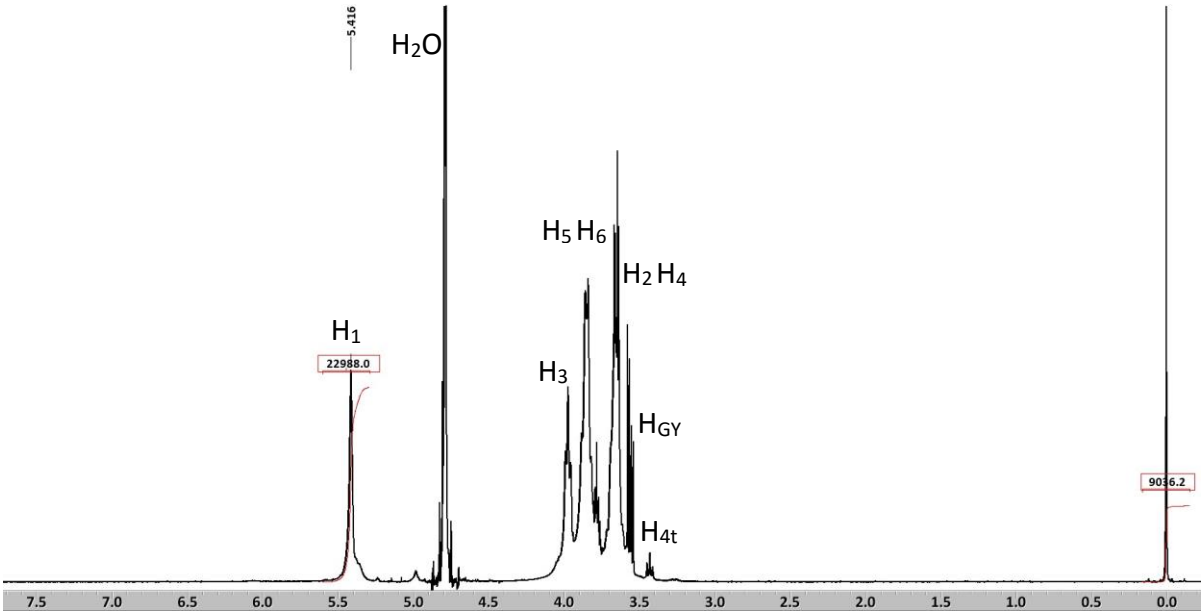

Figure 2.1. ^{1}H-NMR spectrum of CSNPs in D_2O containing TMSP-d_4. The anomeric proton of α-1,4-linked AGUs appears as a singlet at 5.4 ppm. The methyl groups of TMSP-d_4 appear as a singlet at 0 ppm.

The anomeric proton of α-1,4-linked AGUs appears as a singlet peak at 5.4 ppm. The integration of the peak corresponding to the anomeric protons was compared to the integration of the methyl peak in TMSP-d_4. The anomeric proton peak was used since it can be integrated with good accuracy without any overlapping signals from other peaks. The number of grams of AGUs in the sample was determined using **Equation 2.1**:

$$\text{Grams of AGUs} = \frac{I_{\text{H1 of SNP}}}{I_{\text{TMSP-}d4}/9} \times \text{mols of TMSP-}d_4 \times 162 \text{ g/mol} \quad \text{(Eqn. 2.1)},$$

where $I_{\text{H1\_of\_SNP}}$ is the integration of the anomeric proton, $I_{\text{TMSP-}d4}$ is the integration of the peak corresponding to the methyl groups from the TMSP-d_4 standard (this value was divided by 9, as there are three methyl groups for a total of 9 protons) and 162 g/mol is the molecular weight of an AGU. The % AGUs in the CSNPs was obtained using **Equation 2.2**:

% AGUs in the CSNPs = $\frac{\text{grams of calculated AGUs}}{\text{weighed amount of CSNPs}}$ x 100% ..... (**Eqn. 2.2**).

The data from four separate determinations indicated that the CSNPs contained approximately 64 ± 0.04 % AGUs. In other words, 1 g of the CSNPs contain an average of 0.64 ± 0.04 g of actual SNPs. Similar results were reported by Li.[81] Moisture, GX and GY would most likely account for the missing 36% in the CSNP sample. With this knowledge, the mols of AGUs in a weighed quantity of CSNPs was determined by **Equation 2.3**:

mols AGUs in the CSNPs = $\frac{\text{grams of weighed CSNPs x 0.64}}{\text{162 g/mol}}$ ..... (**Eqn. 2.3**).

2.2 Hydroxybutylation of SNPs

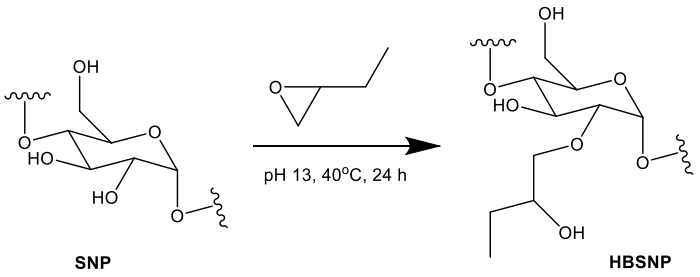

Scheme 2.1. Hydroxybutylation of SNPs.

The hydroxybutylation of the SNPs was performed using the procedure modified from the one that was developed by Karski (**Scheme 2.1**).[79] First, the CSNPs were fully dispersed in water at 40°C for a sufficient amount of time (usually over 2 h) and allowed to cool to room temperature. Then, 10 M NaOH was added drop-wise with vigorous stirring until a pH of 13 was reached. Previous studies by Karski showed that the SNPs do not undergo significant

degradation at this pH at 40°C even over 24 h.[79] Butene oxide (BO) was introduced and the biphasic mixture was stirred at 40°C for 24 h, during which the solution became homogeneous. In some instances, a precipitate formed (discussed below). The solution was neutralized with 1 M HCl, then dialyzed (MW_{cutoff} = 1000 g/mol or 1kD) against water. The resulting solution was lyophilized to give the hydroxybutyl SNPs (HBSNPs) as white powders. Before systematically preparing HBSNPs with different molar substitution of HB groups (MS_{HB}), a control experiment as well as a kinetic study of the BO reaction were conducted.

2.2.1 Formation of Poly(1,2-butylene glycol)

One possible side reaction during the modification of SNPs with BO is the formation of poly(1,2-butylene glycol) (**Fig. 2.2**). Before we began modifying the SNPs with BO, we performed an experiment to determine if a significant amount of poly(1,2-butylene glycol) would be formed under our reaction conditions. The reaction was carried out with 1.7 g BO and without any SNPs using the same protocol as described above. Before the reaction, the reaction mixture was biphasic upon the addition of BO (**Fig. 2.3A**). This is expected, as BO is known to have a poor water solubility. After the 24 h reaction, the reaction mixture appeared to be homogeneous and transparent, indicating that some kind of reaction certainly took place (**Fig. 2.3B**). After dialysis against water, there was no observable precipitate in the dialysis tubing (**Fig. 2.3C**). The dialyzed reaction mixture was lyophilized to remove water. Approximately 8 mg of white powder was left in the flask. The ^{1}H NMR spectrum of the white

powder in dimethyl sulfoxide-d_6 (DMSO-d_6) with a couple drops of trifluoroacetic acid-*d* (TFA-*d*) confirmed the absence of peaks corresponding to poly(1,2-butylene glycol) (**Fig. 2.4**). This indicates that either the concentration of the NMR solution was too low or that the formation of poly(1,2-butylene glycol) with a molecular weight larger than 1 kD did not occur. Either way, this control experiment shows that the polymerization of BO was negligible.

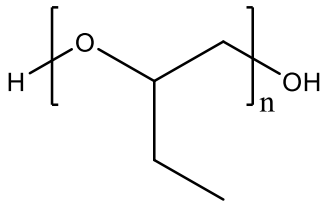

Figure 2.2. Chemical structure of poly(1,2-butylene glycol).

(A) **(B)** **(C)**

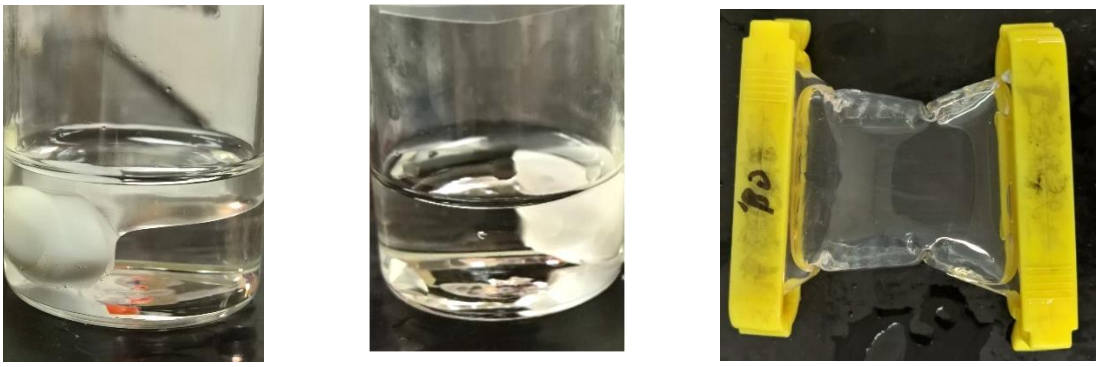

Figure 2.3. Pictures taken for the reaction mixture of the BO control reaction **(A)** before and **(B)** after stirring at 40°C for 24 h and **(C)** after dialysis against water for 2 days.

Figure 2.4. ^{1}H NMR spectrum for the product of the BO control experiment in DMSO-d_6 and two drops of TFA-*d*.

2.2.2 Kinetic Study of the Reaction of BO with SNPs

Wayne Vuong, a student in the Taylor group, performed a kinetic study of the reaction of BO with SNPs. The SNPs used in this kinetic study were different from the ones used throughout this thesis, in that they contained less glycerol (the SNPs were used without purification). Nevertheless, this study provided us with an idea as to how fast the reaction between BO and the SNPs takes place.

The reaction was followed by ^{1}H NMR, and 1 mol equiv of BO to AGU was used. **Fig. 2.5** shows a plot of MS_{HB} vs. time. From this plot, it can be seen that the reaction is more-or-less complete after 5 h. The rate is remarkably linear over the first 2-3 h of the reaction. This may be due to the BO being poorly soluble in the aqueous medium. Hence, for a significant part of the reaction, the aqueous phase was saturated with BO and so the concentration of

BO dissolved in the aqueous phase did not change significantly until the latter half of the reaction. Moreover, since the OH groups in the dispersed SNPs would be in considerable excess as compared to solubilized BO in the first half of the reaction, then the concentration of OH groups on the SNPs would not change considerably until the latter half of the reaction. Therefore, zero-order-like kinetics are seen in the first half of the reaction. The best line fit to the data over the first 2 h of the reaction has an R^2 value of 0.96. The slope of this line provides a zero-order rate constant (k) of 0.19 mols substituted OH groups/h for the first 2 h of the reaction.

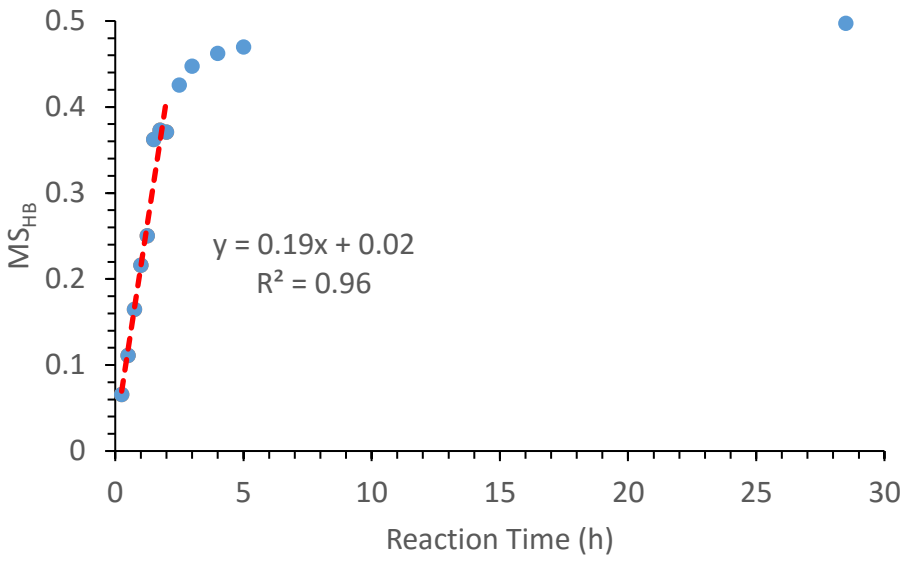

Figure 2.5. Kinetic study of 1 mol equiv BO reaction conducted by Vuong.

It is important to reiterate that the SNPs used in this kinetic study contained considerably less glycerol as compared to the SNPs used to prepare HBSNPs presented in subsequent sections in this chapter. The amount of glycerol may affect the rate of these

reactions. It would certainly be expected to compete for BO, and so to affect the degree of substitution of the modified SNPs. Moreover, different amounts of BO added may have an effect on the total reaction time needed for the reaction to go to completion. Intuitively, a smaller amount of BO in the reaction would be consumed in a shorter period of time. If larger than 1 mol equiv of BO were used, the reaction may require more than 5 h to reach completion. Thus, for a fair comparison of the reaction results, all subsequent reactions between BO reaction and SNPs discussed in this thesis were reacted for 24 h.

2.3 ^{1}H NMR Spectral Analysis of HBSNPs

By varying the amount of BO used in the reactions, HBSNPs with different MS_{HB}s were obtained. A typical ^{1}H NMR spectrum for an HBSNP is shown in **Fig. 2.6**. The peak at 0 ppm belongs to the internal standard, TMSP-d_4. Peaks at 1.1-0.8 ppm correspond to the methyl protons in the HB group (labeled **D**), whereas the peaks at 1.7-1.3 ppm represent the methylene protons in the HB group (labeled **C**). The peaks between 4.2-3.3 ppm are assigned to the 6 protons (labeled **2-6**) in the AGU and the 3 protons (labeled **A** and **B**) from the HB group. The largest peak at 4.8 ppm corresponds to the water peak. Lastly, the peaks at 5.7-5.3 ppm are assigned to the anomeric proton (labeled **1**). Three distinctive peaks can be found in this region for HBSNPs with low MS_{HB}. The peaks are at approximately 5.7, 5.5, and 5.4 ppm. The specific assignments of these peaks are based on where the substituents are attached onto the AGU.[82] The chemical shift of the anomeric protons depends on the

proximity between the anomeric proton and the substituting position.[83] As mentioned in **Section 1.8**, the possible sites of substitution on an AGU are at the O-2, O-3, and O-6 positions. The chemical shift of the anomeric proton can be affected by the position of substitution. In the simplest case where only monosubstitution occurs, the chemical shift of the anomeric proton will shift downfield the most when the O-2 position is substituted. This is due to the fact that the substituting position is the closest to the anomeric proton. Similarly, the chemical shift of the anomeric proton in the O-3 substituted AGU is also affected but to a lesser degree because the O-3 substituting position is further away than O-2. Lastly, O-6 is too far away from the anomeric proton to induce any effect so that the chemical shift of the anomeric proton is more-or-less the same as the one found in an unsubstituted SNP. Thus, the peaks at 5.7, 5.5, and 5.4 ppm correspond to the anomeric protons of the AGUs with substitution at O-2, O-3, and O-6 or unsubstituted at any position, respectively.

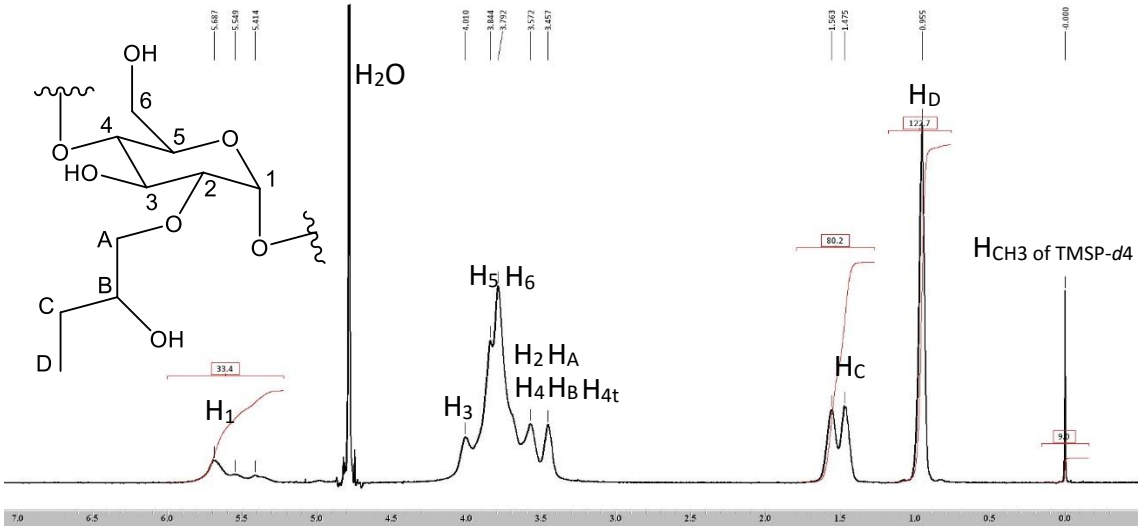

Figure 2.6. ^{1}H-NMR spectrum of $HB_{1.2}$SNPs, with a MS_{HB} of 1.2, in D_2O.

Merkus et al. reported that hydroxyethylation of starch proceeds with O-2 substitution dominating over O-3 substitution, which in turn is favored over O-6 substitution.[1] They briefly discussed that this substitutional preference is due to the differences in the acidity of the hydroxyl groups at different positions on an AGU. The hydroxyl group at C-2 is more acidic than those at C-3 and C-6. This means that under basic conditions, there is a greater concentration of the conjugate base of the OH at C-2. The differences in acidity are possibly caused by the electron-withdrawing effect of the close-by oxygen atoms. The C-2 hydroxyl group is comparatively more electron-deficient because it has three oxygen atoms within the range of three bond lengths. The C-3 hydroxyl group has two oxygen atoms within the range of three bond lengths, so it experiences less electron-withdrawing effects than the C-2 hydroxyl group does but more than the one at C-6. Merkus et al. also suggested that the hydroxyl groups at C-2 and C-3 are in proximity to each other to provide stabilization by inductive effect for the negative alkoxy ion that is generated after the deprotonation step.[84]

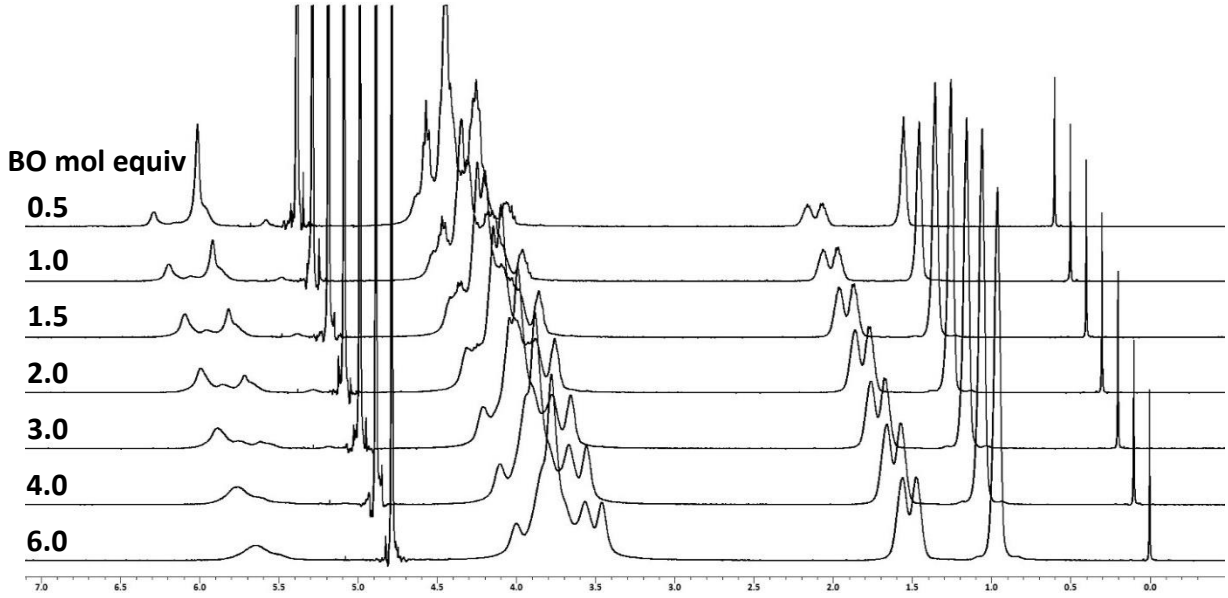

Figure 2.7. ^{1}H NMR spectra of HBSNPs prepared with an increasing amount of BO. The spectra are slant-stacked and magnified to approximately the same intensity based on the internal standard peak at 0 ppm.

Consistent with Merkus et al.'s studies on the hydroxyethylation of starch, the O-2 position was the more favourable site for substitution to occur than either O-3 or O-6 for the hydroxybutylation of SNPs.[84] This is supported by analysis of the ^{1}H-NMR spectra of HBSNPs modified using increasing mol equiv of BO (**Fig. 2.7**). At low mol equiv of BO, the O-2 position was the more favourable substitution site, as evidenced by the appearance of the furthest downfield-shifted anomeric peak at 5.7 ppm. As the mol equiv of BO increases, this peak clearly increases in height and peak area. At the same time, the appearance of a second but smaller peak at 5.5 ppm indicates that the substitution at O-3 position also took place but was less favourable than O-2. As the mol equiv of BO increases above 2.0, the peaks corresponding to the anomeric protons overlap and broaden. When two or more HB groups

attach onto one AGU, it is possible to get different combinations of substitution. Moreover, it is possible that the HB groups could be oligomerizing or polymerizing. Whether the HB groups oligomerize or polymerize cannot be determined by ^{1}H NMR alone. This issue will be discussed in more detail in **Section 2.8**. The possibilities for the combination of substitution increase exponentially as the number of HB groups on one AGU increases. For example, a disubstituted AGU theoretically has six possible constitutional isomers. The broadening of the anomeric peaks could be a consequence of different isomers that may have slightly different chemical shifts. Despite the broadening effects, it is clear that the population of the O-2 substituted AGUs are more than the population of the O-3 substituted ones based on the size of the underlying peaks.

The anomeric peak at 5.4 ppm decreases with the addition of an increasing amount of BO. As mentioned earlier, this peak represents the anomeric proton of the unsubstituted AGU and/or the one of the O-6 monosubstituting AGU. Further increase in the amount of BO used results in the disappearance of this peak eventually at high mol equiv of BO. This suggests that the amount of HBSNPs having only monosubstitution at O-6 position is very small. However, for the AGUs with more than one substituent, it is still not clear if O-6 substitution is taking place. For example, the anomeric proton peak for an HBSNP having an O-2 and O-6 disubstituted AGU would be expected to have a very similar chemical shift as an HBSNP with just an O-2 monosubstituted AGU.

2.4 The MS_{HB} and the Reaction Efficiency of the Hydroxybutylation Reactions

The molar substitution for the hydroxybutylation reaction (MS_{HB}) was determined from the ratio of one third of the integration of the methyl peak from the HB group and the integration of the anomeric peak in the ^{1}H-NMR spectra of the modified HBSNPs. The MS_{HB} as well as other key parameters for nine different hydroxybutylation reactions are given in **Table 2.1**.

Table 2.1. Molar substitution (MS_{HB}), reaction efficiency, % yield and cloud point temperature (T_c) of HBSNPs.

Entry	BO:AGU[a]	MS_{HB}[b]	Efficiency	% Yield	T_c (°C)[c]
1	0.5	0.22 ± 0.00	44% ± 0%	92% ± 8%	-
2	1	0.48 ± 0.01	48% ± 1%	88% ± 6%	-
3	1.5	0.73 ± 0.03	48% ± 2%	85% ± 1%	-
4	2	0.93 ± 0.02	47% ± 1%	75% ± 8%	> 70
5	2.5	1.29 ± 0.05	52% ± 2%	72% ± 2%	52 ± 2
6	3	1.45 ± 0.05	48% ± 2%	71% ± 3%	46 ± 1
7	4	1.64 ± 0.01	41% ± 0%	63% ± 5%	39 ± 0.5
8	5	1.80 ± 0.04	36% ± 1%	49% ± 7%	35 ± 0.5
9	6	1.85 ± 0.05	31% ± 1%	49% ± 3%	33 ± 1

[a] BO:AGU is the mole ratio between BO and AGUs
[b] MS_{HB} is the molar substitution of HB groups obtained by ^{1}H NMR
[c] T_c is the cloud point temperature obtained from transmittance curves of 10 g/L aqueous HBSNP dispersions and reported as the temperature at the inflection point.

The relationship between the MS_{HB} and the amount of BO added is shown in **Fig. 2.8**. The entire data set was best fitted to a quadratic function. For the reactions with 0.5 to 3 mol equiv of BO, the MS_{HB} increases linearly with the amount of BO.

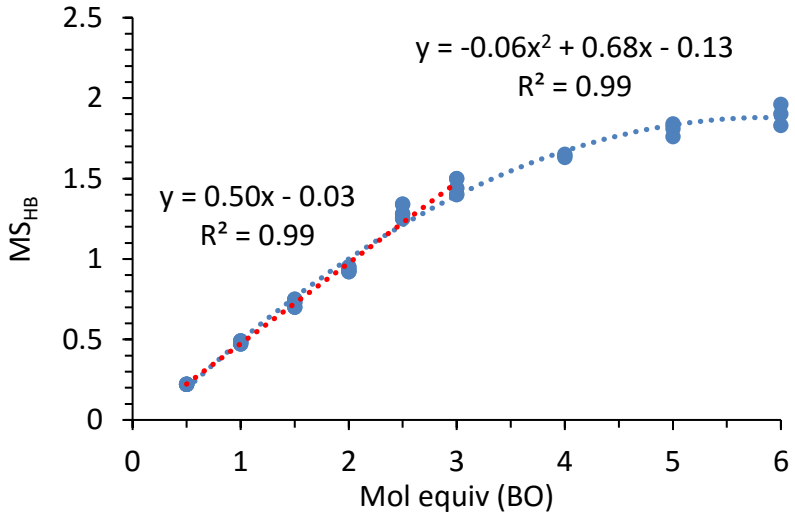

Figure 2.8. The relationship between the MS_{HB} of the HBSNPs and the amount of BO used in each reaction.

The reaction efficiency was calculated by dividing the actual MS_{HB} by the theoretical maximum MS_{HB}. For example, if 4 mol equiv of BO were used in a reaction, the maximum and theoretical MS_{HB} would be 4. For the reactions where the MS_{HB} increased linearly with the amount of BO, the reaction efficiency ranged from 44% to 52% (**Table 2.1**, entries **1**-**6**). When the mol equiv of BO increased from 3 to 6, the reaction efficiency decreased from 50% to 30% (**Table 2.1**, entries **7**-**9**).

In general, the hydroxybutylation reactions were found to proceed with poor reaction efficiency. This could be due to a number of reasons. First, BO can react with water or

hydroxide to form the corresponding glycol. Second, the reaction is initially heterogeneous, as BO is not miscible with water. Third, some of the reaction sites on the SNPs might not be accessible during the reaction.

The decrease in efficiency as the BO:AGU ratio increases above 3 may be attributed to two factors. First, as the more favorable substitution sites are occupied, subsequent reactions may take place at a much slower rate, which translates into poorer efficiency. This rationalization is based on the above discussion that there are differences in the reactivity of the sites of substitution. It was noticed that the reaction mixtures became cloudy when the BO:AGU ratio was greater 3. This was due to the T_c of the resulting HBSNPs being less than 40^{o}C (see **Table 2.1**, entries **7**-**9**). Therefore, another reason for the decrease in reaction efficiency may be that, as the BO:AGU ratio increases above 3, the modified SNPs precipitate and aggregate during the reaction, which causes the population of the active substitution sites to decrease.

2.5 Determination of % Yield of the HB Reactions

The % yields reported in **Table 2.1** are the yields of an average of 3 sets of reactions, that they are calculated in a way slightly different than the conventional method. The conventional method for % yield calculation can be expressed by the following **Equation 2.4**:

$$\% \text{ Yield} = \frac{\text{mass recovered}}{\text{theoretical mass}} \times 100\% \quad \text{(Eqn. 2.4)}$$

In the case of HBSNPs, this method often overestimates the true % yield due to the presence of moisture in these purified and freeze-dried HBSNPs. For a more accurate % yield calculation, the moisture content of the HBSNP sample needs to be determined and accounted for. One way to determine the correct % yield is with ^{1}H-NMR. Assuming that the sample is pure (after dialysis and freeze drying) without impurities other than moisture, the moisture content will be the part of a HBSNP sample that is not the actual HBSNPs. The actual amount of HBSNPs in an HBSNP sample can be determined using ^{1}H NMR and an internal standard (TMSP-d_4). As the amount of the internal standard added is known, the relative amount of AGUs and the HB groups can be calculated based on the integration of the anomeric peaks and the methyl peak, respectively. The unmodified and modified AGUs (not accounting for the substituent yet) in the NMR sample was calculated using **Eqn. 2.1**. The grams of HB groups in the NMR sample was calculated using **Equation 2.5**:

$$\text{Grams of HB groups} = \frac{I_{\text{CH3 of HB}}}{I_{\text{CH3's of TMSP-}d4}/3} \times \text{mols of TMSP-}d_4 \times 72 \text{ g/mol} \quad \textbf{(Eqn. 2.5)},$$

where $I_{\text{CH3 of HB}}$ is the integration under the peak corresponding to the methyl group of the hydroxybutyl group. The molecular weight of an HB group is 72 g/mol. The sum of the amounts of the modified and unmodified AGUs and the amount of HB groups approximates the total amount of HBSNPs. The assumptions here were: first, the end groups of the HBSNP chains are negligible; second, the modified and unmodified AGUs are the same. In fact, the modified and unmodified AGUs are slightly different. If a monosubstituting AGU is compared to an unmodified one, their molecular weight differs by 1 g/mol. But due to the fact that the

exact proportion of every type of substituting AGU species is not known, the current method remains the closest approximation to the true amount of HBSNPs in the NMR sample. As the amount of the HBSNPs that were used to prepare the NMR sample was known, the ratio of the amount calculated from NMR analysis and the amount used to make the NMR sample is therefore the actual HBSNP content in the HBSNP sample.

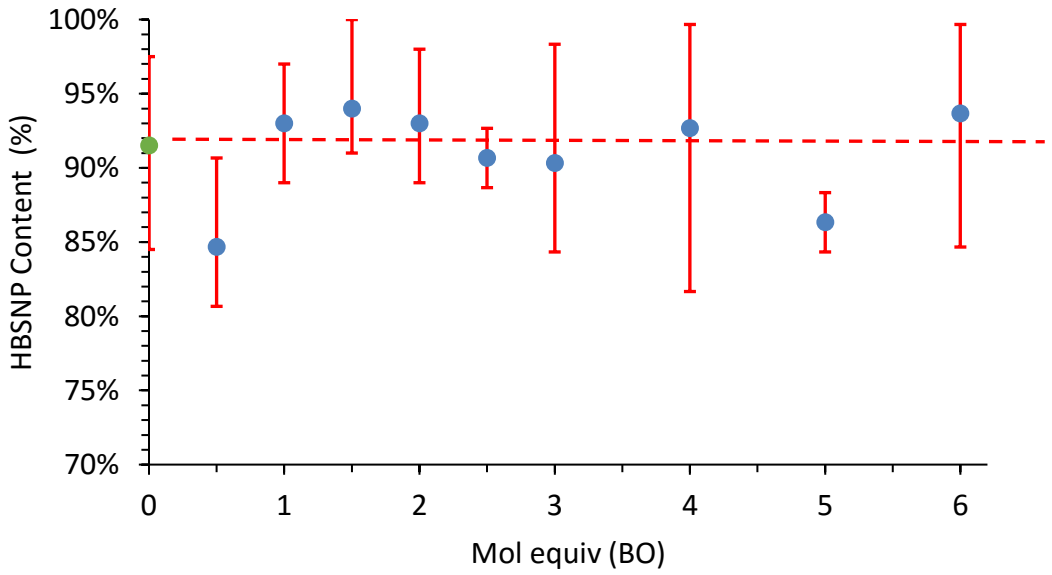

Figure 2.9. The average HBSNP content in HBSNP samples that are modified with 0 to 6 mol equiv of BO.

Fig 2.9 shows a plot of the average HBSNP content in a HBSNP sample over the amount of BO used in the reactions. The control experiment (the green dot in **Fig. 2.9**) was done in the exact same way as the HBSNP reactions without the addition of BO. The control experiment shows on average about 90% of the sample are actual SNPs and therefore, the rest 10% should most likely be moisture content. Looking at the HBSNP samples, the true HBSNP content fluctuates around 90% as indicated by the dotted red line going through most

of the error bars. Some of the error bars are relatively large, indicating large differences in the dryness of the HBSNP samples. No correlation between the HBSNP content and the amount of BO used can be found.

With the obtained percentage of the actual HBSNP content in each HBSNP sample, a better estimate of the true % yield for each reaction was calculated using **Equation 2.6**:

$$\% \text{ Yield} = \frac{\text{mass recovered} \times \text{HBSNP content}}{(\text{g of CSNP} \times 0.64) + \text{g BO}} \times 100\% \quad \textbf{(Eqn. 2.6)}.$$

The mass recovered is the amount of the HBSNP sample recovered after dialysis and lyophilisation. The theoretical mass is the total mass of the reactants which include the mass of SNP and BO. This takes into account that there is 0.64 g of SNP in every gram of CSNP.

Another way to calculate the % yield of the HBSNP reactions is based on the reaction efficiency. Reaction efficiency basically depicts the proportion of HB groups that are successfully incorporated onto the SNPs. Taking the efficiency into consideration, the % $\text{yield}_{\text{Eff}}$ can be obtained using **Equation 2.7**:

$$\%\ \text{Yield}_{\text{Eff}} = \frac{(\text{g of CSNP} \times 0.64) + (\text{Eff.}_{\text{BO}} \times \text{g BO})}{(\text{g of CSNP} \times 0.64) + \text{g BO}} \times 100\% \quad \textbf{(Eqn. 2.7)}.$$

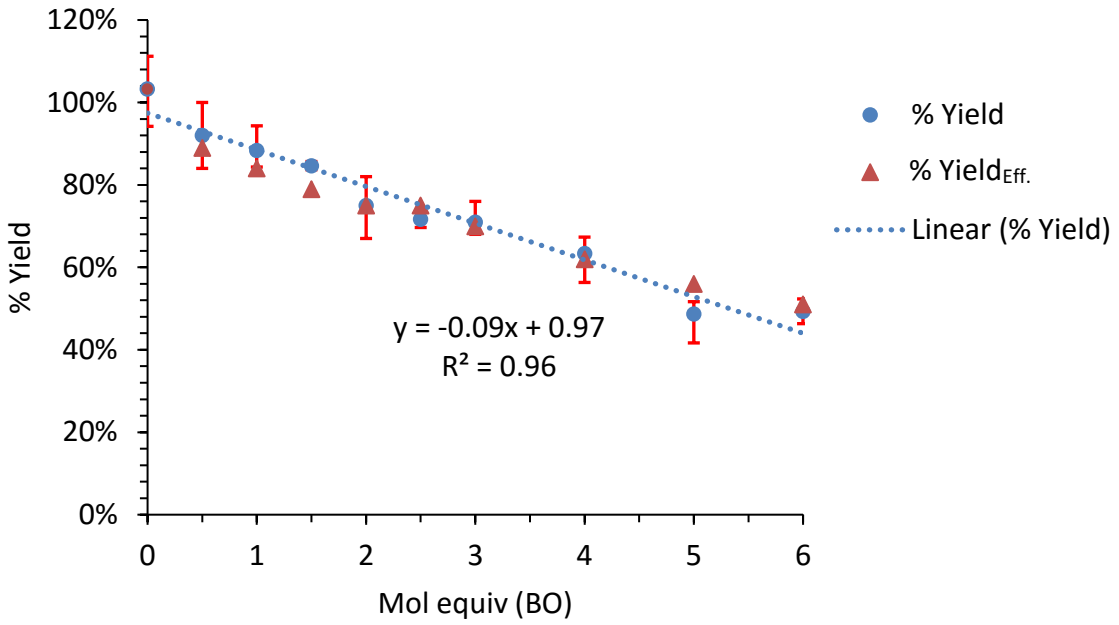

Figure 2.10. Correlation between the amount of BO used in the reactions and % yields. Two types of % yields are shown; one is based on NMR analysis (% yield), and the other one is based on reaction efficiency (% $yield_{Eff.}$).

Fig 2.10 shows the % yields calculated based on the HBSNP content corrected mass recovery (%yield) as well as the reaction efficiency (% $yield_{Eff.}$). The difference between the % yield and % $yield_{Eff}$ is very small as the two sets of data overlap in most cases. Both yields decrease as the amount of BO used increases. This is expected, as more BO is lost due to the inability to be incorporated into the SNPs. The fact that both types of yields are very similar suggests that there is a minimal amount of product loss during sample preparation other than the loss due to unsuccessful incorporation of the HB groups (i.e. sample transfer or purification). This is further supported by a near 100% recovery obtained for the control experiments that are performed in the exact same way without the addition of BO. This is important as it provides the ultimate proof for the stability of SNPs under these specific

reaction conditions (pH 13, 40°C, 24 h). If any differences between the % yield and % $yield_{Eff.}$ were to be discovered, it would be the indication of sample loss. One possible way for sample loss is through SNP degradation. The degraded SNPs would get removed during dialysis, leading to an overall decrease in % yields.

2.6 Thermoresponsive Behavior of HBSNPs

The thermoresponsivity of the HBSNPs was determined by dispersing the HBSNPs in water for 16 h and then measuring the light transmittance of the resulting dispersions as a function of temperature. The light transmittance curves for several HBSNPs with MS_{HB}s ranging from 0.73-1.9 are shown in **Fig. 2.11**. The cloud point (T_c, also referred to LCST in this thesis) was defined as the temperature corresponding to the point of inflection on a transmittance curve. The inflection point is where the curve has the maximum derivative or the maximum rate of change in transmittance over temperature. The T_cs for nine HBSNPs are given in **Table 2.1**. There is an inverse correlation between the MS_{HB} and T_c. This is expected, as the T_c depends on the degree of hydrophobic modification. As shown in **Fig. 2.11**, $HB_{0.95}$SNP (this is a HBSNP with a MS_{HB} of 0.95) does not undergo a total collapse up to 70°C, but $HB_{1.23}$SNP exhibits a drastic decrease in transmittance at about 55°C. It appears that a MS_{HB} greater than 1 is required for the HBSNPs to exhibit thermosensitive behavior. This is in close agreement with the results in Karski's M.Sc. thesis.[79] A linear relationship was found between

the MS_{HB} and T_c (**Fig. 2.12**). This linear correlation enables one to predict the T_c of thermoresponsive HBSNPs with MS_{HB}s greater than 1.

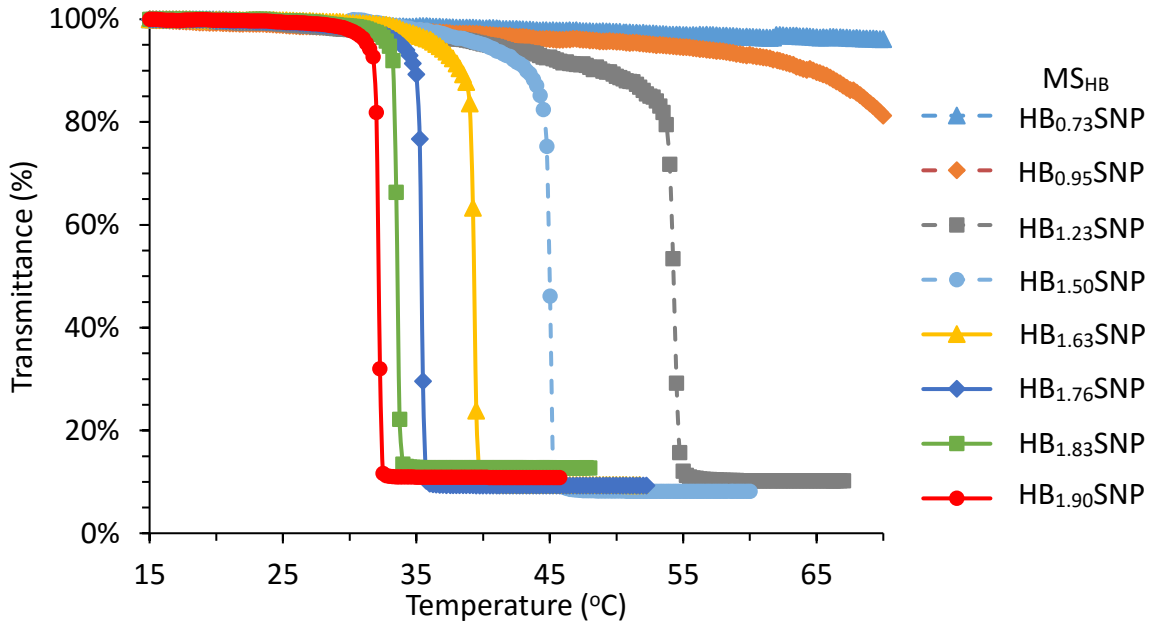

Figure 2.11. Light transmittance curves for aqueous dispersions of HBSNPs (10 g/L) with MS_{HB}s ranging from 0.7-1.9.

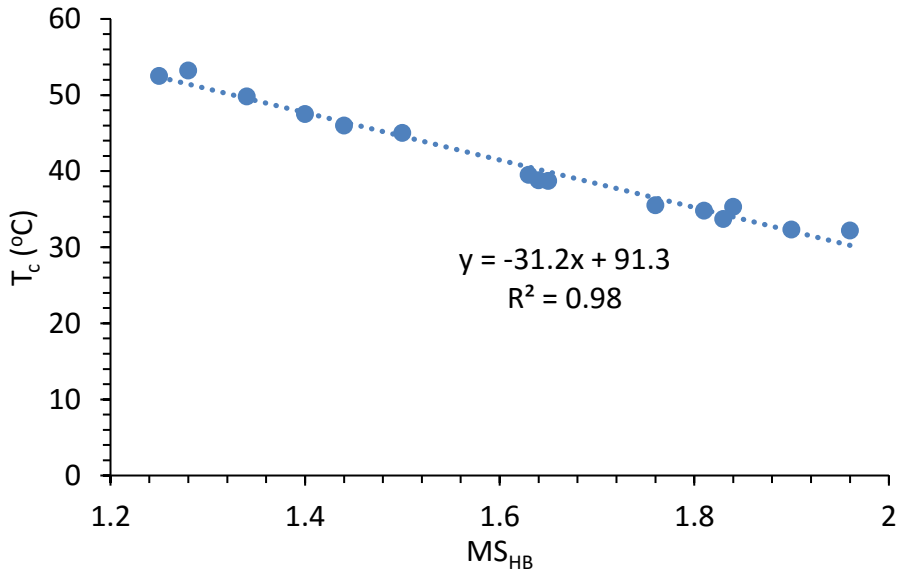

Figure 2.12. Correlation between MS_{HB} and T_c for HBSNPs.

2.6.1 The Shape of Transmittance Curves

Looking more closely at the transmittance curves in **Fig. 2.11**, it is very noticeable that for some curves, especially for the HBSNPs with MS_{HB}s from 1.0 to 1.5, the transmittance of the underlying HBSNP dispersions starts to decrease at a temperature that is much lower than the temperature at which the drastic drop in transmittance occurs. **Table 2.2** shows the temperatures at which the dispersions of HBSNPs with different MS_{HB}s at 95%, 90%, 80%, and 50% transmittance, denoted by $T_{95\%}$, $T_{90\%}$, $T_{80\%}$, and $T_{50\%}$, respectively. It is clear that the difference in temperature between the 95% and 50% transmittance ($T_{50\%}$ - $T_{95\%}$) is much larger when the MS_{HB} is below 1.5 and becomes very small at high MS_{HB}s. For example, the temperature gap is 13.9^{o}C for $HB_{1.23}$SNP, whereas it is much smaller for $HB_{1.90}$SNP at only 0.8^{o}C (**Table 2.2**, entry **3** and **8**). This temperature gap essentially describes the shape of the transmittance curve and a larger temperature gap means a shallower curve or a slower thermotransition and vice versa.

Table 2.2. Temperatures at which the dispersions of HBSNPs with different MS_{HB}s at 95%, 90%, 80%, and 50% transmittance. ($T_{50\%}$ - $T_{95\%}$) is the change in temperature when the transmittance of an HBSNP dispersion decrease from 95% to 50%.

Entry	MS_{HB}	$T_{95\%}$ (°C)	$T_{90\%}$ (°C)	$T_{80\%}$ (°C)	$T_{50\%}$ (°C)	$T_{50\%}$ - $T_{95\%}$ (°C)
1	0.73	>70	>70	>70	>70	-
2	0.95	53	64.8	>70	>70	>17
3	1.23	40.3	49	53.5	54.2	13.9
4	1.50	39.8	43.3	44.6	45	5.2
5	1.63	36.5	38.3	39.1	39.3	2.8
6	1.76	33.8	34.8	35.1	35.3	1.5
7	1.83	32.6	33.3	33.4	33.6	1
8	1.90	31.3	31.8	32	32.1	0.8

To the best of our knowledge, this type of slow thermotransition has not been reported for thermoresponsive hydrophobically modified starch or starch nanoparticles in the literature, but in the case of thermoresponsive cellulose, examples are readily available.[85,86] In most cases, this slow thermotransition is speculated to be caused by the differences in substitution patterns for different samples. The substitution pattern here refers to the homogeneity of the substitution, which describes the uniformity of either the degree of substitution between different chains or the distribution of substituents on one chain.

If there are differences in the MS_{HB} between different HBSNP chains that together have an average MS_{HB}, the chains with an actual MS_{HB} higher than the average MS_{HB} would

intuitively have lower T_c. Hence, these chains precipitate first and cause the initial decrease in transmittance, before the total collapse occurs when the T_c of the majority of HBSNP chains with an MS_{HB} closer to the average MS_{HB} is reached. In contrast, if the MS_{HB} of all the HBSNP chains are very similar, only a total collapse would be observed at their T_c. An assumption needs to be considered here is that the decrease in transmittance correlates with the amount of HBSNPs that are precipitated. This theory suggests that a homogenous sample would have a faster thermotransition when compared to a heterogeneous sample. Fitzpatrick et al. reported that a lower T_c and a steeper transmittance curve can be found with a homogeneous methyl cellulose sample and a shallower transmittance curve is associated to the heterogeneous sample.[86] The substitution patterns were determined by enzymatic degradation studies.

If the distribution of HB groups is non-uniform along a HBSNP chain, meaning some segments of the chain are more substituted than the others, this heterogeneously substituted chain may undergo a different thermotransition mechanism, which is reflected by a different transmittance curve than a homogeneously substituted chain. More specifically, when the T_c of HBSNP chains that are homogeneously and highly substituted by HB groups is reached, these chains would quickly find each other due to hydrophobic interaction and collapse as aggregates, together to induce the sudden decrease in transmittance. On the contrary, if the HBSNP chains are heterogeneously substituted, the more substituted segment would hydrophobically associate with other more substituted segments when T_c is reached. These

aggregates consisting of the more substituted segments would not collapse right away due to the unsubstituted or less substituted segments that are still soluble. At this stage, the aggregates might resemble a micelle-like system which consists of a hydrophobic core and a hydrophilic outer layer. This would be reflected by a small decrease in transmittance at the beginning of a transmittance curve. A total collapse would occur at a higher temperature and gives the steep transmittance curve. Viriden et al. examined the transmittance curve and rheological properties of both heterogeneously and homogeneously substituted thermoresponsive hydroxypropyl methyl cellulose (HPMC) samples and found that the thermotransition was faster in the latter case.[85] The more substituted segments in the heterogeneous HPMC sample interact hydrophobically but stay in solution with the aid of the less substituted segment to form a gel-like structure.[85] This enables a steep transmittance curve and a slower thermotransition, similar to the HBSNP samples with MS_{HB} below 1.5.

On the basis of the results from hydroxybutylation reactions, it is reasonable to suggest that there are differences in the substitution patterns across the HBSNP samples that were prepared using a different amount of BO. Assuming the substitution onto any SNP chains is completely random at first, there should be a Poisson-distribution of the differently substituted chains for the reactions with BO as the limiting reafgent. The reaction would stop at the moment when all the BO is consumed (either successfully incorporated or reacted to form side products). Thus, this HBSNP sample would consist of differently substituted HBSNP chains. As the amount of BO added increases and the active substitution sites in the SNPs

become the limiting factor, most of unsubstituted chains or segments in a chain would be substituted eventually which results in a more homogenously substituted HBSNP sample. Thus, a HBSNP sample with low MS_{HB} would be more heterogeneous than the ones with higher MS_{HB}. However, it is important to point out that the discussion above is only a reasonable speculation, further studies need to be conducted to gain more insight into the substitution pattern of the HBSNP samples.

2.6.2 Reversibility of Thermoresponsivity

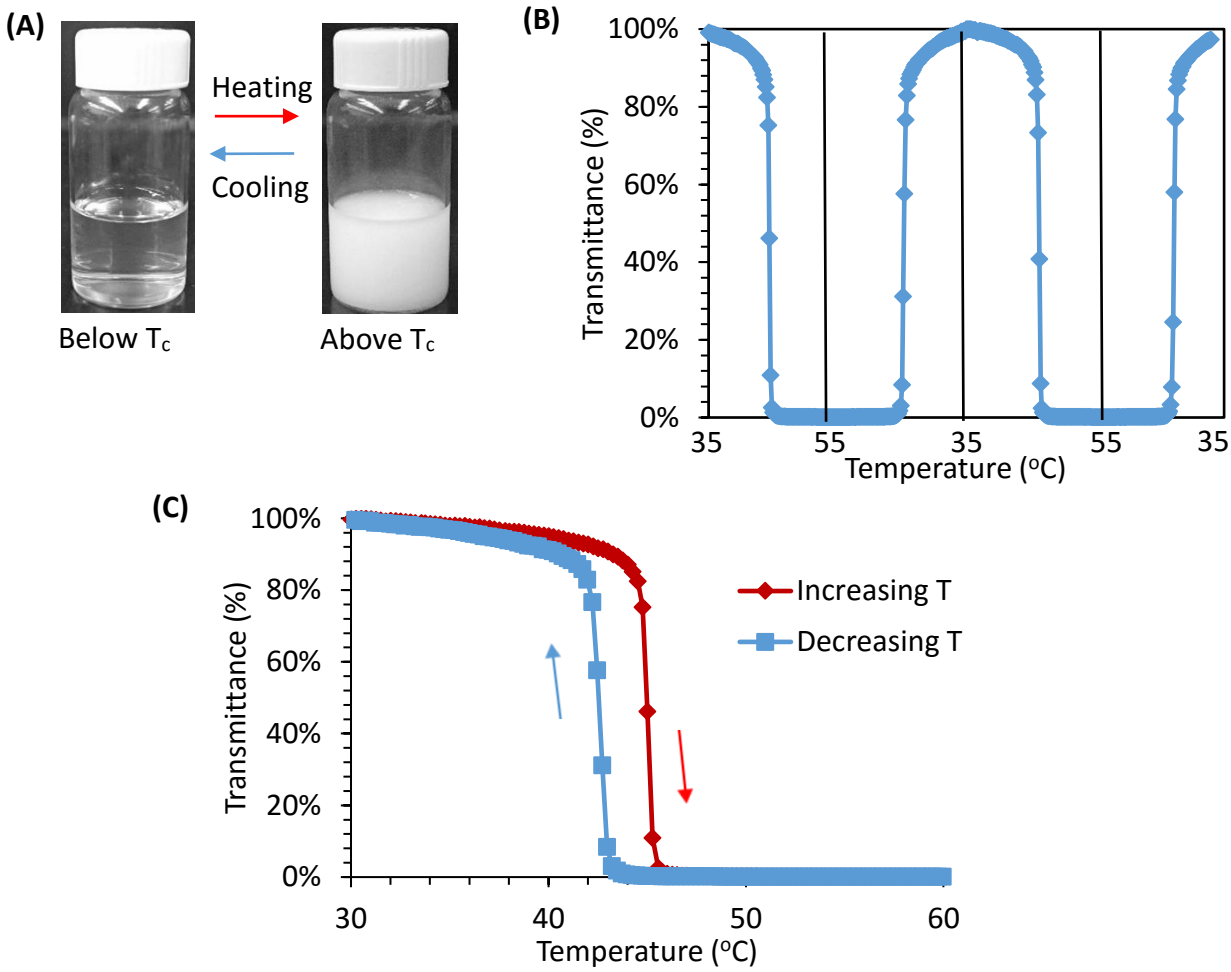

Figure 2.13. (**A**) Pictures of an $HB_{1.8}$SNP aqueous dispersion (10 g/L, T_c = 35°C) taken at 25 and 55°C; (**B**) the reversible changes in the turbidity of an aqueous dispersion of $HB_{1.5}$SNPs (10 g/L, T_c = 45°C) with temperature; (**C**) the hysteresis of a $HB_{1.5}$SNP aqueous dispersion (10 g/L) between heating and cooling cycles.

The thermotransition of the HBSNPs is easily observable by the naked eye. For example, **Fig. 2.13A** shows the sudden and drastic change in the turbidity of an aqueous dispersion of $HB_{1.8}$SNP (T_c = 35°C) from transparent (below the T_c) to cloudy (above the T_c).

The transmittance curves of a 10 g/L $HB_{1.5}$SNP dispersion (T_c = 45°C) for heating and cooling cycles show that the thermotransition process is highly reversible (**Fig. 2.13B**). An approximately 2.5°C temperature gap between the heating and cooling transmittance curves was observed, showing a pronounced hysteresis in the heating and cooling cycles (**Fig. 2.13C**). Similar to the hysteresis of PNIPAAm,[26] the hysteresis of a $HB_{1.5}$SNP dispersion can be attributed to the presence of both intra- and inter-chain hydrogen bonding within the aggregates above T_c. These hydrogen bonds tend to persist in the cooling process and limit the accessibility of the water molecules to the inside of the aggregates. Hence, a relatively noticeable hysteresis can be observed.

2.6.3 The Effect of HBSNP Concentration on the T_c

The effect of HBSNP concentration on the T_c was examined for aqueous dispersions of $HB_{1.5}$SNPs ranging from 0.1-50 g/L (**Fig. 2.14A** and **B**). There is very little change in T_c for HBSNP concentrations of 5-50 g/L. A decrease in the sample concentration below 5 g/L reduces the sharpness of transmittance curves and results in an increase in the T_c. A 3.2°C drop in the critical temperatures was observed when the dispersion was diluted 100-fold from a concentration of 50 to 0.5 g/L (**Fig. 2.14B**). This decrease in T_c could be a result of the inability to form large aggregates when the original T_c was reached, hence, more time and energy input (higher T) were required.[87]

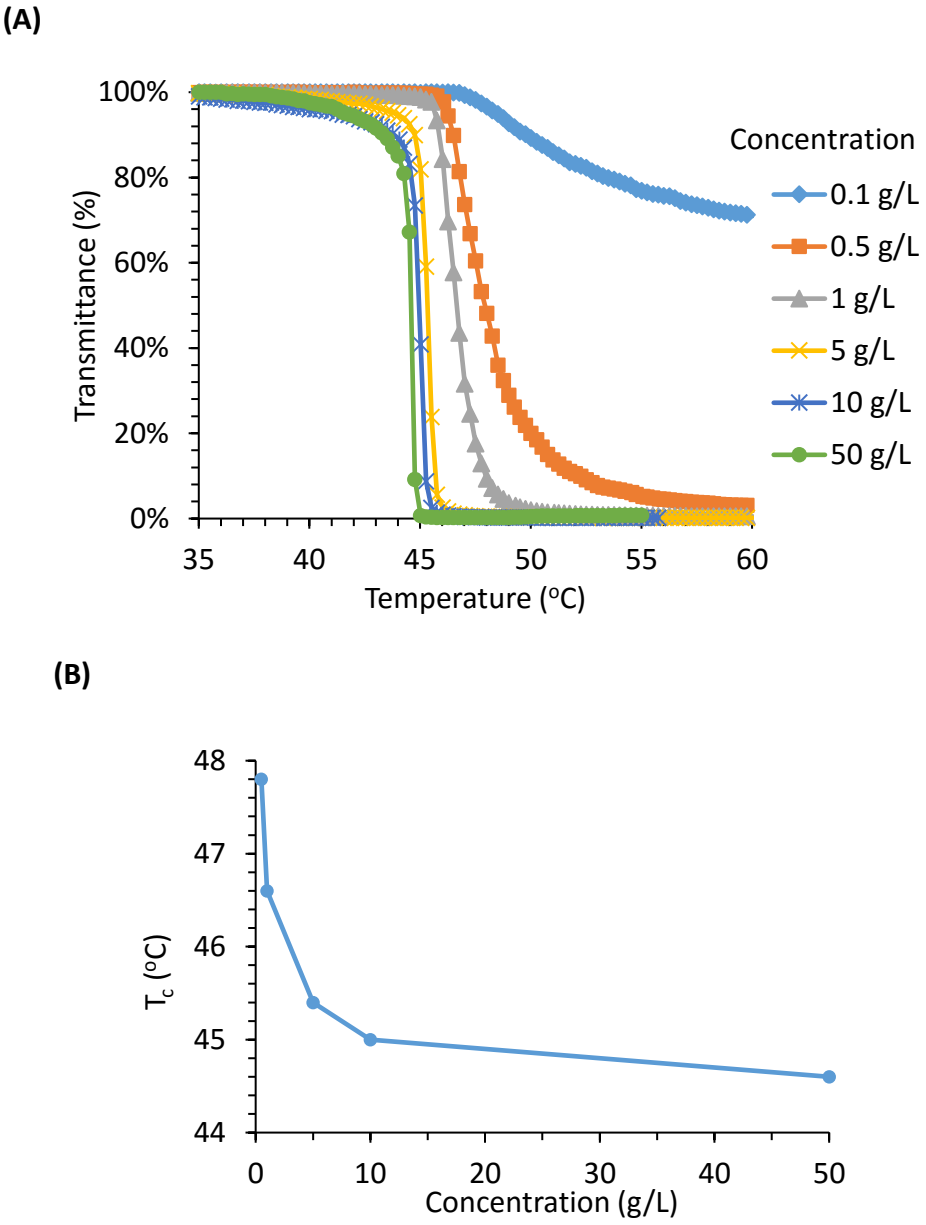

Figure 2.14. The effect of $HB_{1.5}$SNP concentration on T_c. (**A**) Transmittance curves for a series of $HB_{1.5}$SNP dispersions with concentration ranging from 0.1 to 50 g/L; (**B**) a plot of T_c vs. $HB_{1.5}$SNP concentration.

2.6.4 The Effect of Salts on the T_cs of HBSNPs

The effect of salts on the T_c of a 10 g/L aqueous dispersion of $HB_{1.2}$SNP is shown in **Fig. 2.15**. Salts are generally classified into two types: kosmotropic and chaotropic salts. Kosmotropic salts contain anions that have a stronger interaction with water molecules. This anion-water interaction is much stronger than the SNP-water interaction. As a result, kosmotropic anions disrupt the hydrogen bonds that enable the SNPs to stay solvated. Therefore, an increase in the hydration strength or the concentration of kosmotropic salts in the solution will disrupt more SNP-water hydrogen bonds and cause the SNPs to precipitate out faster and at a lower temperature. Examples of kosmotropic anions are listed in the order of decreasing hydration strength: $SO_4^{2-} > H_2PO_4^- > F^- > Cl^- > Br^-$ (following the order of the Hofmeister series).

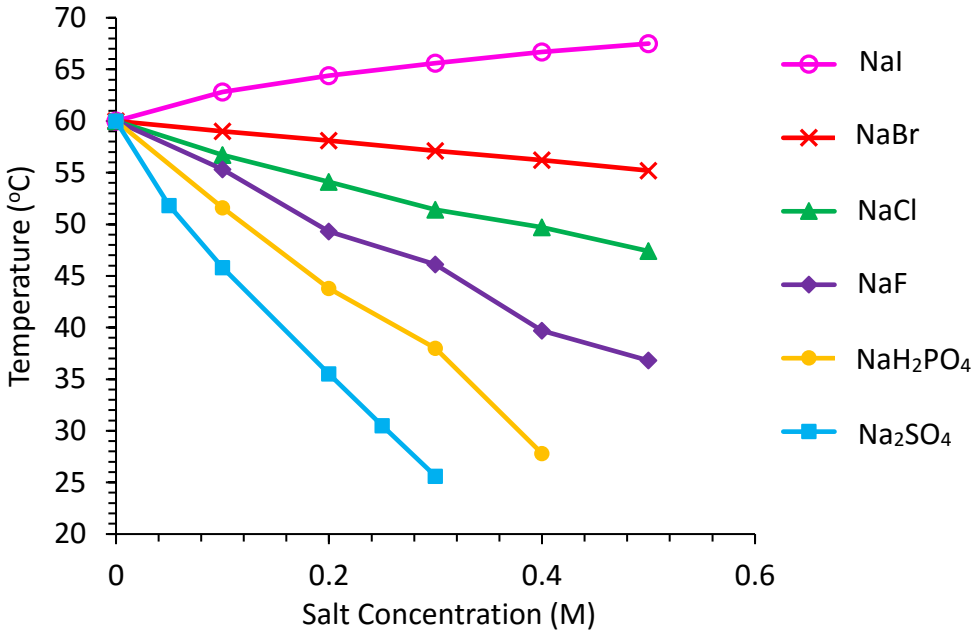

Figure 2.15. Effect of salts and salt concentration on the T_c of 10 g/L aqueous dispersions of $HB_{1.2}$SNPs.

As expected, the T_c of the $HB_{1.2}$SNP dispersion was affected by the addition of kosmotropic salts and by the salt concentration (**Fig. 2.15**). The hydration strength of the salts determines the effectiveness of T_c lowering. For example, when the $HB_{1.2}$SNP dispersion contains Na_2SO_4 with a final concentration of 0.3 M, the T_c decreases substantially to 26°C from the original 60°C. In contrast, for the dispersion containing 0.3 M NaBr, the T_c decreases only slightly to 57°C.

Chaotropic salts, such as NaI, do not interact with water as strongly as kosmotropic salts do. Du et al. suggested that direct interactions between the cation, Na^+, and the amide oxygen atoms on PNIPAAm chains affect the T_c of a PNIPAAm dispersion.[88] Stronger cation-PNIPAAm interactions result in a larger increase in T_c. The strength of cation-PNIPAAm

interactions is in turn affected by the cation-anion interactions in the dispersion. Chaotropic salts such as NaI have weaker cation-anion interactions when compared to kosmotropic salts. In this case, the cation-PNIPAAm interactions are stronger, which causes an increase in T_c. Since the HBSNPs have an ether oxygen atom in every modified AGU, similar cation-HBSNP interactions may occur and an increase in T_c upon the addition of chaotropic salts may be observed. Experimental data comfirm that the T_c increases when the NaI concentration increase from 0.1 to 0.5 M (**Fig. 2.15**). In summary, kosmotropic salts decrease the T_c of an HBSNP while chaotropic salts increase the T_c.

2.7 Dynamic Light Scattering Studies on HBSNPs

Dynamic light scattering (DLS) was employed to measure the particle size of the SNPs in an aqueous dispersion before and after the modification. Briefly, the HBSNPs were dispersed in deionized water and stirred for 16 h at 4^{o}C. The concentration of all the DLS samples was 3 g/L. Each DLS sample was filtered through a 0.2 µm polytetrafluoroethylene (PTFE) filter prior to the measurements. The duration of each measurements was 100 seconds and a scattering angle of 173^{o} was used. Hydrodynamic diameters (D_h, *Z*-average size) and polydispersity index (PDI) were obtained from DLS measurements. The D_hs and PDIs of a series of aqueous dispersions of HBSNPs at 15^{o}C, which is below the T_c of all of the HBSNPs that were examined, are given in **Table 2.3**.

Table 2.3. Summary of D_hs and PDIs for aqueous dispersions of HBSNPs (3 g/L) at 15 °C.

Entry	Sample	D_h (nm)[a]	PDI[b]
1	$HB_{0.3}$SNP	32.6 ± 0.2	0.386 ± 0.002
2	$HB_{0.6}$SNP	35.8 ± 0.1	0.372 ± 0.003
3	$HB_{0.9}$SNP	33.4 ± 0.2	0.273 ± 0.003
4	$HB_{1.3}$SNP	31.1 ± 0.1	0.215 ± 0.002
5	$HB_{1.4}$SNP	30.6 ± 0.1	0.200 ± 0.000
6	$HB_{1.6}$SNP	31.2 ± 0.1	0.198 ± 0.004
7	$HB_{1.8}$SNP	36.8 ± 2.0	0.278 ± 0.020
8	$HB_{1.9}$SNP	32.5 ± 0.4	0.224 ± 0.006

[a] D_h is the *Z*-average size from DLS measurement
[b] PDI is the polydispersity index given by DLS.

The average D_h of unmodified commercial grade SNPs (CSNPs) was determined to be 58.3 ± 2 nm (*Z*-average size, PDI: 0.53 ± 0.03) in water. This is larger than the diameter of the dry SNPs, which was estimated to be 40 nm by scanning electron microscopy (information according to the supplier). It is not surprising that the diameter of the dry particles is different from the D_h given by DLS. In addition, the D_h obtained here is also slightly larger than what was found by Chakraborty et al., who reported an average D_h of 50 nm for an aqueous dispersion of SNPs.[78] This discrepancy in size may arise from the differences in the DLS protocols. For example, the scattering angle and the concentration of SNP dispersions in the two studies are different, which should certainly affect the measurements to some degree.

The D_h of HBSNPs generally is slightly larger than 30 nm, which is about half of the size of the unmodified SNPs. This observation suggests that D_h of SNPs in water decreases after hydrophobic modification. It is important to note that the D_h of a particle depends on the interactions between the particle and its surrounding solvent. Due to the particle-solvent interactions, DLS probes not only the size of the particle, but also the layer of solvent that associate with the particle as it moves under the influence of Brownian motion. A change in the particle-solvent interactions would result in a change in the solvent layer, and therefore the D_h. In the case of HBSNP, as the interaction with water has certainly changed after the modification, the change in D_h that was observed is reasonable. However, no correlation can be found between the D_hs of the HBSNPs and their MS_{HB}s.

At 65°C, which is above the T_C of all of the HBSNPs that were examined, the D_hs of thermoresponsive HBSNPs (with MS_{HB} greater than 1) increased substantially as shown in **Fig. 2.16**. This was expected, as the thermoresponsive HBSNPs remain as isolated particles in a dispersion below the T_c but form aggregates due to a change in the hydrophobicity when the T_c is reached. For $HB_{1.3}$SNP and $HB_{1.4}$SNP, the D_h above their T_c is approximately 400 nm. For HBSNPs with MS_{HB} greater than 1.4, the D_h above T_c decreases to around 200 nm. It is still not entirely clear as to why the D_h of the aggregates decreases suddenly when MS_{HB} is greater than 1.4, and remains constant when MS_{HB} is 1.6-1.9. However, the result here can somewhat correlate to the discussion about substitution pattern and transmittance mechanisms in **Section 2.6.1**. Different HBSNP samples may undergo thermotransition differently due to the

differences in substitution patterns (i.e. heterogeneously substituted segments in a chain). The samples with MS_{HB} below 1.5 may have heterogeneously substituted segments and exhibit the gel-like structure before a total collapse. Because of this process, the HBSNP chains would have more time to engage and entangle with each other and form larger aggregates before the total collapse. Comparing to the HBSNP samples with more homogeneously substituted segments (referring to the HBSNPs with a MS_{HB} greater than 1.5), the formation of the gel-like structure would not occur. The HBSNP chains would be likely to form smaller aggregates upon sudden collapse, hence, a smaller D_h can be observed in DLS.

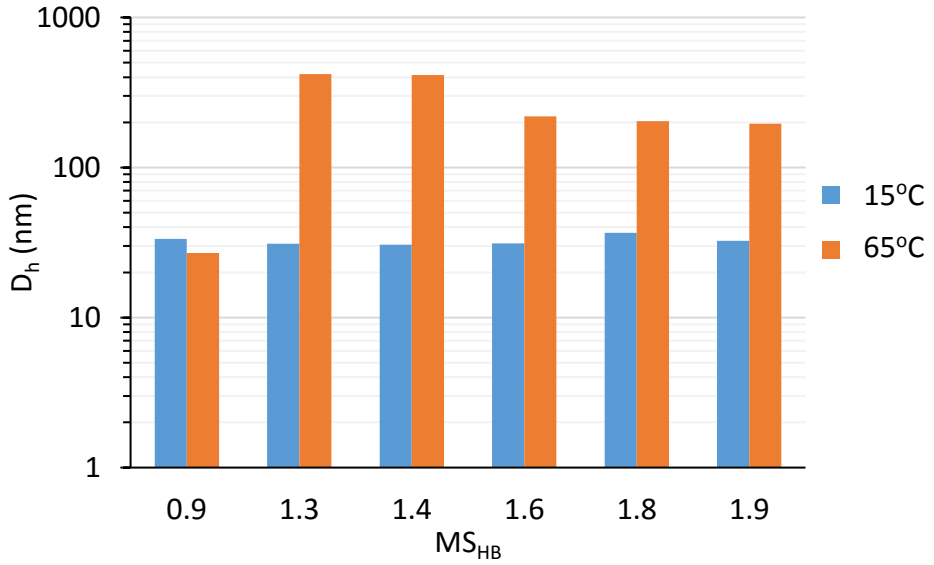

Figure 2.16. D_hs of HBSNPs at 15°C and 65°C. Measurements were performed with 3 g/L aqueous dispersions of the HBSNPs with different MS_{HB}s.

At 65°C, the PDI of thermoresponsive HBSNPs (with MS_{HB} greater than 1) changes substantially as shown in **Fig. 2.17**. The PDI describes the narrowness of the Poisson size distribution that represents the fitted DLS data. A particle with PDI value below 0.1 is

generally considered as monodisperse. PDI values of the HBSNPs decrease to close to 0 as the MS_{HB} increases (**Fig. 2.17**). This reflects that the Gaussian size distribution are very narrow and close to an infinitely thin delta function. The aggregates for these HBSNPs with large MS_{HB} above T_c are monodispersed.

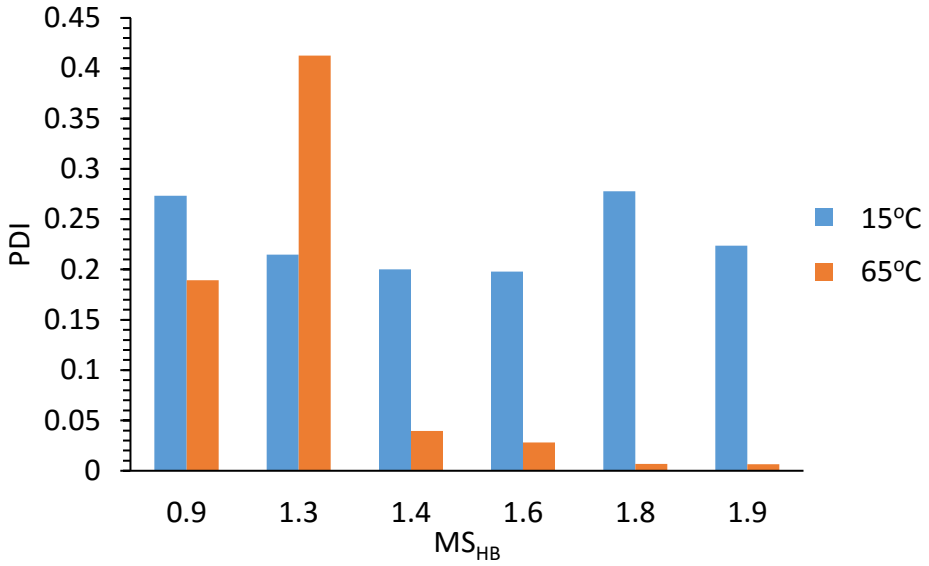

Figure 2.17. PDI of HBSNPs at 15°C and 65°C. Measurements were performed with 3 g/L aqueous dispersions of the HBSNPs with different MS_{HB}s.

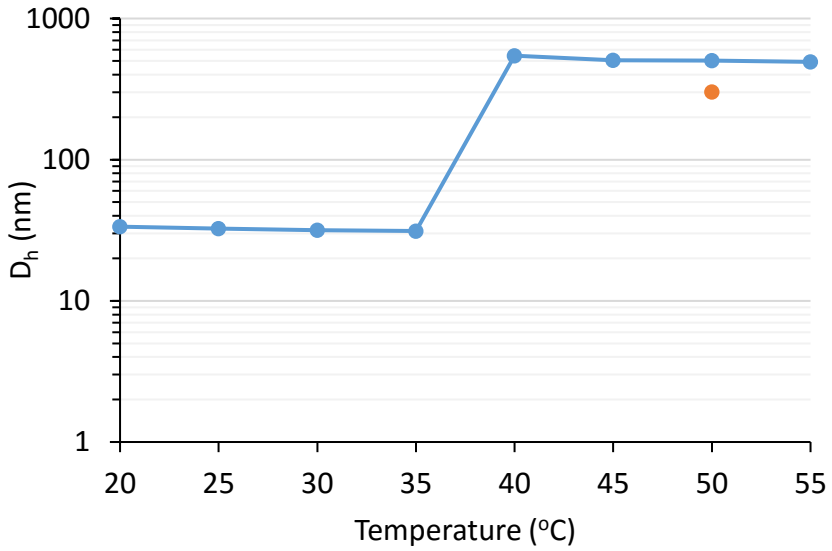

Figure 2.18. Temperature dependence of the D_h of an aqueous dispersion of $HB_{1.8}$SNPs. The temperature range was from 20 to 55°C, with a rate of heating at approximately 5°C/30 min, represented by the blue dots. The D_h of the aggregates at 50°C with a faster heating rate at 15°C/min is represented by the orange dot.

The rate at which the temperature is increased, affects the size of the aggregates above T_c. For an aqueous dispersion of $HB_{1.8}$SNPs, a D_h of 301.4 ± 1.5 nm (*Z*-average size, PDI: 0.115 ± 0.001) was obtained when the dispersion was heated from 25°C to 50°C in less than 2 minutes, whereas a D_h of 502.5 ± 0.5 nm (*Z*-average size, PDI: 0.076 ± 0.006) when the heating process for the same temperature change over 2 h (**Fig. 2.18**). Examples for the heating rate dependence of D_h are readily available in the literature. Viriden et al. observed that the growth of aggregates of thermoresponsive hydroxypropyl methylcellulose (HPMC) above T_c depended on the rate of heating.[85] They attributed this observation to the fact that there is less time for the polymers to diffuse and hydrophobically interact with each other when the rate of heating is fast. Thus, as the T_c is reached, the polymer chains would collapse

and form a greater number of smaller aggregates. On the contrary, when the rate of heating is slower, more time is given for the polymer chains to diffuse and interact with each other, until they collapse as the T_c is reached. Hence, a slower heating rate tends to promote a smaller amount of larger aggregates. A similar behavior was observed in the case of aggregate formation by HBSNPs above T_c. With a faster heating rate, the HBSNPs have less time to diffuse and interact with each other, resulting in a greater amount of smaller aggregates when the T_c is reached.

2.8 Substitution Patterns of HBSNPs

As mentioned earlier, knowledge of the substitution pattern is critical for further understanding of these thermoresponsive HBSNPs. It is of particular interest to answer the following questions regarding substitution pattern: first, whether the HB groups are randomly and evenly substituting onto the OHs of the AGUs of SNPs (there are three substituting positions on an AGU); second, whether the HB groups can oligomerize or polymerize (if substitution occurs on the OH of the HB group that is already attached to an AGU). One way to ascertain the substitution pattern is to hydrolyze the HBSNPs to individual glucose units, and to analyze these glucose derivatives qualitatively as well as quantitatively.

The HBSNPs were hydrolyzed by dispersing them in a 15% v/v aqueous solution of trifluoroacetic acid (TFA), and heating the resulting mixture to 90^{o}C for 16 h in a pressure

tube. ^{1}H NMR spectra for $HB_{0.6}$SNPs before and after hydrolysis are shown in **Fig. 2.19**. The sharp lines and the appearance of both of the α and β anomeric protons in the spectrum of the hydrolysate confirm that the HBSNPs were degraded.

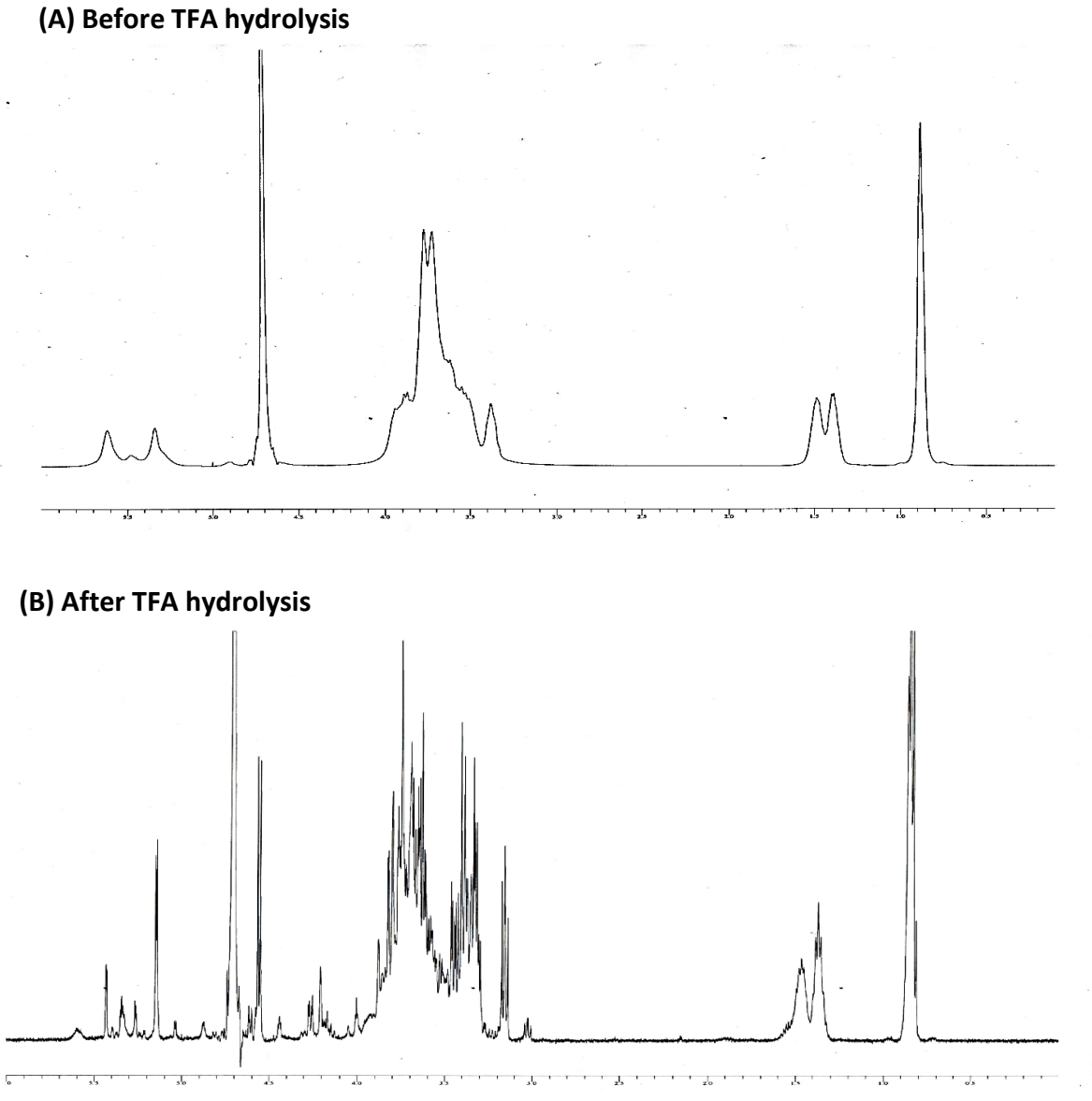

Figure 2.19. ^{1}H-NMR spectra of $HB_{0.6}$SNPs (**A**) before and (**B**) after hydrolysis in an aqueous solution of TFA.

High resolution positive electrospray ionization mass spectrometry (HR+ESIMS) was employed in order to qualitatively identify the different components in the hydrolysate of the HBSNPs. The hydrolysates of $HB_{0.6}$SNPs (not thermoresponsive) and $HB_{1.8}$SNPs (T_c = 37°C) were examined to give a direct comparison between components present in non-thermoresponsive and thermoresponsive SNPs (see **Fig. 2.20** and **Fig. 2.21** for mass spectra). Those components that were unequivocally identified from the hydrolysates of $HB_{0.6}$SNPs and $HB_{1.8}$SNPs are summarized in **Table 2.4** and **Table 2.5** respectively.

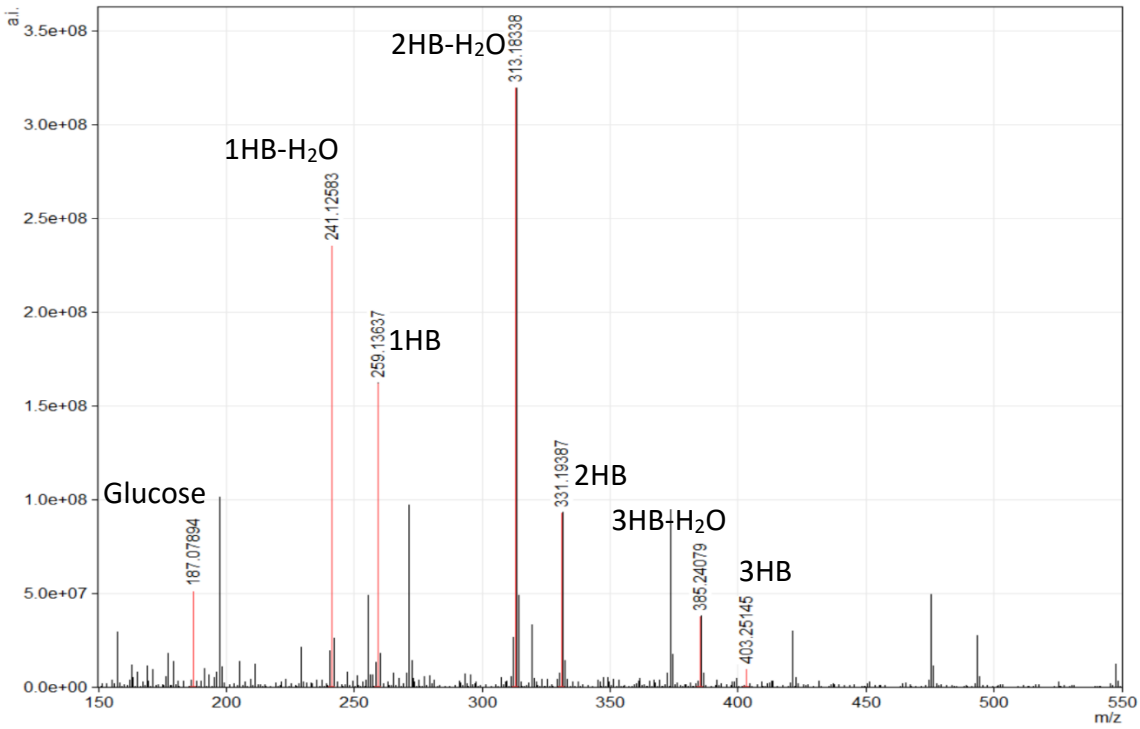

Figure 2.20. HR+ESIMS spectrum of the hydrolysates of $HB_{0.6}$SNPs.

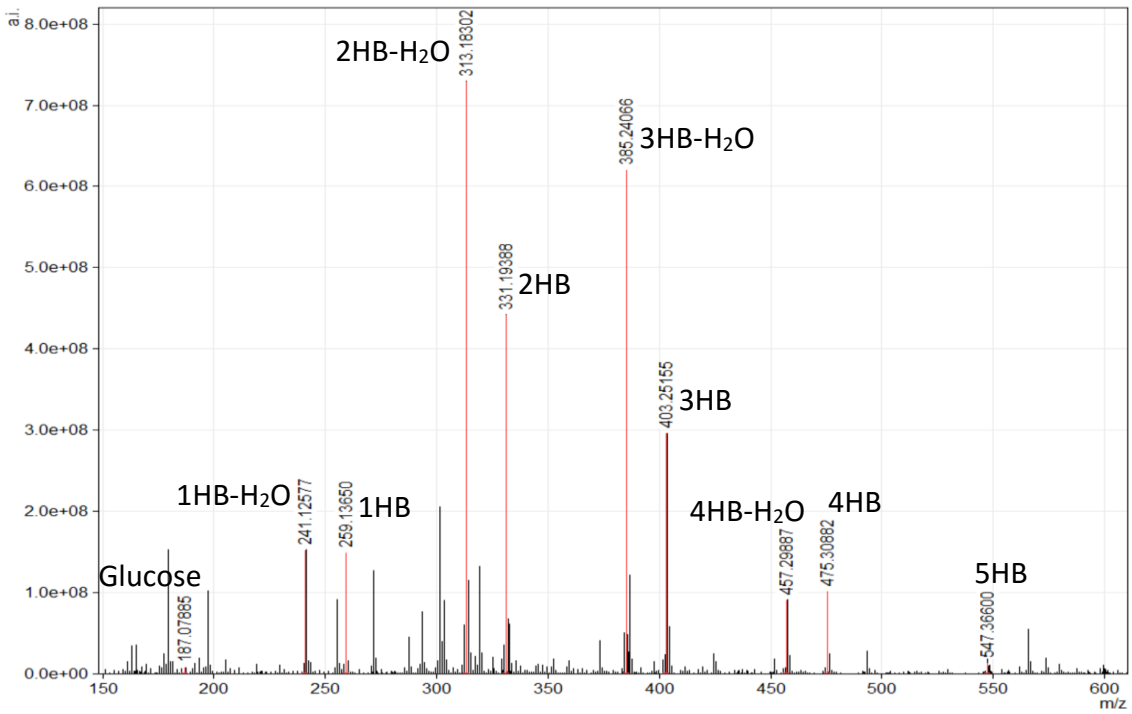

Figure 2.21. HR+ESIMS spectrum of the hydrolysates of $HB_{1.8}$SNPs.

Table 2.4. Components identified from the hydrolysates of $HB_{0.6}$SNPs using HR+ESIMS.

	Glucose Deriv.	Composition	Theo. Mass	Observed Mass	Delta (ppm)
1	Glucose	$C_6H_{12}O_6Li$	187.07884	187.07891	0.36
2	1HB	$C_{10}H_{20}O_7Li$	259.13636	259.13641	0.20
3	1HB-H_2O	$C_{10}H_{18}O_6Li$	241.12579	241.12576	-0.14
4	2HB	$C_{14}H_{28}O_8Li$	331.19387	331.19388	0.02
5	2HB-H_2O	$C_{14}H_{26}O_7Li$	313.18331	313.18329	-0.06
6	3HB	$C_{18}H_{36}O_9Li$	403.25139	403.25141	0.05
7	3HB-H_2O	$C_{18}H_{34}O_8Li$	385.24082	385.24081	-0.03

Table 2.5. Components identified from the hydrolysates of $HB_{1.8}$SNPs using HR+ESIMS.

	Glucose Deriv.	Composition	Theo. Mass	Observed Mass	Delta (ppm)
1	Glucose	$C_6H_{12}O_6Li$	187.07884	187.07890	0.30
2	1HB	$C_{10}H_{20}O_7Li$	259.13636	259.13638	0.08
3	1HB-H_2O	$C_{10}H_{18}O_6Li$	241.12579	241.12578	-0.06
4	2HB	$C_{14}H_{28}O_8Li$	331.19387	331.19383	-0.13
5	2HB-H_2O	$C_{14}H_{26}O_7Li$	313.18331	313.18330	-0.03
6	3HB	$C_{18}H_{36}O_9Li$	403.25139	403.25130	-0.22
7	3HB-H_2O	$C_{18}H_{34}O_8Li$	385.24082	385.24086	0.09
8	4HB	$C_{22}H_{44}O_{10}Li$	475.30890	475.30892	0.04
9	4HB-H_2O	$C_{22}H_{42}O_9Li$	457.29834	457.29837	0.07
10	5HB	$C_{26}H_{52}O_{11}Li$	547.36642	547.36622	-0.36

The species that can be found in both mass spectra include glucose derivatives with one (1HB), two (2HB), or three (3HB) HB groups attached as well as their corresponding dehydrated glucose derivatives (1HB-, 2HB-, 3HB- or 4HB-H_2O, see **Fig. 2.22**). The presence of the dehydrated glucose derivatives provides unequivocal proof that the substitution definitely occurs at, but is not limited to, the O-2 position, since only glucose derivatives with an unsubstituted OH on the O-2 substituting HB group can yield these dehydrated species. They are likely formed during the TFA treatment.

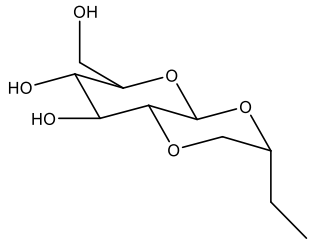

Figure 2.22. Chemical structure of 1,2-O-butylidineglucose (1HB-H_2O).

Glucose derivatives with a fourth (4HB or 4HB-H_2O) and a fifth HB group (5HB) attached were identified in the mass spectrum of $HB_{1.8}$SNPs. The identification of the glucose derivatives with four or five HB groups strongly suggests that at least one of the HB group must have attached onto the OH of another HB group (an AGU has only three sites of substitution, unless it is the end groups of the starch chain which contain four sites). Glucose derivatives with five HB groups unequivocally confirms the presence of oligomerization with the HB groups on the AGUs.

Although we could not get quantitative data from these studies, the intensity of the peaks in both spectra corresponding to 2HB and 2HB-H_2O were the largest, suggesting that disubstituted HBSNPs were the dominant components of the mixtures. Peaks corresponding to glucose derivatives with a fourth (4 HB or 4HB-H_2O) and a fifth HB group (5HB) attached were very small, suggesting that these were formed in very small quantities. Moreover, mass spectra are incapable of differentiating different species with the same chemical composition (i.e. isomers). In order to determine the structure of the hydrolysate components, the

different components will have to be separated by high performance liquid chromatography (HPLC). The resultant fractions will then be analyzed by MS and NMR.

2.9 The Effect of GX and GY on the Hydroxybutylation Reactions

The commercial grade SNPs (CSNPs) that were used for all of the above-mentioned studies contained glyoxal (GX) and glycerol (GY). It would be expected that perhaps the GX and especially the GY would affect the MS_{HB} of the hydroxybutylation reaction. To determine the effect of GX on the MS_{HB}, the hydroxybutylation of SNPs that did not contain GY but contained varying quantities of GX was examined. The SNPs used for these studies are named as GXMGYN, where M is the amount of GX in the sample (in parts per hundred) and N is the amount of GY in the sample (in parts per hundred). For example, a GX2GY0 SNP contains 2 parts GX per 100 parts of the sample and no glycerol. Due to the differences in the composition of various SNPs, the SNP content in these samples should be different accordingly. The SNP content is an approximation of the actual amount of SNPs in a particular SNP sample, excluding any GX, GY or moisture. The knowledge of the SNP content for each SNP sample is critical as it enables the accurate calculation of the amount of modifying reagents in use. Fortunately, such measurements have been performed by Duncan Li, a former M.Sc. student in Taylor lab, and the results were reported in his M.Sc. thesis.[81]

The reaction conditions for all the reactions reported in this section were identical to that of the other hydroxybutylation reactions reported in the earlier sections, but the starting material, the SNP sample, varied. Specifically, SNP samples including GX0-5GY0 SNPs, commercial grade SNP (CSNPs) and purified CSNPs (PSNPs) were used. The PSNPs were prepared by dialyzing the CSNPs in water followed by lyophilisation to remove water. The reactions with the PSNPs were performed with the assumption that the PSNP sample contained SNP only (SNP content was assumed to be 100%).

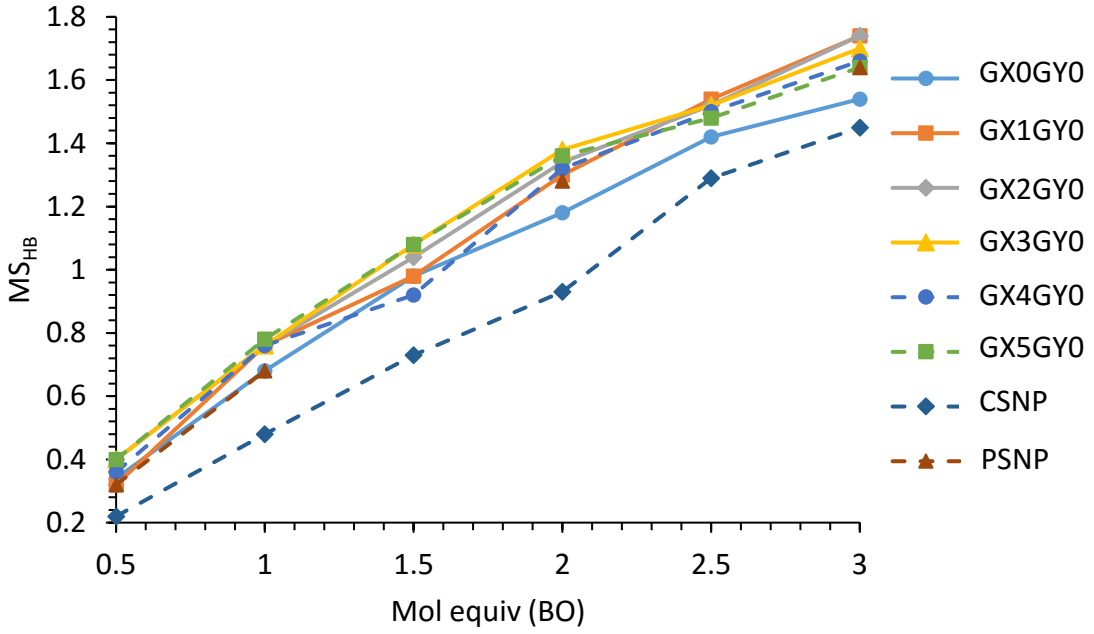

Figure 2.23. Comparison of MS_{HB}s of HBSNP samples prepared from different starting materials, SNPs. GX_MGY_N represents a SNP sample containing M parts of glyoxal per 100 parts of the sample and N parts of glycerol per 100 parts of the sample. In this case, the amount of GX varied from 0 to 5 and the amount of glycerol was 0. CSNPs represent the commercial grade SNPs provided by Ecosynthetix Inc., and the CSNPs contained certain amount of GX and GY, but the exact amounts were not disclosed by the company. PSNPs represent the purified CSNPs via dialysis, and it was expected that all of the GX and GY in the CSNPs would be dialyzed away.

HBSNP samples prepared from the various types of SNP samples were obtained. **Fig. 2.23** shows a plot of the MS_{HB} values versus mol equiv of BO used in these reactions. The CSNPs have the lowest MS_{HB}s of all. This is to be expected, as they contain GY which can compete with the SNPs for the BO. Thus, a greater amount of GY in the reaction mixture may result in a greater consumption of BO, which in turn yields HBSNPs with lower MS_{HB}.

Overall, HBSNPs prepared from GX1-5GY0 SNPs and the purified CSNPs have similar MS_{HB} values when the same mol equiv of BO were used. There is no observable trend between the amount of GX in the starting materials and the resultant MS_{HB} (**Fig. 2.24**). Hence, the MS_{HB} of HBSNPs seems not to be affected by the amount of GX in the SNP samples across the mol equiv range of BO that was examined with the exception of GX0GY0 samples. The HBSNPs prepared from GX0GY0 SNPs show slightly lower MS_{HB} values than the GX1-5GY0 SNPs. This could be a result of the more viscous dispersion obtained with the GX0GY0 SNPs, which causes inefficient stirring during the reaction.

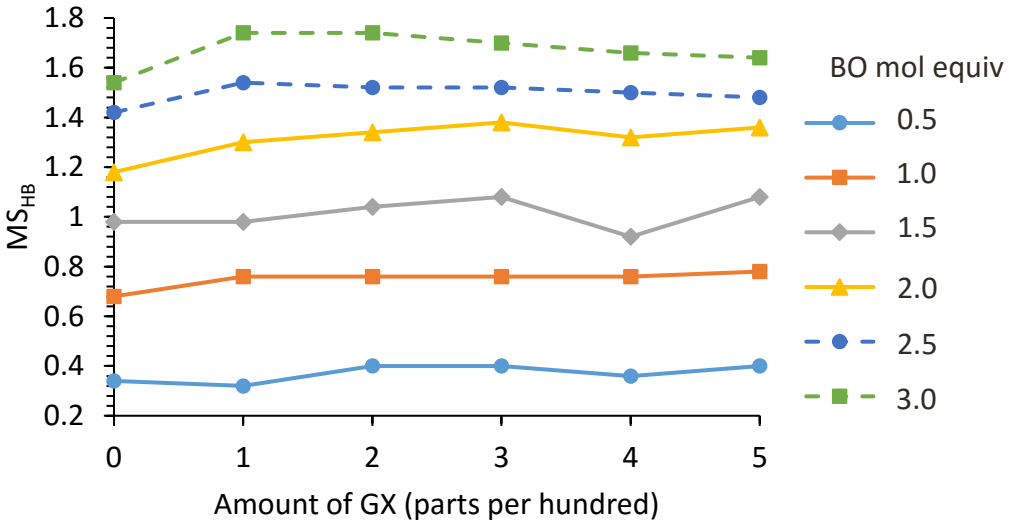

Figure 2.24. Effect of the amount of glyoxal on MS_{HB}. HBSNP samples were obtained from GX0-5GY0 SNP samples reacting with 0.5-3 mol equiv of BO.

Based on unpublished GPC results from Ryan Amos in the Gauthier lab at the University of Waterloo, the molecular weight of the SNPs increases with decreasing amount of GX in the samples.[89] It is believed that GX facilitates the breakdown of starch chains into smaller chains during the extrusion process. Thus, the amount of GX added in the process of producing the SNPs in the extruder should affect the molecular weight of the final products (i.e. GX0GY0 SNPs have larger molecular weight than GX5GY0 SNPs). Combined with the findings above, the molecular weight of the SNPs does not seem to play a significant role in the MS_{HB} of the hydroxybutyl products. However, whether the molecular weight of the products has an effect on T_c remains to be investigated in the future.

Chapter 3

Synthesis and Characterization of Phenyl Hydroxyethyl Starch Nanoparticles

3.1 A Novel Type of Hydrophobically Modified SNPs

As mentioned in Chapter 1, TRPs with a T_c close to body temperature are required for many potential applications of TRPs. In the case of HBSNPs, more than five mol equiv of BO were required to react with the SNPs to yield HBSNPs with a T_c below body temperature. It is highly impractical to produce these HBSNPs on a large scale for any potential applications, due to the need of using a large amount of BO, not to mention that the reaction efficiency is relatively poor (see **Section 2.4**). Thus, a more economical way to produce these thermoresponsive SNPs is needed. One way to solve this problem could be to produce TRSNPs with a more hydrophobic reagent. From Karski's M.Sc. thesis, TRSNPs can also be obtained by hydroxypentylation of SNPs with pentene oxide.[79] More importantly, due to differences in the hydrophobicity of the substituents, the MS of the hydroxypentyl SNPs does not have to be as high as the MS of HBSNPs in order to exhibit thermoresponsive behavior. By substituting a more hydrophobic substituent, TRSNPs with a desired T_c can be obtained with a lower degree of modification. Thus, the amount of the modifying agent can be reduced if the reaction efficiency stays the same. Unfortunately, it was found that the efficiency of the PO reactions was worse than that of the BO reactions.[79] This is mainly due to the decrease in reactivity as the length of the alkane chain increases. Thus, an alkene oxide that is more

hydrophobic and does not compromise the reaction efficiency should be used instead. We anticipated that styrene oxide (SO) would be a good candidate, as it has a hydrophobic aromatic ring and should exhibit a reactivity greater than pentene or hexene oxide. Moreover, SO is relatively inexpensive.

3.2 Preparation of Phenyl Hydroxyethyl SNPs

Phenyl hydroxyethyl SNPs (PHESNPs) were prepared by reacting SNPs with SO (**Scheme 3.1**). The general reaction protocol for the SO reactions was identical to that of the BO reactions.

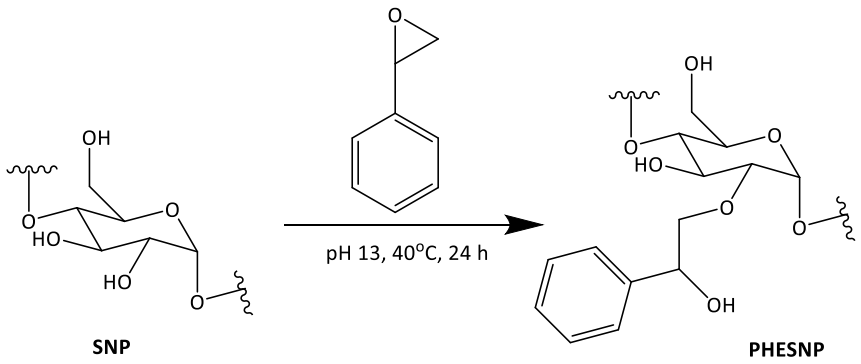

Scheme 3.1. SNP reactions with styrene oxide.

3.2.1 Formation of Poly(styrene oxide)

Experiments were conducted to find out if there was any formation of poly(styrene oxide) (PSO, see **Fig. 3.1**) during the SO reactions. One of the control reactions was carried out with 2.85 g SO and without SNPs. **Fig. 3.2** shows the reaction mixtures before and after

reacting at pH 13 in a 40°C water bath for 24 h. After dialysis of the reaction mixture against water for an extended period of time and water replacements, a white and insoluble substance remained in the dialysis tubing with a MW_{cutoff} of 1 kD (**Fig. 3.3A**). The dialyzed reaction mixture was then split into two portions. The first portion was further subjected to dialysis against water, and the second portion was dialyzed against DMSO. Interestingly, after dialysis against DMSO for one day, the white precipitate still remained in the dialysis tubing and was not completely soluble in DMSO (**Fig. 3.3B**). After the dialysis against DMSO, this portion of the reaction mixture was dialyzed with water again to remove DMSO. Together with the first portion (dialyzed against water only), both portions were lyophilized to recover the insoluble substance that was trapped inside the dialysis tubing. A total of approximately 15 mg of pale yellow to white powder was obtained (9 mg from the first portion and 6 mg from the second). The ^{1}H NMR spectrum of this powder in DMSO-d_6 and a few drops of TFA-*d* shows a broad set of peaks at 7.2 ppm, which potentially correspond to the phenyl protons (**Fig. 3.4**). This suggests that the control reaction yielded a polymer with phenyl functional groups. However, considering the fact that only 15 mg of the polymeric by-product were obtained from a 2.85 g SO reaction, this side reaction is negligible. Moreover, the amount of SO used in the control reaction was much greater than in any of the SO reactions with the SNPs. Typically, the amount of SO used in the reactions with the SNPs would be less than 0.24 g. Thus, another control experiment was conducted with 0.24 g SO and no quantifiable amount of polymeric by-product could be obtained.

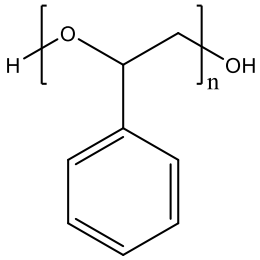

Figure 3.1. Chemical structure of poly(styrene oxide).

(A) **(B)**

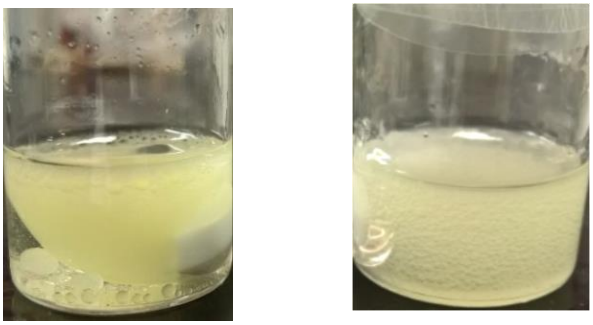

Figure 3.2. Reaction mixtures **(A)** before and **(B)** after the reaction.

(A) **(B)**

Figure 3.3. Reaction mixture in dialysis tubing after dialyzing **(A)** with water and **(B)** with DMSO.

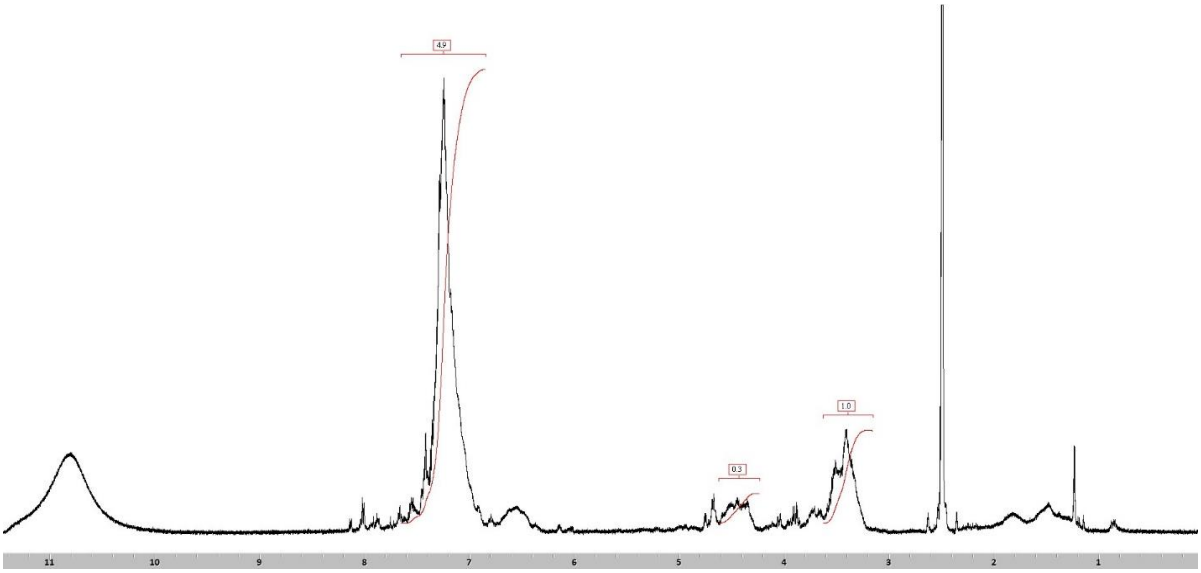

Figure 3.4. ^{1}H NMR spectrum of the white precipitate recovered from the control experiment with 2.85 g SO. The NMR solvent was DMSO-d_6 with a few drops of TFA-*d*.

3.2.2 Kinetic Studies of the SO Reactions

Wayne Vuong, a student in the Taylor group, performed a kinetic study of the reaction of SO with SNPs. The SNPs used in this kinetic study were different from the ones used throughout this thesis, in that they contained less glycerol. Nevertheless, this study provided us with an idea as to how fast the reaction between SO and the SNPs takes place.

The reaction was followed by ^{1}H NMR and 0.3 mol equiv of SO to AGU was used. **Fig. 3.5** shows a plot of MS_{PHE} vs. time. From this plot it can be seen that the reaction is more-or-less complete after 8 h. The plot is linear within the first hour and a zero-order rate constant of 0.023 mols of OH modified/h was obtained. The possible reasons behind this linear relationship are the same as those given for the BO reaction discussed in **Section 2.2.2**. To

ensure that all subsequent reactions discussed in this chapter went to completion, these reactions were allowed to proceed for 24 h.

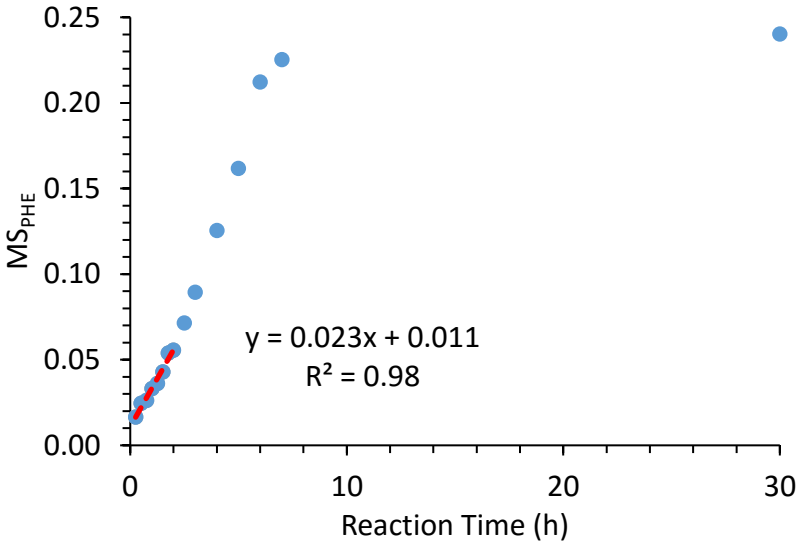

Figure 3.5. Plot of MS_{PHE} versus reaction time.

3.3 ^{1}H NMR Spectral Analysis of PHESNPs

A typical ^{1}H NMR spectrum of a PHESNP in D_2O is shown in **Fig. 3.6**, and the specific peak assignments are provided as follows. The peak at 0 ppm belongs to the internal standard, TMSP-d_4. The peaks between 4.2 - 3.3 ppm are assigned to the 6 protons (labeled **2 - 6**) in the AGU and the 3 protons (labeled **A** and **B**) from the PHE group. The largest peak at 4.8 ppm corresponds to the water peak. The peaks at 5.9 - 5.3 ppm are assigned to the anomeric proton (labeled **1**). Lastly, the peak at 7.9 - 7.3 ppm corresponds to the five phenyl protons from the PHE group.

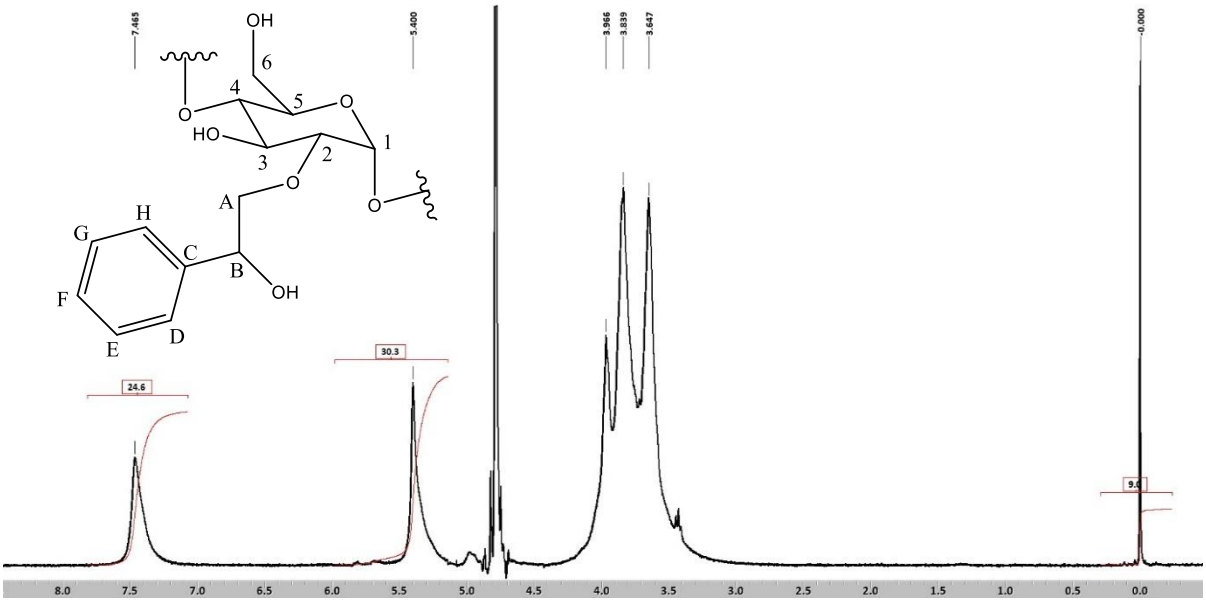

Figure 3.6. ^{1}H NMR spectrum of $PHE_{0.18}SNP$, with a MS_{PHE} of 0.18, in D_2O and TMSP-d_4 as an internal standard.

3.3.1 ^{1}H NMR Spectral Comparison of the Dispersible and the Non-dispersible PHESNPs

For the reactions with a relatively large amount of SO (greater than 0.3 mol equiv of SO), the resultant PHESNPs were just partially dispersible in water. The reaction mixture essentially separated into two phases: an aqueous layer and a non-dispersible precipitate. Hence, one of the questions that needs to be answered is: what are the compositional differences between the dispersible and the non-dispersible products. From **Section 3.2.1**, the chance that the non-dispersible precipitate in the reaction mixture is the polymeric by-products is very low, as the side reaction produced only very limited amount of a by-product based on the control experiments. Thus, it would be interesting to find out what the composition of the non-dispersible products is.

To compare the composition of the dispersible and the non-dispersible products, a reaction was performed to produce a sufficient amount of non-dispersible products for analysis. Specifically, an SNP reaction with 6 mol equiv of SO was carried out following the standard reaction procedure (**Section 4.3.1**). After neutralizing with HCl, the reaction mixture was allowed to settle and then carefully decanted to yield the dispersible aqueous layer and the non-dispersible precipitate. Then, both the aqueous layer and the precipitate were lyophilized (without dialysis) to yield a fine white powder and large agglomerates, respectively. ^{1}H NMR spectra were obtained in both D_2O and DMSO-d_6.

(A)

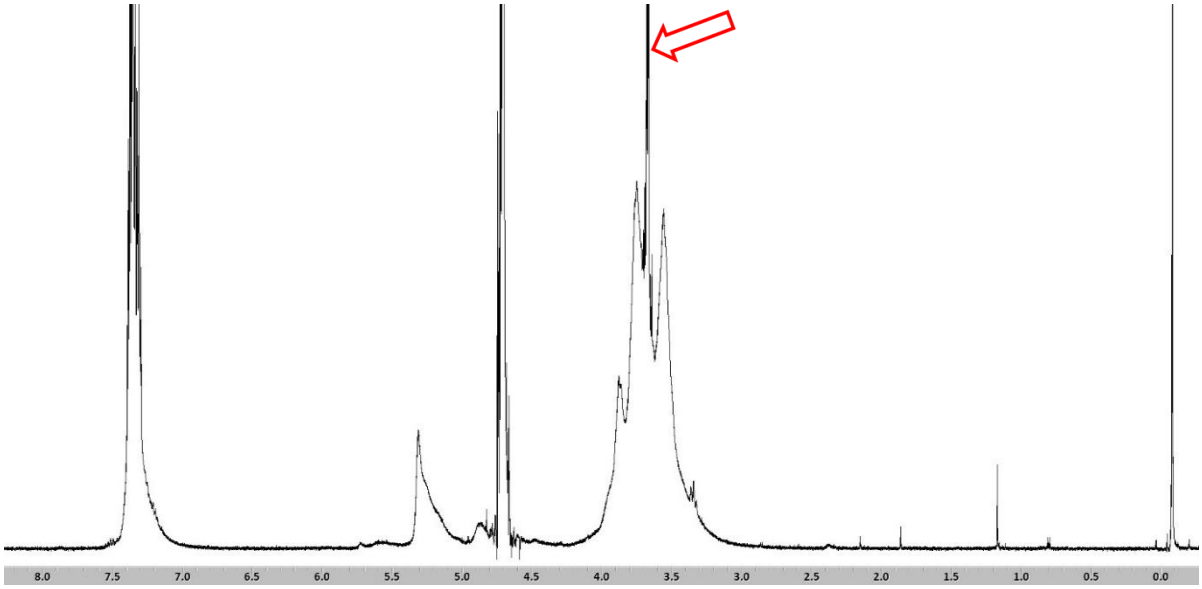

(B)

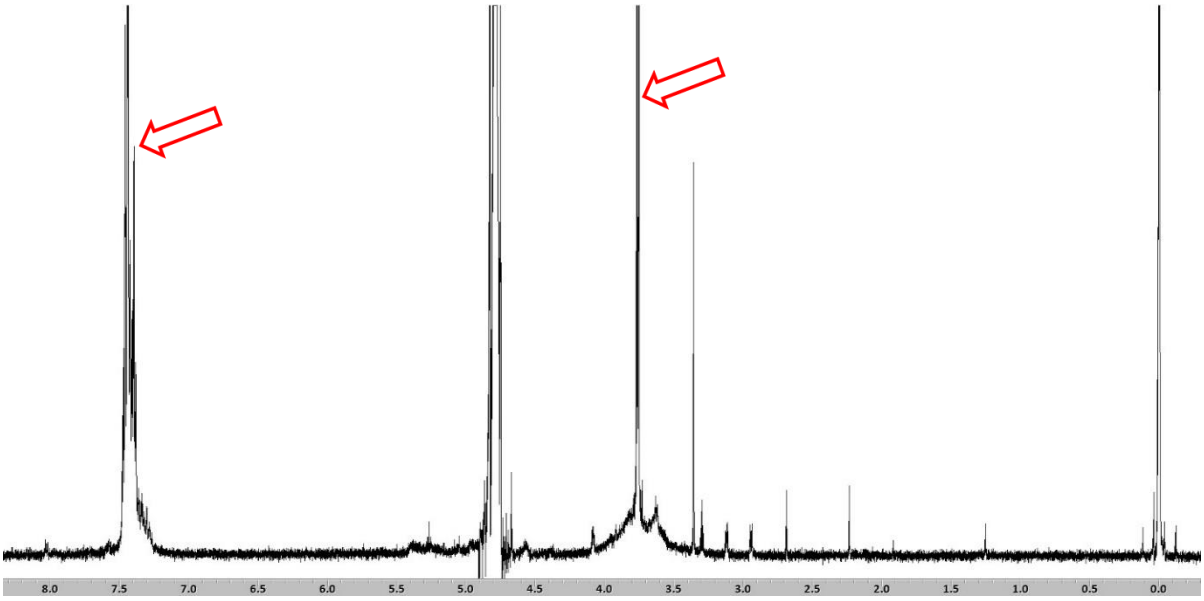

Figure 3.7. ^{1}H NMR spectra for the **(A)** dispersible and **(B)** non-dispersible products in D_2O. The red arrows point out the major peaks that are not seen in a typical spectrum of a purified PHESNP.

The dispersible product in D_2O shows similar peaks as in a typical PHESNP spectrum (compare **Fig. 3.7A** to **Fig. 3.6**). An exception is that there is a sharp peak hidden under the broad set of peaks at approximately 3.7 ppm (indicated by a red arrow). These peaks could arise from hydrolyzed SO. **Fig. 3.7B** shows two major peaks at 7.4 and 3.7 ppm, which could also arise form hydrolyzed SO. Moreover, the signals for the peaks of PHESNPs are very weak, suggesting that the low dispersability of the precipitate is not due to concentration but to the composition of the precipitate (i.e. the molar substitution of the PHE groups, MS_{PHE}, may be too high).

(A)

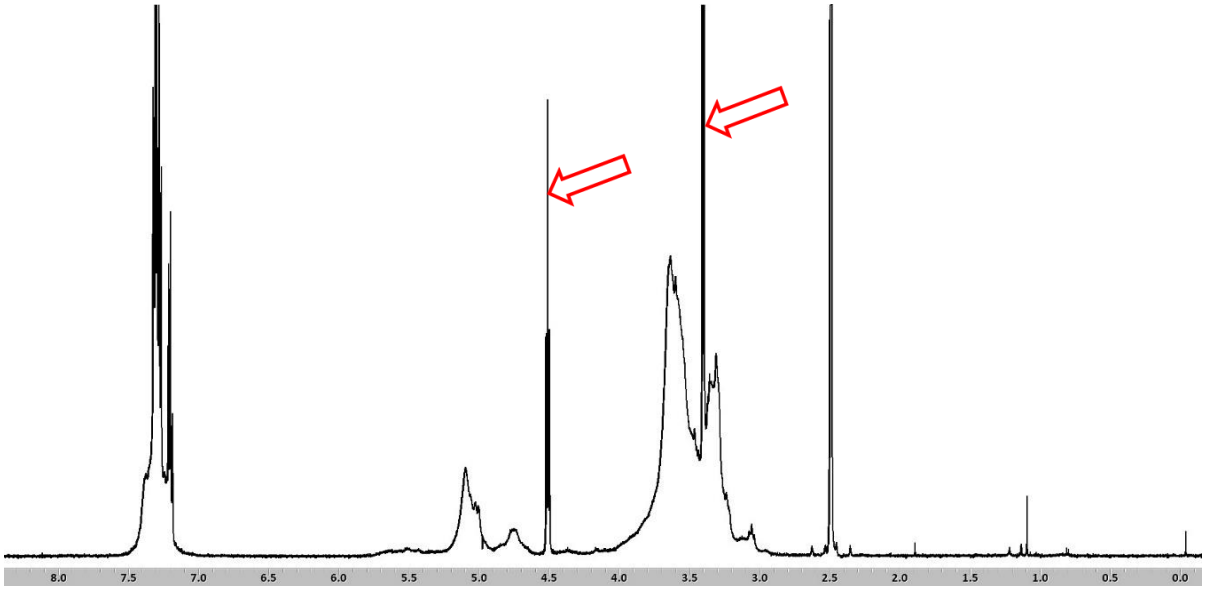

(B)

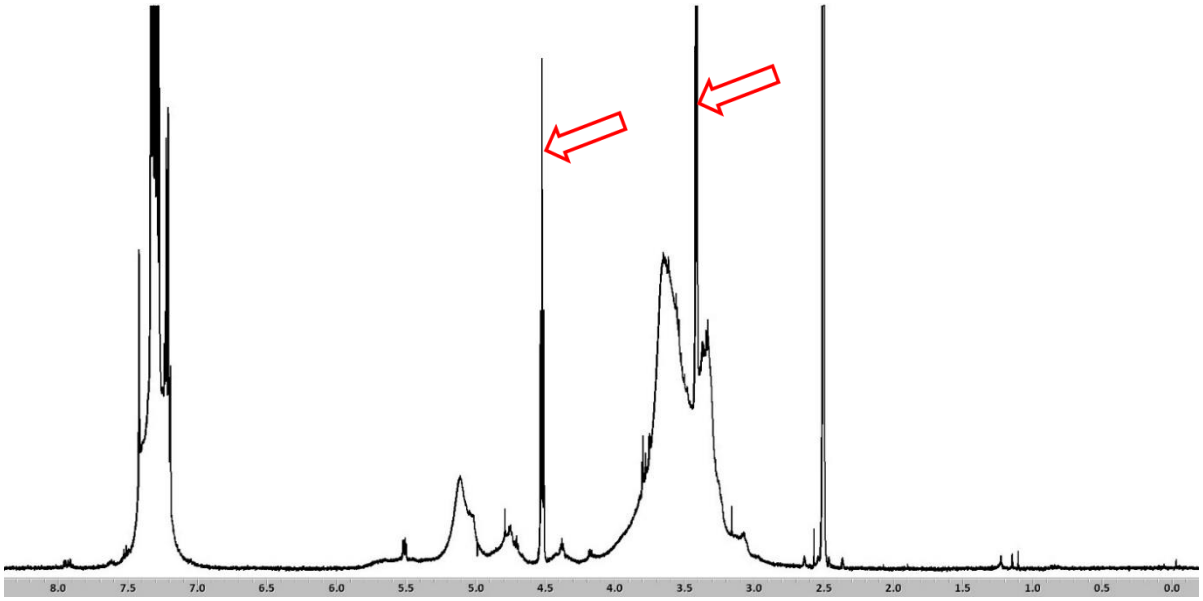

Figure 3.8. ^{1}H NMR spectra for the **(A)** dispersible and **(B)** non-dispersible products in DMSO-d_6 with a few drops of TFA-*d*. The red arrows point out the major peaks that are not seen in a typical spectrum of a purified PHESNP.

The ^{1}H NMR spectra of the dispersible and non-dispersible products in DMSO-d_6 are almost identical (compare **Fig. 3.8A** and **B**). This strongly suggests that the composition of the dispersible and the non-dispersible products are very similar. The difference in the dispersability could be caused by the difference in MS_{PHE}, though it is not directly investigated here. The red arrows indicate the peaks corresponding to a low molecular weight by-product. A spiking experiment with SO shows that the low molecular weight compound is not SO, as the peaks of SO do not overlap with the peaks indicated by the red arrows (**Fig. 3.9A**). This suggests that the starting material, SO, was completely consumed after the 24 h of reaction. **Fig. 3.9B** shows the ^{1}H NMR spectrum of 1-phenyl-1,2-ethanediol (the hydrolysis product of SO). The peaks of the by-product match the peaks of the 1-phenyl-1,2-ethanediol perfectly, thus, the identity of the by-product is confirmed to be 1-phenyl-1,2-ethanediol. When compared to a typical ^{1}H NMR spectrum of PHESNPs in DMSO-d_6 (**Section 3.5.2, Fig. 3.16**), the absence of the peaks corresponding to the by-product strongly suggests that the removal of the by-product by dialysis in water from the PHESNP samples is effective.

(A)

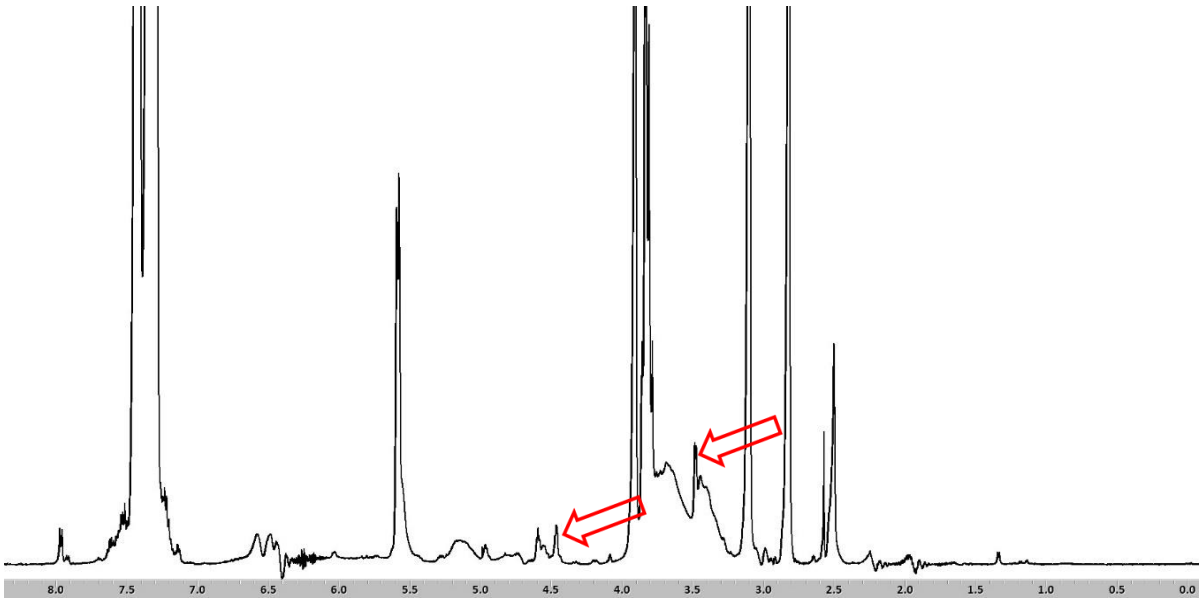

(B)

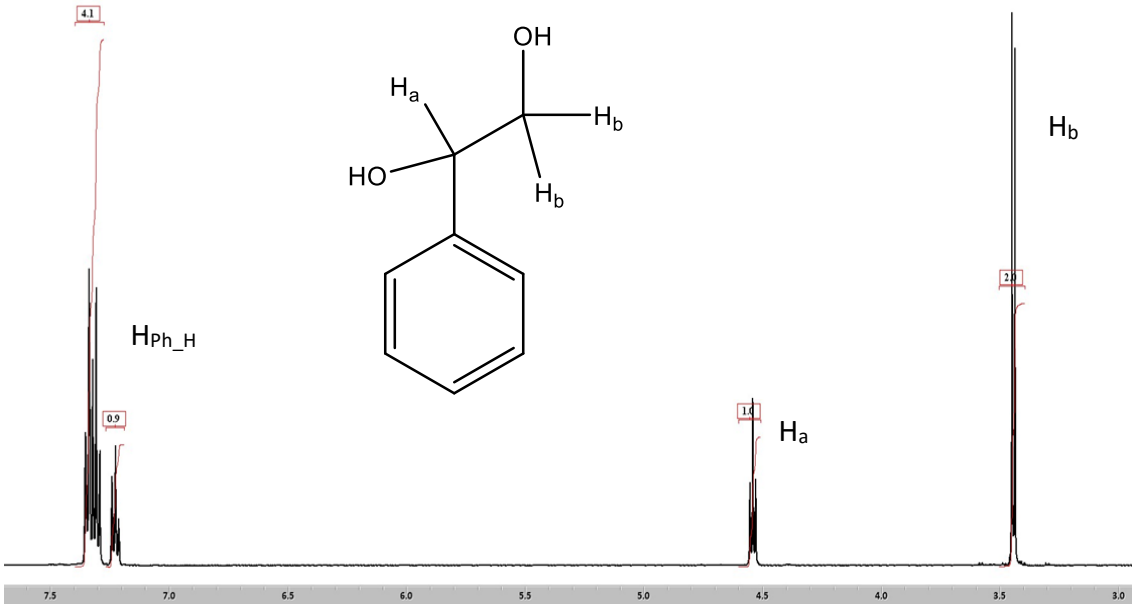

Figure 3.9. ^{1}H NMR spectra for the **(A)** dispersible product spiking with SO and **(B)** 1-phenyl-1,2-ethanediol in DMSO-d_6 with a few drops of TFA-*d*. The red arrows in (**A**) represent the peaks of the by-products found in the control experiment.

3.4 Molar Substitution of PHESNPs

By varying the amount of SO used in the reactions, PHESNPs with different MS values of PHE groups (MS_{PHE}) were obtained. Reactions performed with SO:AGU ratios greater than 0.5 resulted in a highly non-dispersible paste-like substance in D_2O; therefore, the MS_{PHE} of these samples was not obtained using ^1H NMR with D_2O as solvent, but rather in DMSO-d_6. The MS_{PHE} was obtained using **Equation 3.1**:

$$MS_{PHE} = \frac{I_{Phenyl\ H}}{(I_{H1} \times 5)} \quad \text{(Eqn. 3.1)}.$$

The integration of the anomeric proton is multiplied by 5, as there are five phenyl protons from one PHE group whereas each AGU contains only one anomeric proton. The key characteristics of a series of PHESNPs are summarized in **Table 3.1**. Additionally, a linear correlation between MS_{PHE} and the amount of SO added was found as shown in **Fig. 3.10**.

Table 3.1. Molar substitution (MS_{PHE}), reaction efficiency and % yield of PHESNPs.

	SO:AGU[a]	MS_{PHE}[b]	Efficiency	% Yield[c]
1	0.05	0.025	50%	96%
2	0.1	0.073	73%	93%
3	0.15	0.103	69%	89%
4	0.2	0.129	65%	77%
5	0.25	0.182	73%	82%
6	0.3	0.231	77%	73%
7	0.4	0.319	80%	66%
8	0.45	0.365	81%	71%
9	0.5	0.400	80%	65%

[a] SO:AGU is the mole ratio between SO and AGUs
[b] MS_{PHE} is the molar substitution obtained by ^1H NMR
[c] The % yield calculation has accounted for an estimation of 10% moisture content in the PHESNP sample.

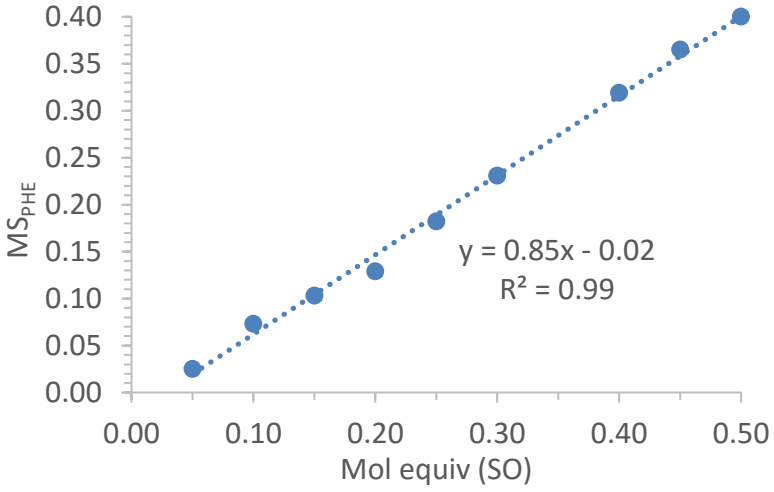

Figure 3.10. Relationship between the MS_{PHE} of the PHESNPs and the amount of SO used in each reaction.

Similar to the HB groups, the PHE groups may be substituting onto different OH groups in different combinations. Additionally, SO can react through the α and β carbon with an OH group, thus two positional isomers each with two diastereomers can be expected.[90] Depending on the α or β carbon, the reaction mechanism can be quite different. In addition to the S_N2 type substitution reaction, in which a nucleophile attacks the least sterically hindered site (**Fig. 3.11B**), an S_N1 type reaction may occur. In the case of SO reactions, an S_N1 type reaction involves a nucleophilic attack at the α carbon of SO (**Fig. 3.11A**). This could be made possible by the formation of benzylic carbocation, which is stabilized by resonance delocalization of the carbocation positive charge distributed across the aromatic ring.[90]

(A)

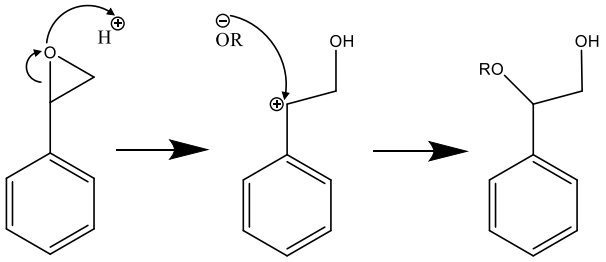

(B)

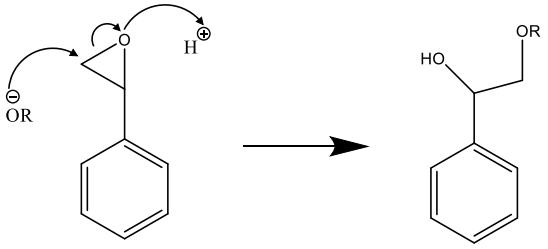

Figure 3.11. Mechanism of the nucleophilic attack at the **(A)** α or **(B)** β carbon on SO.

3.5 An Investigation into the Challenges of MS_{PHE} Determination

A series of ^1H NMR spectra in D_2O of PHESNPs modified by increasing the mol equiv of SO is shown in **Fig. 3.12**. At low mol equiv from 0.05 to 0.15, the peak corresponding to the phenyl protons at 7.9 – 7.3 ppm has a definite increase in size. This is expected, as on average more PHE groups are incorporated onto the AGUs for the increasing mol equiv of SO used. However, after 0.15 mol equiv and up to 0.30 mol equiv, the peak appears to be unchanged. This is not expected, as the MS_{PHE}s clearly increase for these PHESNP samples (**Table 3.1**, entries **3**-**6**), which means the peak has to increase with respect to the anomeric peak as well as the internal standard peak. Moreover, the peak decreases drastically along with other major peaks on the spectra for PHESNPs of 0.4 to 0.5 mol equiv SO reactions. The peak area of all the peaks in these spectra (except for the internal standard, TMSP-d_4) is very small, which generally indicates that there was not enough sample in the NMR solution. However, since the concentration of the PHESNP dispersions was at 20 g/L for all NMR measurements, the decrease in overall peak area must arise from the decrease in the dispersability of the PHESNP samples as the MS_{PHE} increases. A decrease in peak size for certain protons peaks may have occurred when there was formation of micelles. For example, in an aqueous system, the peak corresponding to the protons of hydrophobic groups should decrease in size as compared to those belonging to the hydrophilic groups in the same polymer. But it is clearly not the case here because a decrease in the overall peak size was observed.

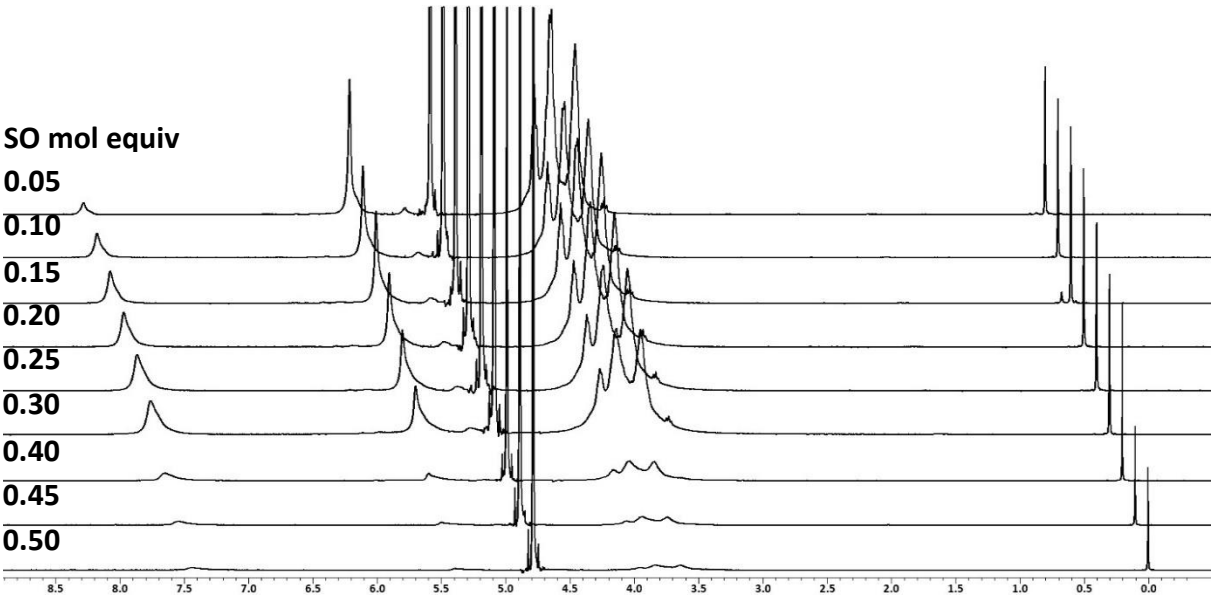

Figure 3.12. ^{1}H NMR spectra for PHESNPs prepared with an increasing amount of SO. The spectra are slant-stacked and magnified to approximately the same intensity based on the internal standard, TMSP-d_4, peak at 0 ppm. The magnitude of the TMSP-d_4 peaks for 0.45 and 0.5 mol equiv is half of that of the rest of TMSP-d_4 peaks because only half of the amount of TMSP-d_4 was added.

3.5.1 Dispersability Study of PHESNPs

One of the methods to determine the dispersability of PHESNPs is by turbidity measurements. More specifically, a series of 10 g/L dispersions were made by dispersing PHESNPs with different MS_{PHE} in deionized water. The dispersions were stirred overnight in a fridge at 4^{o}C and allowed to equilibrate to 15^{o}C prior to the measurements. The absorbance of the PHESNP dispersions was measured at 500 nm at 15^{o}C, and deionized water was used as blank. The experimental control was obtained by processing SNPs in the same conditions as in the SO reactions, but without the addition of SO. **Fig. 3.13** shows the transmittance

versus MS_{PHE} plot. In general, the transmittance decreases as the MS_{PHE} increases. More specifically, below a MS_{PHE} value of 0.1, the transmittance of the PHESNP dispersions is similar to that of the control. The transmittance decreases slightly as the MS_{PHE} increases from 0.1 to 0.3. Beyond MS_{PHE} of 0.3, the transmittance decreases drastically to as low as 20% when MS_{PHE} is at 0.4. The differences in the transmittance of the dispersions could reflect the differences in the dispersability of PHESNPs with various MS_{PHE}. The MS_{PHE} is comparable to the concentration of PHE groups. In a 10 g/L PHESNP dispersion, the higher the MS_{PHE} the more the PHE groups are present in the dispersion. Thus, the dispersability of PHESNPs here can be correlated to MS_{PHE}. Below a MS_{PHE} of 0.1, the dispersability of PHESNPs are comparable to the dispersability of the unmodified SNPs. The dispersability decreases slightly for an increase in MS_{PHE} up to 0.23. Beyond that, a drastic decrease in dispersability can be observed. This is also in agreement with the experimental observation that non-dispersible products can be obtained from the reactions with 0.5 mol equiv or more SO (which gives an MS_{PHE} of 0.4).

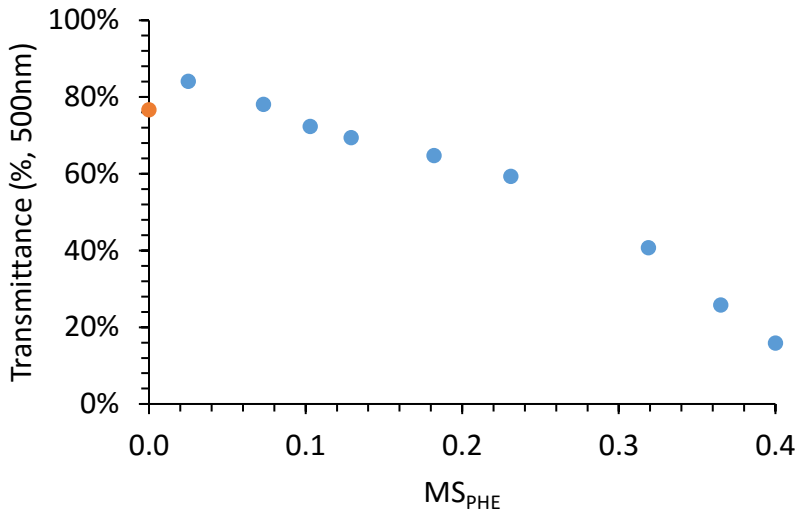

Figure 3.13. Turbidity assay of the dispersions of PHESNPs at different MS_{PHE}s. The measurements were done at 500 nm at 15°C with a dispersion concentration of 10 g/L.

3.5.2 MS_{PHE} Determination using DMSO-d_6 as NMR Solvent

Due to the poor dispersability of PHESNPs in water, there is a concern that the MS_{PHE} calculated from the NMR analysis with D_2O as the NMR solvent is not accurate. Assuming that the PHESNP sample is heterogeneous (i.e. some fractions of the sample may have a higher MS_{PHE} than the others), the fractions with higher MS_{PHE} will intuitively have lower water-dispersability. Hence, these PHESNPs with higher MS_{PHE} may not be detected by NMR and reflected on the calculated MS_{PHE}, resulting in an underestimate of the true MS_{PHE}. Therefore, it is important to consider another way to determine the MS_{PHE} and to ensure that the same MS_{PHE} can be obtained regardless of the choice of the method of determination.

Another method to determine MS_{PHE} involves changing the NMR solvent from D_2O to DMSO-d_6. An assumption here is that the dispersability of PHESNPs is better in DMSO than in

water. **Fig. 3.14** shows a series of ^{1}H NMR spectra of PHESNPs which are prepared using 0 to 0.5 mol equiv of SO. In the case of the spectra for PHESNPs in D_2O, the overall peak size decreases when the PHESNPs are prepared using more than 0.4 mol equiv of SO (**Fig. 3.14**). The decrease in overall peak size is not observed when using DMSO-d_6 as NMR solvent. The increase in peak size of the phenyl proton peaks is quite noticeable as the amount of SO used increased (**Fig. 3.14**). Another peak that also increased in size is at 4.8 ppm (**Fig. 3.14**). It should be noted that this peak is present in the spectrum of the unmodified SNPs, and it is assigned to the anomeric protons of the AGUs at branching point.[91] Since the calculation of MS_{PHE} requires the accurate determination of the integration of the anomeric proton peak, the assignments of the peaks in the region from 5.5 to 4.5 ppm were carefully investigated.

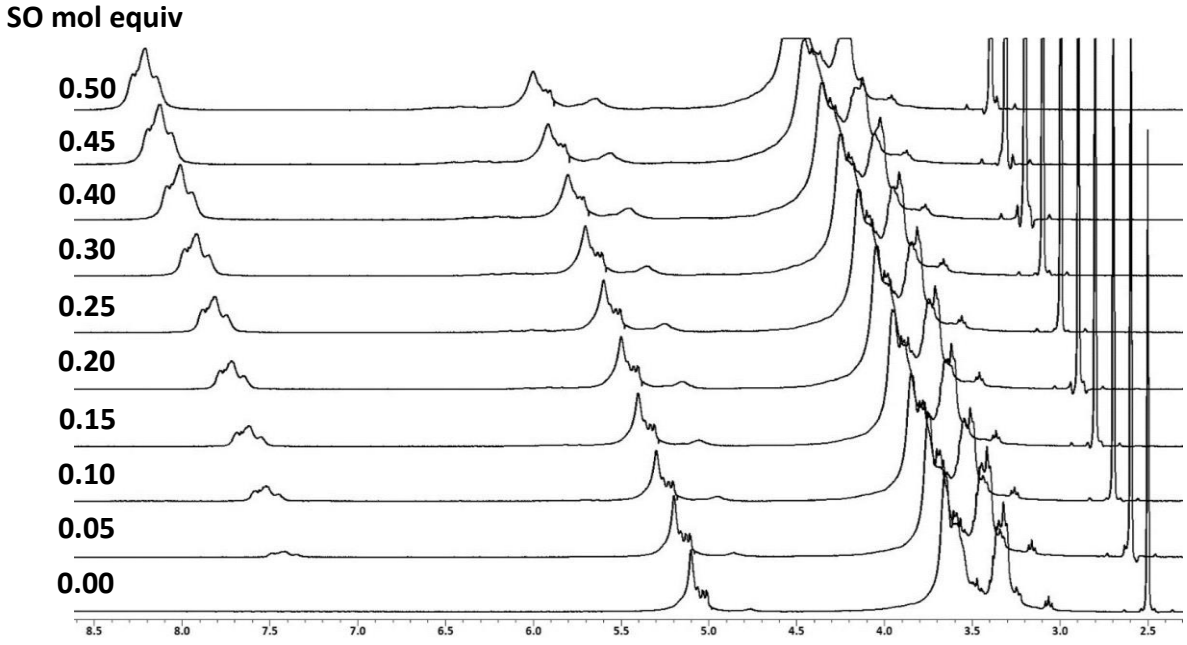

Figure 3.14. A series of ^{1}H NMR spectra of PHESNPs prepared from 0 to 0.5 mol equiv SO in DMSO-d_6 with a few drops of TFA-*d*.

The anomeric peak of the unmodified SNPs is at 5.2-5.0 ppm, which is confirmed by the overlapping of the peak labeled as "**b**" in the anomeric region and the anomeric peak in spectrum of the unmodified SNPs (**Fig. 3.15**, compare the spectra for PHESNP and the unmodified SNP). The peaks labeled as "**a**" have a small integration but they are observable under magnification in that region (**Fig. 3.15**, PHESNP). A set of peaks can also be found in this region in the spectrum of HBSNP (**Fig. 3.15**, HBSNP). Based on the discussion of the downfield-shifting post-modification anomeric proton peak in **Section 2.3**, this set of peaks can be assigned to the anomeric proton of the O-2 and O-3 substituted AGU. The small peak at 4.7 ppm (labeled as "**c**") has the same chemical shift as the anomeric peak at the branching AGU. This peak increases in size as the amount of SO used increases (**Fig. 3.14**), suggesting

that there is an overlap of peak(s) contributed by protons of the substituting PHE groups. According to the spectral analysis of the by-product, 1-phenyl-1,2-ethanediol, the peak at 4.6-4.5 ppm corresponds to the proton at α carbon (**Fig. 3.9B**). As the PHE group has a similar proton at this position, it is expected that the chemical shift of this proton approximates the chemical shift of the proton in 1-phenyl-1,2-ethanediol. Hence, the peak labeled "**c**" should correspond to a combined signal from the anomeric proton at a branching point and the proton from the PHE group.

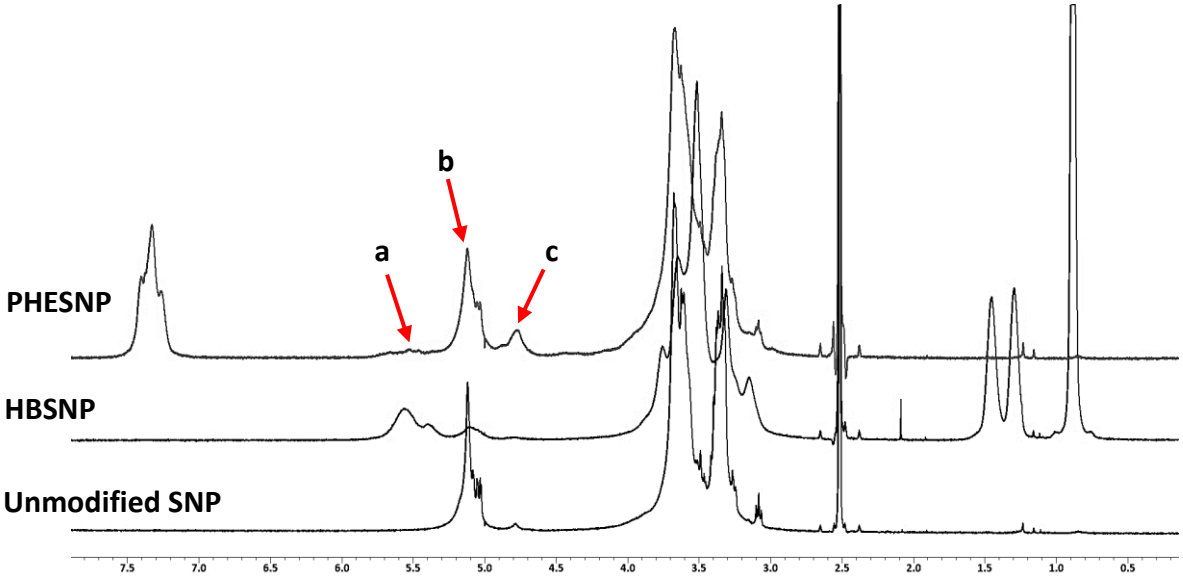

Figure 3.15. ^{1}H NMR spectral comparison of PHESNP, HBSNP and the unmodified SNP in DMSO-d_6 with a few drops of TFA-*d*.

Due to the complexity of the anomeric proton peak of PHESNPs, the determination of MS_{PHE} is greatly affected by how the integration of the anomeric proton peak is defined (**Fig. 3.16**). For example, if the integration of the anomeric proton is defined as "**a + b + c_0**" (i.e. the

sum of the integration of the anomeric proton on the modified, unmodified and branching point AGU), the MS_{PHE} can be calculated as in **Equation 3.2**:

$$MS_{PHE} = \frac{(p/5)}{(a + b + c_0)} \quad \text{(Eqn. 3.2)}.$$

If the integration of the anomeric proton is defined differently, such as "**a + b + c – p/5**" (i.e. the sum of the integration of all the peaks in the region subtracting the integration of the proton from PHE groups), the MS_{PHE} is calculated differently as shown in **Equation 3.3**:

$$MS_{PHE} = \frac{(p/5)}{(a + b + c - p/5)} \quad \text{(Eqn. 3.3)}.$$

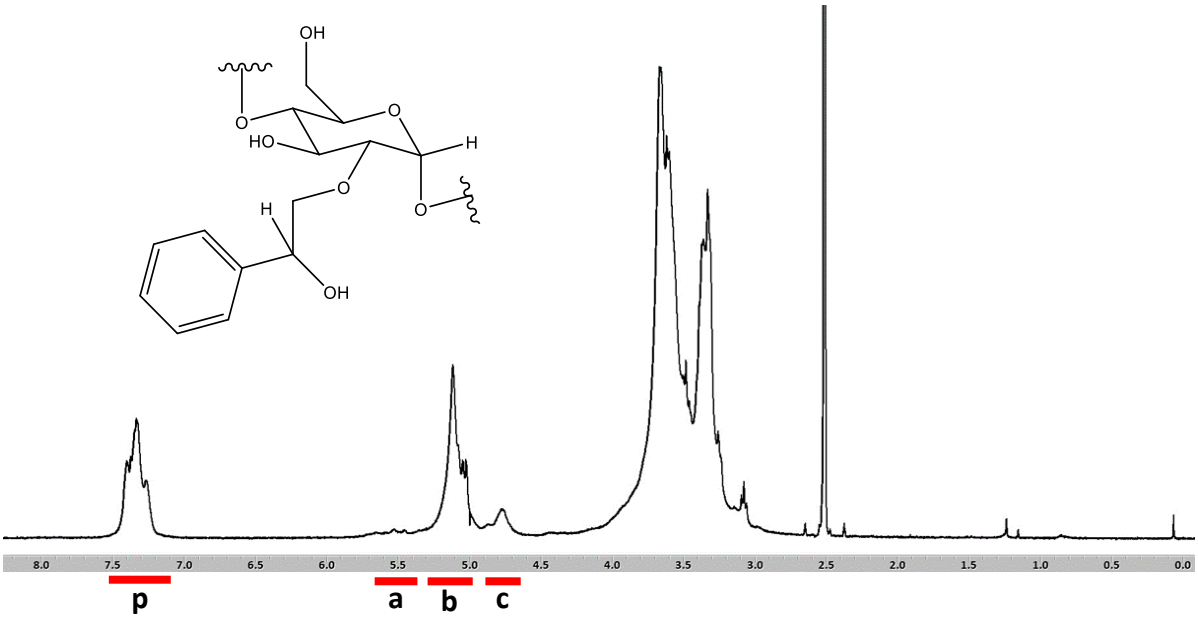

Figure 3.16. ^{1}H NMR spectrum of a typical PHESNP sample in DMSO-d_6 with a couple drops of TFA-*d*. The integration of the phenyl peaks is "**p**", the integration of the anomeric proton peak is separated into three portion: "**a**", "**b**" and "**c**".

Table 3.2 shows different MS_{PHE}s calculated from the differently defined anomeric proton integrations. The MS_{PHE}s based on "**b + c_0**" share the most similarity with the MS_{PHE_D2O}s calculated from NMR analysis of PHESNPs in D_2O (green). Some MS_{PHE}s are slightly higher (light blue) and some are slight lower (light brown) than their corresponding MS_{PHE_D2O}s. Other MS_{PHE}s can be very different from the MS_{PHE_D2O}s, for example, the MS_{PHE}s based on "**b + c**" or "**a + b + c**" are much lower (dark brown) and the ones based on "**b + c – p/5**" or "**a + b + c – p/5**" are much higher (dark blue), especially for the samples with higher MS_{PHE}s. The same observations can be made when all MS_{PHE}s are plotted against the mol equiv of SO used to prepare the PHESNP samples (**Fig. 3.17**). Up to 0.3 mol equiv, the MS_{PHE}s calculated from different methods are relatively similar. However, at 0.4 mol equiv or higher, the MS_{PHE}s are relatively inconsistent. Due to this inconsistency, the MS_{PHE}s calculated from the NMR analysis with D_2O as the NMR solvent appear to be a better choice for now.

Table 3.2. A summary of MS_{PHE}s based on different integration of the anomeric proton. The green means the same as the MS_{PHE}s calculated from NMR measurements using D_2O (MS_{PHE_D2O}s), the brown means lower and the blue means higher than MS_{PHE_D2O}s. The darker the color the larger difference there is between the MS_{PHE}s (from NMR measurements using DMSO-d_6) and MS_{PHE_D2O}s. The darker the color means the larger the difference.

	D_2O	DMSO-d_6							
mol equiv		**b**	**b+c$_0$**	**a+b**	**a+b+c$_0$**	**b+c**	**a+b+c**	**b+c-p/5**	**a+b+c-p/5**
0	0.00	0.00	0.00	0.00	0.00	0.00	0.00	0.00	0.00
0.05	0.03	0.03	0.03	0.03	0.03	0.03	0.03	0.03	0.03
0.1	0.07	0.09	0.08	0.09	0.08	0.08	0.08	0.09	0.09
0.15	0.10	0.11	0.11	0.11	0.11	0.10	0.10	0.12	0.11
0.2	0.13	0.15	0.14	0.14	0.14	0.13	0.13	0.15	0.15
0.25	0.18	0.19	0.19	0.19	0.18	0.17	0.17	0.21	0.20
0.3	0.23	0.22	0.22	0.21	0.21	0.19	0.19	0.24	0.23
0.4	0.32	0.33	0.32	0.31	0.30	0.28	0.26	0.39	0.36
0.45	0.37	0.39	0.38	0.37	0.36	0.32	0.30	0.47	0.43
0.5	0.40	0.42	0.41	0.39	0.38	0.34	0.31	0.51	0.46

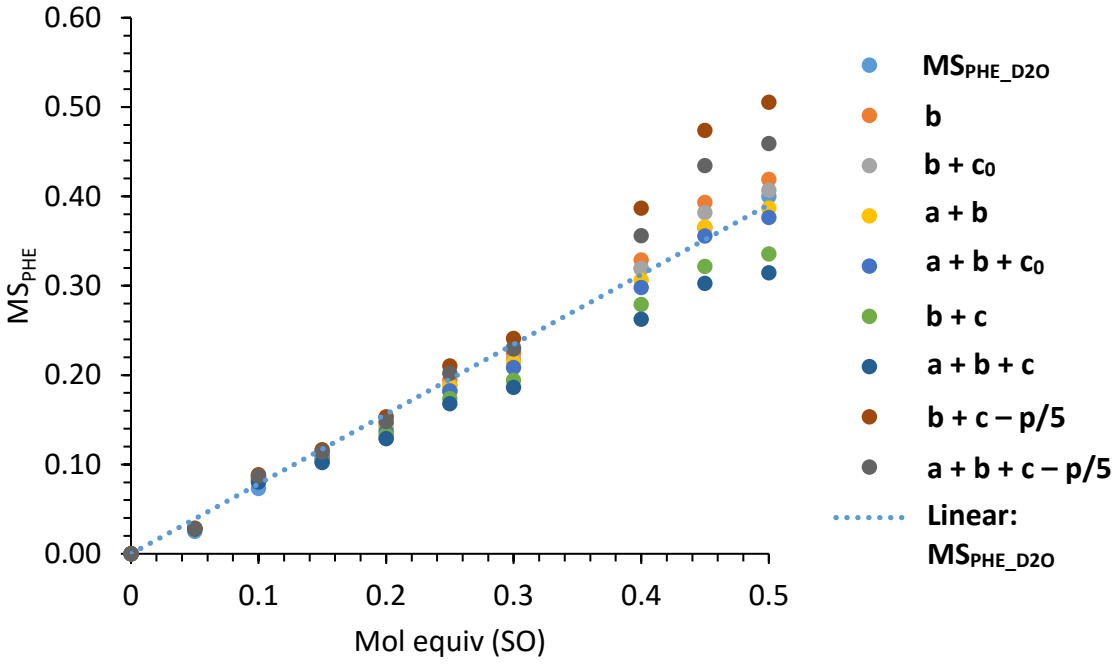

Figure 3.17. Comparison of MS_{PHE}s calculated from different integration of the anomeric proton. The MS_{PHE_D2O}s and the linear best-fit line are also shown, same as in **Fig. 3.10**.

3.6 Efficiency of SO Reactions

Efficiency of the SO reactions are reported in **Table 3.1**. The efficiency was calculated via dividing the actual MS_{PHE} by the theoretical MS_{PHE}. The theoretical MS_{PHE} is the maximum MS_{PHE} based on the mol equiv of SO used in the reactions. An increase in the efficiency from 50% to 80% was observed when the mol equiv of SO increased 10-fold from 0.05 to 0.5. The efficiency of the SO reactions is generally higher than those of the BO reactions. When comparing both reactions with 0.5 mol equiv of reagents, the SO reaction gives an 80% reaction efficiency whereas the BO reaction efficiency is only at 44%.

3.7 % Yields of the SO Reactions

Due to the dispersability issues with the PHESNP samples, the ^{1}H NMR method is not reliable for the determination of PHESNP or the water content in the PHESNP samples that are not fully dispersible in water. As discussed in **Section 2.5**, the water content of the unmodified SNPs and HBSNPs was very similar, both at 10%. It is reasonable to assume that the water content of the PHESNP samples was also similar to that of the unmodified SNPs. In other words, PHESNP content can be assumed to be 90% in a PHESNP sample. With this assumption, the % yield of SO reactions was calculated using **Equation 3.4**:

$$\% \text{ Yield} = \frac{\text{mass recovered} \times 90\%}{0.64 \times g \text{ CSNP} + g \text{ SO}} \times 100\% \quad \text{(Eqn. 3.4)}.$$

The mass recovered was the amount of PHESNP sample recovered after dialysis and lyophilisation. The theoretical mass is the total mass of the reactants, which includes the mass of SNPs and SO. The mass of SNPs has been factored in 0.64, which is the AGU content of the CSNP sample (Section 2.1). There is 0.64 g of AGU in every gram of the starting material (the CSNP sample). The mass of SO is known and can be calculated from the number of mol equiv of SO used in the reaction.

Similar to the BO reactions, another way to calculate the % yield takes into consideration of the reaction efficiency. Again, the reaction efficiency reflects the amount of substituents (the PHE groups) which are successfully incorporated onto the SNPs. The % $yield_{Eff.}$ can be obtained by **Equation 3.5**:

$$\% \text{ Yield}_{Eff.} = \frac{0.64 \times g \text{ CSNP} + Eff._{SO} \times g \text{ SO}}{0.64 \times g \text{ CSNP} + g \text{ SO}} \times 100\% \quad \text{(Eqn. 3.5)}$$

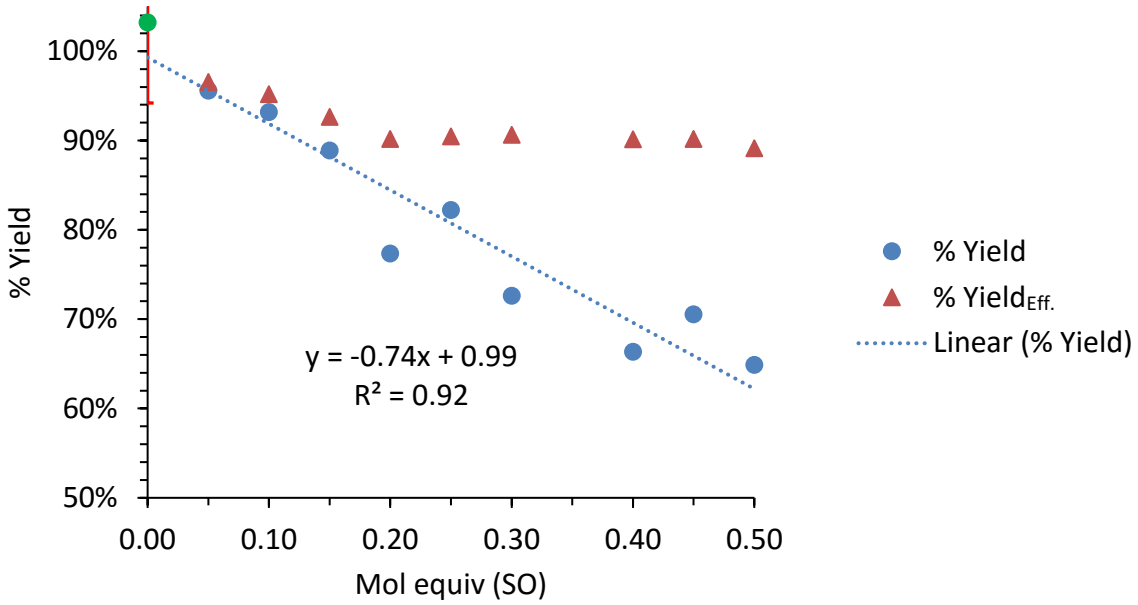

Figure 3.18. % Yields calculated based on the PHESNP content (approximates to 10%) and based on SO reaction efficiency. The data from the control experiment are shown in green.

Fig. 3.18 shows the % yield calculated according to NMR analysis as well as the reaction efficiency with respect to the amount of SO used in the reactions. At low mol equiv SO, the two yields stay close to each other and decrease slightly with the mol equiv of SO used. Again, % $yield_{Eff.}$ is the efficiency-based yield, which has taken into account for the loss of SO that has not been incorporated onto the SNPs, assuming no other sample loss. The fact that both yields are similar suggests that there are very little other types of sample loss during sample preparation. As the mol equiv of SO increases, % $yield_{Eff.}$ stays relatively constant. This is because of the slight increase in reaction efficiency (see **Table 3.1**, entries **5**-**9**). The % yield decreases linearly and the gap between both yields are increasingly larger with the mol equiv of SO (**Fig. 3.18**). This would suggest that sample loss during sample preparation becaming

more severe as more SO was used in the reaction. There are mainly two possible ways to contribute to the loss of sample other than the unsuccessful incorporation of SO. First, degradation of the SNPs could be a primary reason for a major loss of sample if degradation occurs under the reaction conditions (pH 13, 40^{o}C, 24 h). The degraded SNPs would be eliminated during dialysis. Fortunately, this is not likely the case here. Based on the experiment controls, degradation of SNPs under the reaction conditions mentioned above is minimal or not noticeable. The same reaction conditions were used in the BO reactions and no degradation of the SNPs was observed in that case as well. Second, another possibility for sample loss is during sample transfer. Whenever the sample is transferred from one container to another, there will be inevitably some sample loss. In this case, as the PHESNPs become less dispersible due to the increase in MS_{PHE}, it is more difficult to avoid sample loss during the preparation of these samples. The comparison between both % yields clearly reflects this sample loss problem.

3.8 Substitution Pattern Studies for PHESNPs

PHESNPs were subjected to TFA hydrolysis under the same conditions described in **Section 2.8**. Briefly, TFA (15% v/v) was added to a pressure tube containing an aqueous PHESNP dispersion. The reaction was performed at 90^{o}C and stirred over night. Then, the TFA and solvent in the reaction mixture were evaporated off on a high vacuum rotary evaporator with a sufficient number of washes with toluene and then water. The product was lyophilized

for storage. **Fig. 3.19** shows the comparison between the ^{1}H NMR spectra before **(A)** and after TFA hydrolysis **(B)**.

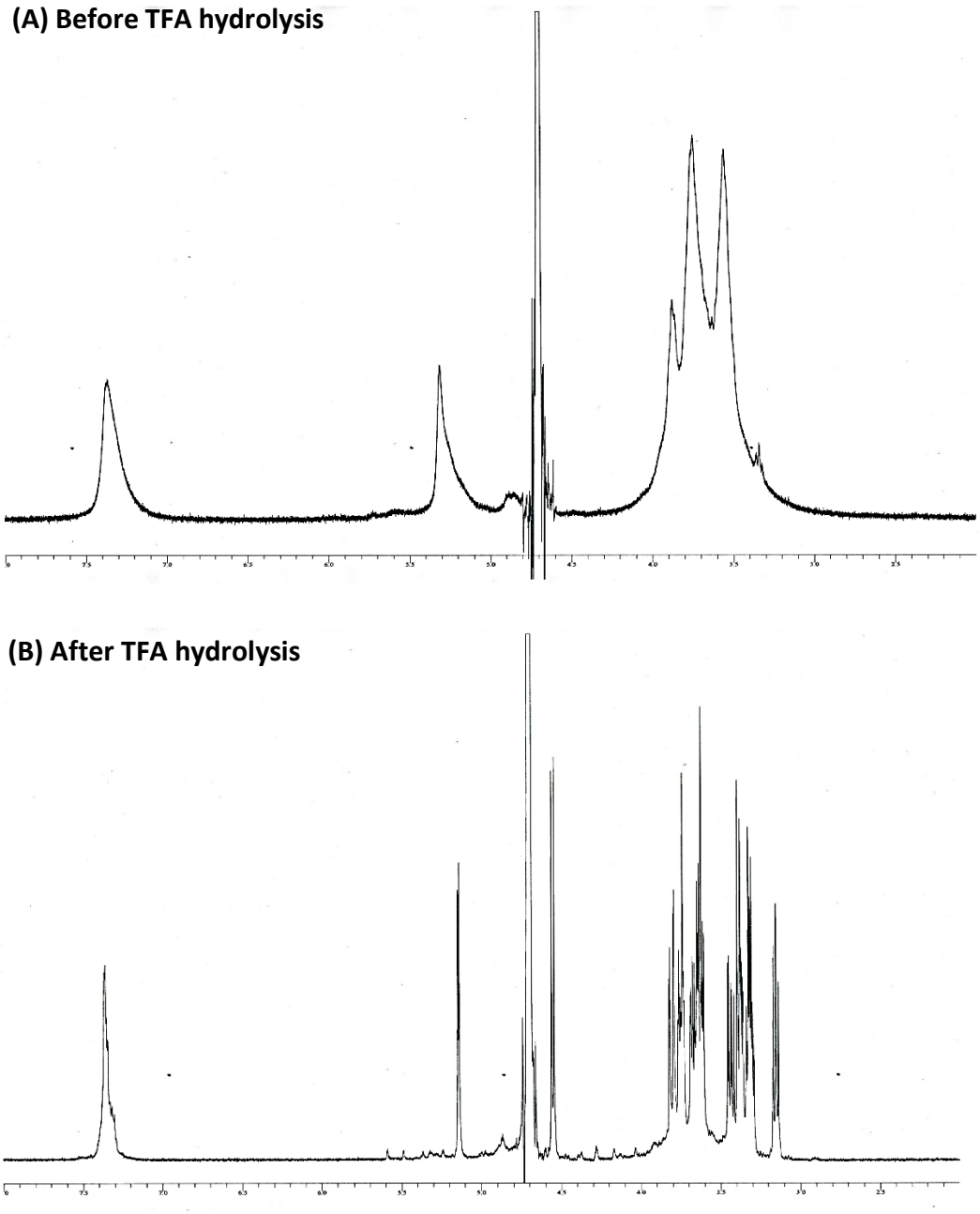

Figure 3.19. NMR spectra of $PHE_{0.32}$SNPs (**A**) before and (**B**) after TFA hydrolysis.

The sharpened peaks and the appearance of both α and β anomeric protons clearly suggest that the hydrolysis reaction was successful. By HR+ESIMS, a number of different components in the hydrolysates of PHESNPs can be identified. **Table 3.3** shows the identifiable species for $PHE_{0.32}SNP$ **(A)** and $PHE_{0.40}SNP$ **(B)**. The corresponding mass spectra are provided in **Fig. 3.20** and **Fig. 3.21** respectively.

Table 3.3. (A) Components identified from the hydrolysate of $PHE_{0.32}SNPs$ using HR+ESIMS.

	Glucose Deriv.	**Composition**	**Theo. Mass**	**Observed Mass**	**Delta (ppm)**
1	Glucose	$C_6H_{12}O_6Li$	187.07884	187.07880	-0.23
2	1PHE	$C_{14}H_{20}O_7Li$	307.13636	307.13412	-7.29
3	1PHE-H_2O	$C_{14}H_{18}O_6Li$	289.12579	289.12572	-0.26
4	2PHE	$C_{22}H_{28}O_8Li$	427.19387	427.19131	-6
5	2PHE-H_2O	$C_{22}H_{26}O_7Li$	409.18331	409.18333	0.05

(B) Components identified from the hydrolysate of $PHE_{0.40}SNPs$ using HR+ESIMS.

	Glucose Deriv.	Composition	Theo. Mass	Observed Mass	Delta (ppm)
1	Glucose	$C_6H_{12}O_6Li$	187.07884	187.07887	0.14
2	1PHE	$C_{14}H_{20}O_7Li$	307.13636	307.13632	-0.13
3	1PHE-H_2O	$C_{14}H_{18}O_6Li$	289.12579	289.12573	-0.22
4	2PHE	$C_{22}H_{28}O_8Li$	427.19387	427.19403	0.37
5	2PHE-H_2O	$C_{22}H_{26}O_7Li$	409.18331	409.18335	0.10
6	3PHE	$C_{30}H_{36}O_9Li$	547.25139	547.25159	0.37

7	3PHE-H_2O	$C_{30}H_{34}O_8Li$	529.24082	529.24103	0.39
8	4PHE	$C_{38}H_{44}O_{10}Li$	667.30890	667.30890	0.00

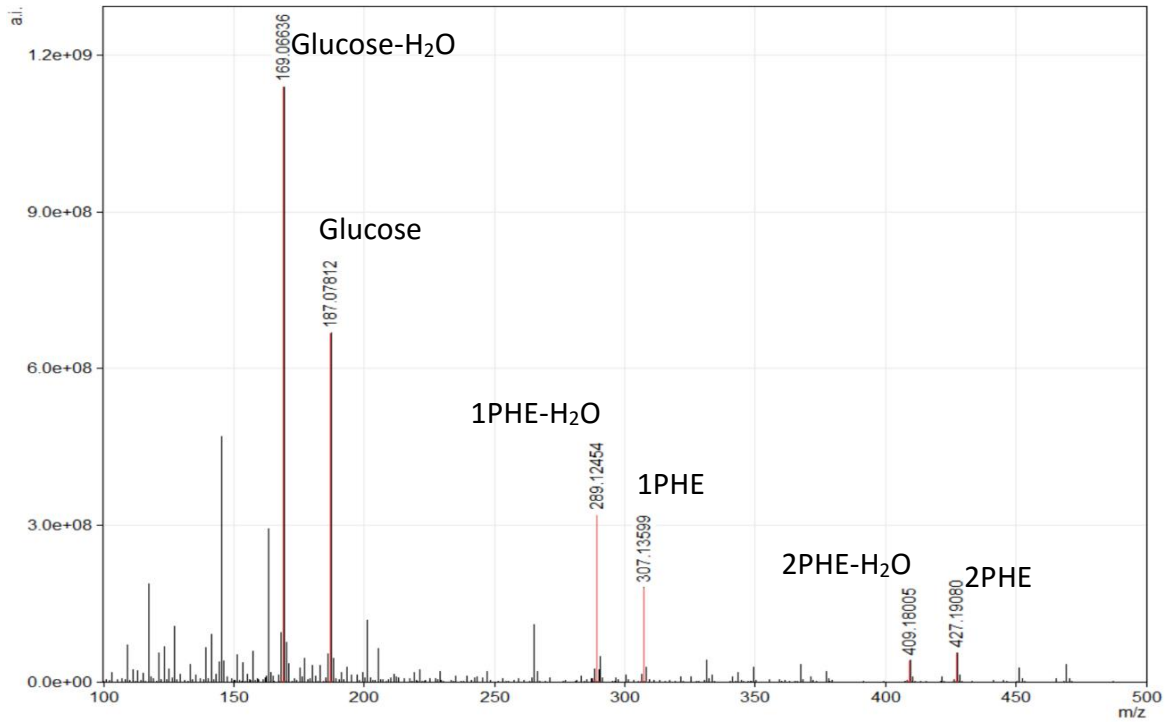

Figure 3.20. HR+ESIMS spectrum of the hydrolysates of $PHE_{0.32}SNPs$.

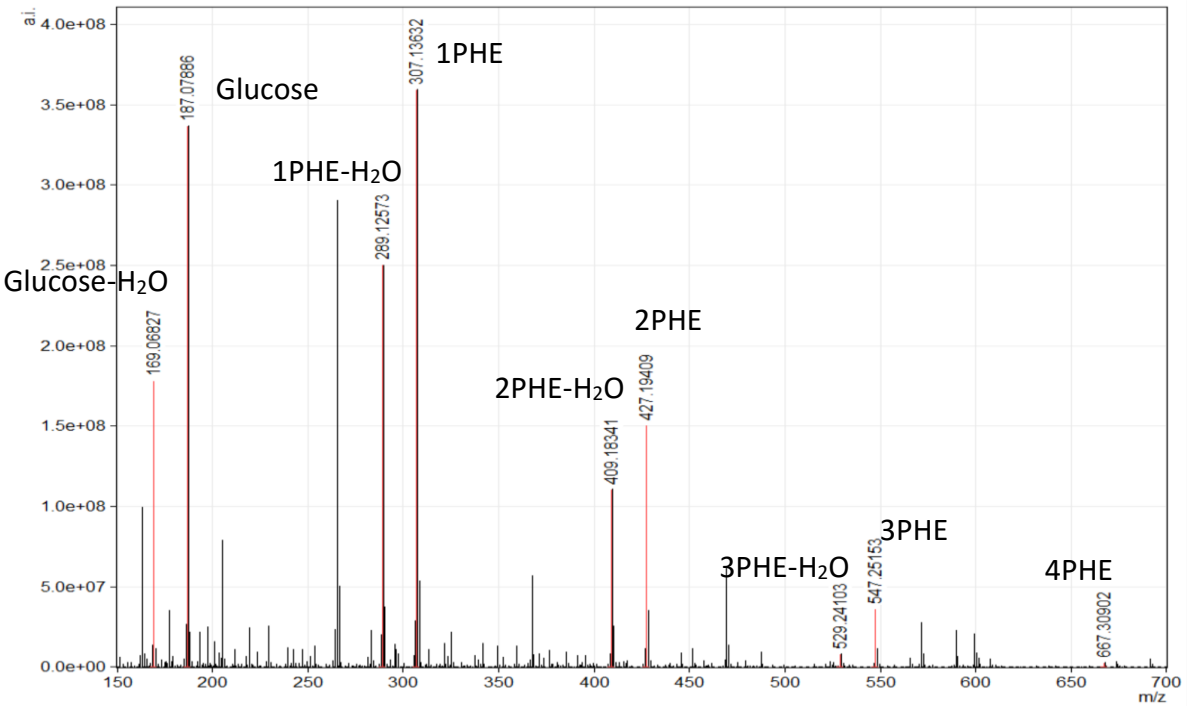

Figure 3.21. HR+ESIMS spectrum of the hydrolysates of $PHE_{0.40}$SNPs.

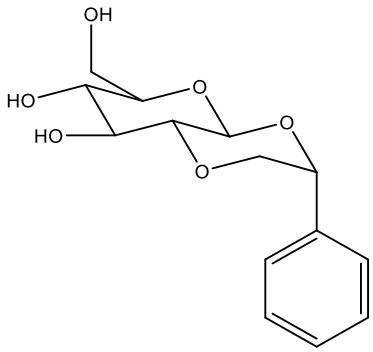

Figure 3.22. Chemical structure of the dehydrated phenyl hydroxyethylglucose (1PHE-H_2O).

Similar to the HBSNPs, a greater number of components in the PHESNP hydrolysates can be found when the MS_{PHE} is higher. The components that can be found in both spectra include glucose derivatives with one substituting PHE group (phenyl hydroxyethylglucose or 1PHE), glucose with two PHE groups (2PHE) and their corresponding dehydrated glucose

derivatives (1PHE-H_2O and 2PHE-H_2O, see **Fig. 3.22**). In addition to those, glucose derivatives with the third (3PHE) and fourth substituting PHE groups (4PHE) can be found in the mass spectrum of the hydrolysates of $PHE_{0.40}$SNPs. The presence of the glucose derivatives with the fourth PHE groups strongly indicates the presence of oligomerizing PHE groups. The dehydrated glucose derivatives suggest that the substitution occurs at, but not limited to, the O-2 position. This is because the formation of the dehydrated glucose derivative is only possible when there is a free OH on the O-2 substituting PHE group. As mentioned before, the analysis by mass spectrometry is only a qualitative measurement. But based on the intensity of the peaks in the spectra, the monosubstituted PHESNPs could be the dominant component in both hydrolysates other than the unsubstituted glucose units. For a more confident analysis, the hydrolysates can be separated by HPLC and the analysis of HPLC fractions potentially reveals more detailed qualitative information regarding the different isomers as well as the information on the quantitative aspect of the hydrolysates.

3.9 Thermoresponsive Behavior of PHESNPs

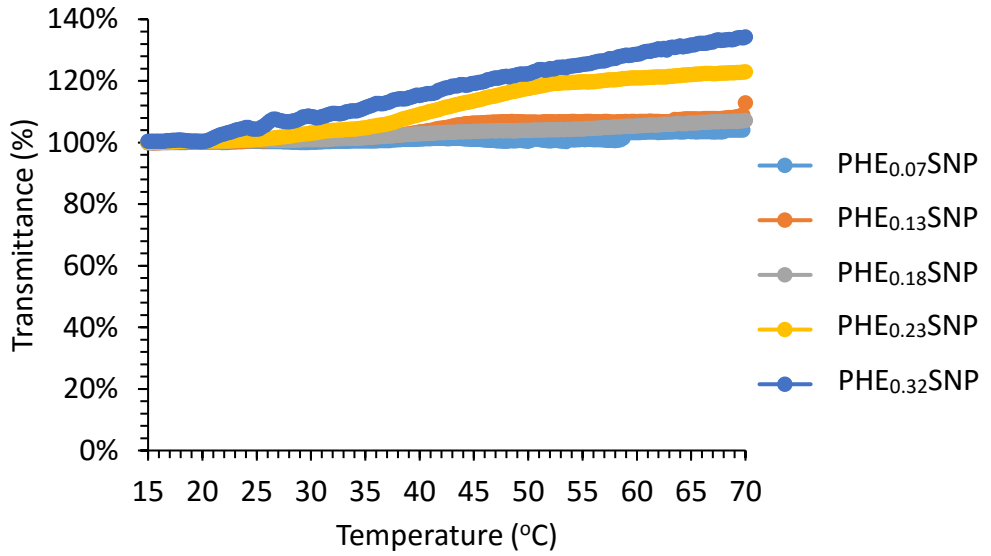

Figure 3.23. Transmittance curves for PHESNPs with different MS_{PHE}s. Measurements were done with 10 g/L dispersions at 500 nm. The initial transmittance was normalized to 100% at 15°C prior to the measurements.

The transmittance curves for PHESNPs show that the PHESNPs are not thermoresponsive up to a MS_{PHE} of 0.32. Again, a dispersion with thermoresponsive SNP would undergo a sudden change in solubility when the cloud point temperature (T_c) is reached, and would be reflected as a decrease in transmittance of the dispersion in a turbidity measurement. All transmittance was initially normalized to 100% at 15°C prior to the measurements. The actual transmittance of the dispersions at 15°C are reported as in **Fig. 3.10** which used deionized water as a blank. **Fig. 3.23** shows that the transmittance of the PHESNP dispersion generally increases with temperature, indicating an increase in the dispersability as the temperature rises. This phenomenon could be due to the settling effect

of the non-dispersible PHESNPs (the ones with relatively high MS_{PHE}). As the measurement proceeds, the non-dispersible PHESNPs could settle at the bottom of the cuvette over time, hence, the absorbance decreases (and the transmittance increases).

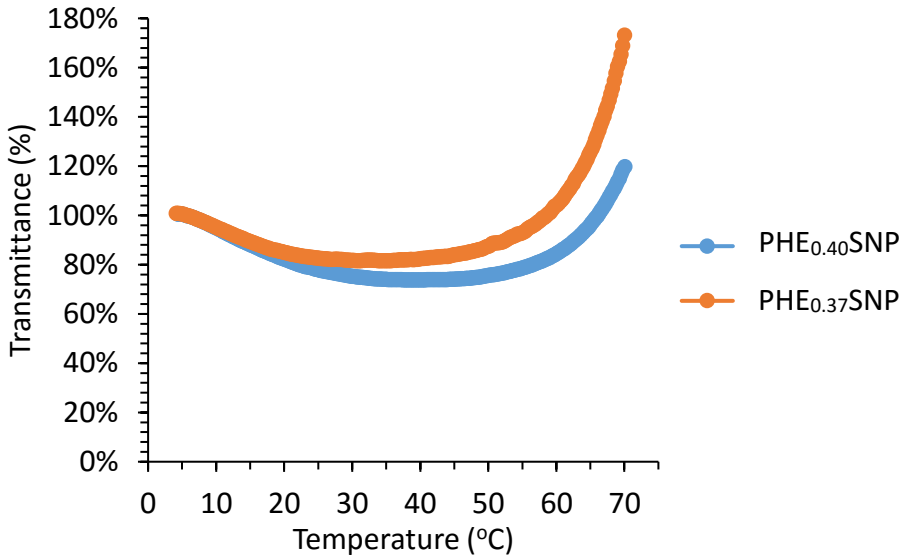

Figure 3.24. Transmittance curves for PHESNPs with MS_{PHE} of 0.37 and 0.40. Measurements were done with 10 g/L dispersions at 500 nm. The initial transmittance was normalized to 100% at 4°C prior to the measurements.

The transmittance curves for $PHE_{0.37}SNP$ and $PHE_{0.40}SNP$ are very different from the ones of the PHESNPs with MS_{PHE} below 0.32. Both transmittance curves decrease gradually at first and then increase as the temperature increases further (**Fig. 3.24**). It is important to note that both PHESNPs start off very non-dispersible, which is not reflected by the normalized transmittance curve (but can be seen in **Fig. 3.10**). Both PHESNPs appear to be least dispersible at around 30 to 40°C and become more dispersible at higher temperature. The rationalization behind this observation is still unknown. But it can be certainly concluded

that PHESNPs in general are not thermoresponsive or they do not exhibit the typical thermoresponsive behavior as in the HBSNPs.

Chapter 4

Summary, Future Directions and Experimental Procedures

4.1 Summary

A number of TRSNPs were successfully synthesized. In particular, HBSNPs with MS_{HB} ranging from 0.22 to 1.85 were obtained, and only those with MS_{HB} values greater than 1 would exhibit thermoresponsive behavior. From the DLS studies, an abrupt change in the hydrodynamic size of the HBSNPs below and above the T_c was observed. The turbidity studies show that the thermotransition was highly reversible, and obvious hysteresis between the heating and cooling cycles was observed. Both the MS of the HB groups and the concentration of the SNP dispersion were inversely correlated with the T_c. Kosmotropic salts decreased T_c, and some salts with strong hydration strength decreased the T_c dramatically. Chaotropic salts increased T_c at low salt concentrations, but decreased it at higher concentrations. Substitution pattern studies strongly support the existence of O-2 substituted AGUs and oligomerization of the HB groups on the HBSNPs.

Another hydrophobically modified SNP, PHESNP, was synthesized. The PHESNPs obtained had MS_{PHE} values from 0.025 to 0.4. The dispersability of the PHESNPs was poorer than that of the HBSNPs, and PHESNPs with a MS_{PHE} greater than 0.4 was essentially non-dispersible in water. The SO reaction efficiency was better than the BO reaction efficiency, however, the yield of the latter was greater instead. PHESNPs with low MS_{PHE} values were not

thermoresponsive, and those with a MS_{PHE} close to 0.4 did not exhibit typical thermoresponsive behavior, for which the transmittance of the dispersion decreases from 100% to close to 0% at T_c.

4.2 Future Directions

4.2.1 Potential Application in Oil Extraction

As briefly mentioned in **Section 1.6.4**, thermorepsonsive polymers have a promising future in the development of a novel method for the extraction of oil from oil sands. Though the synthetic-based TRPs may not be a commercially viable option, the development seems quite possible with the newly discovered thermoresponsive starch nanoparticles introduced in this thesis. A number of the TRSNP samples will be selected to perform the extraction experiments. The experiment conditions will be optimized, and further modification of the SNPs will be performed to improve the extraction efficiency.

4.2.2 Future Characterization of the TRSNPs

Further studies of TRSNPs will focus on the investigation of the substitution patterns, and on the rheological and solution properties of the modified SNPs. In addition to the substitution pattern of the substituents on the AGU, which can be investigated by composition analysis in HR+ESIMS, the substitution patterns of the SNP chain and of the entire sample also contain important information about the modified SNPs. Amylase degradation of the modified SNPs would provide insight into the substitution patterns

according to the degree of degradation. Furthermore, differences in the architecture or the conformation of the modified SNPs should be studied using the static light scattering (SLS). SLS can provide information on the radius of gyration (R_g), and with the hydrodynamic radius (R_h) from DLS, the conformation of the modified SNPs below and above the T_c in an aqueous dispersion can be studied. If the information about the rheological properties of the modified SNP such as viscosity are required, rheological measurements can be conducted using a rheometer. Additionally, electron microscopes such as transmission electron microscope (TEM) can be employed to study the morphology of the modified SNPs.

4.3 Experimental Procedures

4.3.1 General Information

Starch nanoparticles were obtained from EcoSynthetix Inc. (Burlington, ON). Styrene oxide and 1,2-butene oxide were obtained from Sigma-Aldrich Co. (USA). Other reagents and solvents were commercially available and used without further purification unless stated otherwise. ^{1}H NMR was taken with a Bruker Avance 500 MHz NMR machine (Bruker Co., Germany). Turbidity measurements were performed using a Cary 4000 Bio UV-Visible spectrophotometer (Agilent Technology Inc., USA). DLS measurements were performed by a Malvern Nanoseries Zetasizer (Malvern Instruments Ltd., UK). The mass spectrometry in use was a Thermo Scientific Q-Exactive Orbitrap (Thermo Fisher Scientific Inc., USA).

4.3.2 General Hydroxyalkylation Protocol

SNPs (1 g) were dispersed in 2.7 mL deionized water in a 20 mL scintillation vial at 40^{o}C for 2 h. The dispersion was cooled to room temperature (rt) followed by the drop-wise addition of 0.3 mL of 10 M NaOH with vigorous stirring to give a dispersion with a pH 13. The concentration of the SNP dispersion was approximately 25 wt. %. A pre-determined amount of reagent was added at rt, and the reaction vial was capped and sealed. The reaction vial was immediately put into a 40^{o}C water bath and the reaction mixture was vigorously stirred for 24 h. After the 24 h, the reaction mixture was taken out of the water bath and allowed to cool to rt followed by neutralizing with 1 M HCl under vigorous stirring. The neutralized reaction mixture was then subjected to dialysis against deionized water for 1 to 2 days using a dialysis bag with molecular weight cut-off (MW_{cutoff}) of 1 kD. A minimum of 5 water replacements were performed over the course of 1 to 2 days, and the dilution ratio is approximately 1: 10^{10}. The dialyzed SNPs were lyophilized for at least 3 days to yield a white powder. The white powder was stored in a centrifuge tube at rt.

4.3.3 ^{1}H NMR Measurements

To prepare a 20 g/L NMR dispersion, the modified SNPs were stirred in deuterium oxide (D_2O) for 16 h at 4^{o}C. Before taking the measurements, the dispersion was cooled to rt and a known amount of the internal standard, 3-(trimethylsilyl)-2,2',3,3'-tetradeuteropropionic acid (TMSP-d_4), was added. ^{1}H NMR spectra were obtained on a Bruker Avance 500 MHz NMR machine at rt. D1 was set at 2.2 seconds and at least 64 scans were

obtained for each ^{1}H NMR spectrum. The spectra were processed using Mestrec 2.2 software (Mestrelab Research S.L., Santiago de Compostela). Phasing was done manually with the pivot point set to the left of the water peak at 4.8 ppm. Both multi-point baseline correction and automatic integral correction were applied.

4.3.4 Cloud Point Temperature Measurements

T_c measurements were done using 10 g/L dispersions of the modified or unmodified SNPs unless stated otherwise. The modified SNPs were stirred in deionized water for 16 h at 4^{o}C. The optical transmittance of the SNP dispersions was measured by a Cary 4000 Bio UV-Visible spectrophotometer equipped with a multi-cuvette holder and temperature controller. The temperature of the dispersion was measured by a temperature probe in a reference cell. The transmittance was recorded at 500 nm with a heating/cooling rate of 1^{o}C/min. The SNP dispersions were equilibrated for at least 5 minutes at 15^{o}C in the cuvette before the measurements commenced. Absorbance data points were taken every 0.25^{o}C and recorded up to 70^{o}C. T_c is defined as the temperature at the inflection point of the transmittance curve, where the rate of decrease in transmittance is maximum. The maximum transmittance was normalized to 100%.

4.3.5 Dynamic Light Scattering

DLS samples were prepared by dispersing the SNPs in deionized water at a concentration of 3 g/L. The dispersions were stirred for 16 h at 4^{o}C. Prior to the

measurements, the dispersion was filtered through a 0.2 µm PTFE syringe filter directly into a low volume Quartz cell. The measurements were performed by a Malvern Nanoseries Zetasizer. At least 3 measurements per sample, 3 runs per measurement and 100 seconds per run were performed. The equilibrating time for the dispersions at each temperature setting was 5 minutes.

4.3.6 Degradation of the Modified SNPs

To a 20 g/L aqueous dispersion of the modified SNPs in a pressure tube was added TFA drop-wise with vigorous stirring, to a final concentration of 15% v/v. The reaction mixture was then capped and immersed in a 90^{o}C oil bath for approximately 5 h. After that, the reaction mixture was cooled to rt followed by the addition of toluene to assist in the removal of TFA. The mixture was concentrated to dryness using a high vacuum rotary evaporator. Toluene was added and the mixture was concentrated again. This was repeated two more times. Water was added and the mixture was concentrated. This was repeated two more times. A brown glue-like substance was recovered. This material was dissolved in water and lyophilized to yield a brown powder.

4.3.7 HR+ESIMS Measurements

HR+ESIMS samples were prepared using the degraded SNPs prepared using the procedure described in **Section 4.3.6**. A 2 g/L solution in 1:1 methanol/water with 0.1% formic acid was prepared as a stock solution used for further dilution to a concentration of

approximately 0.8 g/L. A drop of lithium acetate solution (in 1:1 methanol/water with 0.1% formic acid) was added to the degraded SNP dispersion described above. The mixture was vortexed and centrifuged prior to injection in the mass spectrometer.

References

1. Gil, E. S.; Hudson, S. M. Stimuli-reponsive polymers and their bioconjugates. *J. Polym. Sci. A Polym. Chem.* **2004***, 29*, 1173-1222.

2. Chung, J.; Yokoyama, M.; Yamato, M.; Aoyagi, T.; Sakurai, Y.; Okano, T. Thermo-responsive drug delivery from polymeric micelles constructed using block copolymers of poly (N-isopropylacrylamide) and poly (butylmethacrylate). *J. Controlled Release* **1999***, 62*, 115-127.

3. Lavigne, M. D.; Pennadam, S. S.; Ellis, J.; Yates, L. L.; Alexander, C.; Górecki, D. C. Enhanced gene expression through temperature profile-induced variations in molecular architecture of thermoresponsive polymer vectors. *J. Gene Med.* **2007***, 9*, 44-54.

4. Nitschke, M.; Gramm, S.; Götze, T.; Valtink, M.; Drichel, J.; Voit, B.; Engelmann, K.; Werner, C. Thermo-responsive poly (NiPAAm-co-DEGMA) substrates for gentle harvest of human corneal endothelial cell sheets. *J. Biomed. Mater. Res. A* **2007***, 80*, 1003-1010.

5. Rotzetter, A.; Schumacher, C.; Bubenhofer, S.; Grass, R.; Gerber, L.; Zeltner, M.; Stark, W. Thermoresponsive polymer induced sweating surfaces as an efficient way to passively cool buildings. *Adv. Mater.* **2012***, 24*, 5352-5356.

6. Yang, B.; Duhamel, J. Extraction of Oil from Oil Sands Using Thermoresponsive Polymeric Surfactants. *ACS Appl. Mater. Interfaces* **2015***, 7*, 5879-5889.

7. Saitoh, T.; Satoh, F.; Hiraide, M. Concentration of heavy metal ions in water using thermoresponsive chelating polymer. *Talanta* **2003***, 61*, 811-817.

8. Wu, C.; Wang, X. Globule-to-coil transition of a single homopolymer chain in solution. *Phys. Rev. Lett.* **1998***, 80*, 4092-4094.

9. Fusco, S.; Borzacchiello, A.; Netti, P. Perspectives on: PEO-PPO-PEO triblock copolymers and their biomedical applications. *J. Bioact. Compatible Polym.* **2006***, 21*, 149-164.

10. Aseyev, V.; Tenhu, H.; Winnik, F. M. Non-ionic thermoresponsive polymers in water. In *Self Organized Nanostructures of Amphiphilic Block Copolymers II* Springer: 2010; pp 29-89.

11. Klouda, L.; Mikos, A. G. Thermoresponsive hydrogels in biomedical applications. *Eur. J. Pharm. Biopharm.* **2008***, 68*, 34-45.

12. Liu, F.; Urban, M. W. Recent advances and challenges in designing stimuli-responsive polymers. *Prog. Polym. Sci.* **2010***, 35*, 3-23.

13. Pasparakis, G.; Vamvakaki, M. Multiresponsive polymers: nano-sized assemblies, stimuli-sensitive gels and smart surfaces. *Polym. Chem.* **2011***, 2*, 1234-1248.

14. Vihola, H.; Laukkanen, A.; Tenhu, H.; Hirvonen, J. Drug release characteristics of physically cross-linked thermosensitive poly (N-vinylcaprolactam) hydrogel particles. *J. Pharm. Sci.* **2008***, 97*, 4783-4793.

15. Stile, R. A.; Healy, K. E. Thermo-responsive peptide-modified hydrogels for tissue regeneration. *Biomacromolecules* **2001***, 2*, 185-194.

16. Twaites, B. R.; de las Heras Alarcón, Carolina; Lavigne, M.; Saulnier, A.; Pennadam, S. S.; Cunliffe, D.; Górecki, D. C.; Alexander, C. Thermoresponsive polymers as gene delivery vectors: cell viability, DNA transport and transfection studies. *J. Controlled Release* **2005***, 108*, 472-483.

17. Frank, H. S.; Evans, M. W. Free volume and entropy in condensed systems III. Entropy in binary liquid mixtures; partial molal entropy in dilute solutions; structure and thermodynamics in aqueous electrolytes. *J. Chem. Phys.* **1945***, 13*, 507-532.

18. Némethy, G.; Scheraga, H. A. Structure of water and hydrophobic bonding in proteins. I. A model for the thermodynamic properties of liquid water. *J. Chem. Phys.* **1962***, 36*, 3382-3400.

19. Southall, N. T.; Dill, K. A.; Haymet, A. A view of the hydrophobic effect. *J. Phys. Chem. B* **2002***, 106*, 521-533.

20. Heskins, M.; Guillet, J. E. Solution properties of poly (N-isopropylacrylamide). *J. Macromol. Sci. , Chem.* **1968***, 2*, 1441-1455.

21. Taylor, L. D.; Cerankowski, L. D. Preparation of films exhibiting a balanced temperature dependence to permeation by aqueous solutions—a study of lower consolute behavior. *J. Polymer Sci. Polymer Chem. Ed.* **1975***, 13*, 2551-2570.

22. Cheng, H.; Xie, S.; Zhou, Y.; Huang, W.; Yan, D.; Yang, J.; Ji, B. Effect of degree of branching on the thermoresponsive phase transition behaviors of hyperbranched multiarm copolymers: comparison of systems with lcst transition based on coil-to-globule transition or hydrophilic−hydrophobic balance. *J. Phys. Chem. B* **2010***, 114*, 6291-6299.

23. Alexandridis, P.; Hatton, T. A. Poly (ethylene oxide) poly (propylene oxide) poly (ethylene oxide) block copolymer surfactants in aqueous solutions and at interfaces:

thermodynamics, structure, dynamics, and modeling. *Colloids Surf. A Physicochem. Eng. Asp.* **1995***, 96*, 1-46.

24. Dimitrov, I.; Trzebicka, B.; Müller, A. H.; Dworak, A.; Tsvetanov, C. B. Thermosensitive water-soluble copolymers with doubly responsive reversibly interacting entities. *Prog. Polym. Sci.* **2007***, 32*, 1275-1343.

25. Lutz, J.; Hoth, A. Preparation of ideal PEG analogues with a tunable thermosensitivity by controlled radical copolymerization of 2-(2-methoxyethoxy) ethyl methacrylate and oligo (ethylene glycol) methacrylate. *Macromolecules* **2006***, 39*, 893-896.

26. Wang, X.; Qiu, X.; Wu, C. Comparison of the coil-to-globule and the globule-to-coil transitions of a single poly (N-isopropylacrylamide) homopolymer chain in water. *Macromolecules* **1998***, 31*, 2972-2976.

27. Cheng, S.; Zhang, J.; Zhuo, R. Macroporous poly (N-isopropylacrylamide) hydrogels with fast response rates and improved protein release properties. *J. Biomed. Mater. Res. A* **2003***, 67*, 96-103.

28. Troll, K.; Kulkarni, A.; Wang, W.; Darko, C.; Koumba, A. B.; Laschewsky, A.; Müller-Buschbaum, P.; Papadakis, C. M. The collapse transition of poly (styrene-b-(N-isopropyl acrylamide)) diblock copolymers in aqueous solution and in thin films. *Colloid Polym. Sci.* **2008***, 286*, 1079-1092.

29. Ward, M. A.; Georgiou, T. K. Thermoresponsive polymers for biomedical applications. *Polymers* **2011***, 3*, 1215-1242.

30. Calejo, M. T.; Sande, S. A.; Nyström, B. Thermoresponsive polymers as gene and drug delivery vectors: architecture and mechanism of action. *Expert Opin. Drug Deliv.* **2013***, 10*, 1669-1686.

31. Yamada, N.; Okano, T.; Sakai, H.; Karikusa, F.; Sawasaki, Y.; Sakurai, Y. Thermo-responsive polymeric surfaces; control of attachment and detachment of cultured cells. *Makromol. Chem. , Rapid Commun.* **1990***, 11*, 571-576.

32. Cunliffe, D.; de las Heras Alarcón, Carolina; Peters, V.; Smith, J. R.; Alexander, C. Thermoresponsive surface-grafted poly (N-isopropylacrylamide) copolymers: effect of phase transitions on protein and bacterial attachment. *Langmuir* **2003***, 19*, 2888-2899.

33. Okano, M. N. T.; Winnik, F. M. Poly (N-isopropylacrylamide)-based Smart Surfaces for Cell Sheet Tissue Engineering. *Material Matters* **2010***, 5*, 56.

34. Ward, M. A.; Georgiou, T. K. Thermoresponsive terpolymers based on methacrylate monomers: Effect of architecture and composition. *J. Polym. Sci. A Polym. Chem.* **2010***, 48*, 775-783.

35. Zhu, X.; Avoce, D.; Liu, H.; Benrebouh, A. Copolymers of N-alkylacrylamides as thermosensitive hydrogels. *Macromol. Symp.* **2004***, 207*, 187-192.

36. Zhang, X.; Chu, C. Fabrication and characterization of microgel-impregnated, thermosensitive PNIPAAm hydrogels. *Polymer* **2005***, 46*, 9664-9673.

37. Sosnik, A.; Cohn, D.; Román, J. S.; Abraham, G. A. Crosslinkable PEO-PPO-PEO-based reverse thermo-responsive gels as potentially injectable materials. *J. Biomater. Sci. Polym. Ed.* **2003***, 14*, 227-239.

38. Cohn, D.; Sosnik, A.; Levy, A. Improved reverse thermo-responsive polymeric systems. *Biomaterials* **2003***, 24*, 3707-3714.

39. Kanazawa, H.; Yamamoto, K.; Matsushima, Y.; Takai, N.; Kikuchi, A.; Sakurai, Y.; Okano, T. Temperature-responsive chromatography using poly (N-isopropylacrylamide)-modified silica. *Anal. Chem.* **1996***, 68*, 100-105.

40. Kanazawa, H.; Nishikawa, M.; Mizutani, A.; Sakamoto, C.; Morita-Murase, Y.; Nagata, Y.; Kikuchi, A.; Okano, T. Aqueous chromatographic system for separation of biomolecules using thermoresponsive polymer modified stationary phase. *J. Chromatogr. A* **2008***, 1191*, 157-161.

41. Kikuchi, A.; Okano, T. Intelligent thermoresponsive polymeric stationary phases for aqueous chromatography of biological compounds. *Prog. Polym. Sci.* **2002***, 27*, 1165-1193.

42. Nagase, K.; Kobayashi, J.; Kikuchi, A.; Akiyama, Y.; Kanazawa, H.; Okano, T. Effects of graft densities and chain lengths on separation of bioactive compounds by nanolayered thermoresponsive polymer brush surfaces. *Langmuir* **2008***, 24*, 511-517.

43. Tanaka, T.; Ando, Y.; Saitoh, T.; Hiraide, M. Preconcentration of traces of cobalt, nickel, copper and lead in water by thermoresponsive polymer-mediated extraction for tungsten filament electrothermal vaporization-inductively coupled plasma mass spectrometry. *J. Anal. At. Spectrom.* **2002***, 17*, 1556-1559.

44. Maeda, Y.; Nakamura, T.; Ikeda, I. Changes in the hydration states of poly (N-n-propylmethacrylamide) and poly (N-isopropylmethacrylamide) during their phase transitions in water observed by FTIR spectroscopy. *Macromolecules* **2001***, 34*, 8246-8251.

45. Kubota, K.; Fujishige, S.; Ando, I. Single-chain transition of poly (N-isopropylacrylamide) in water. *J. Phys. Chem.* **1990***, 94*, 5154-5158.

46. Ito, D.; Kubota, K. Thermal response of poly (Nn-propylacrylamide). *Polym. J.* **1999***, 31*, 254-257.

47. Uğuzdoğan, E.; Çamlı, T.; Kabasakal, O.; Patır, S.; Öztürk, E.; Denkbaş, E.; Tuncel, A. A new temperature-sensitive polymer: Poly (ethoxypropylacrylamide). *Eur. Polym. J.* **2005***, 41*, 2142-2149.

48. Aoki, T.; Muramatsu, M.; Torii, T.; Sanui, K.; Ogata, N. Thermosensitive phase transition of an optically active polymer in aqueous milieu. *Macromolecules* **2001***, 34*, 3118-3119.

49. Maeda, Y.; Sakamoto, J.; Wang, S.; Mizuno, Y. Lower critical solution temperature behavior of poly (N-(2-ethoxyethyl) acrylamide) as compared with poly (N-isopropylacrylamide). *J. Phys. Chem. B* **2009***, 113*, 12456-12461.

50. Uğuzdoğan, E.; Kabasakal, O. S. Synthesis and characterization of thermally-sensitive polymer: Poly (aminomethoxypropylacrylamide). *Colloids Surf. Physicochem. Eng. Aspects* **2010***, 368*, 129-136.

51. Fischer, F.; Zufferey, D.; Tahoces, R. Lower critical solution temperature in superheated water: the highest in the poly (N, N-dialkylacrylamide) series. *Polym. Int.* **2011***, 60*, 1259-1262.

52. Liu, H.; Zhu, X. Lower critical solution temperatures of N-substituted acrylamide copolymers in aqueous solutions. *Polymer* **1999***, 40*, 6985-6990.

53. Xu, J.; Jiang, X.; Liu, S. Synthesis of low-polydispersity poly (N-ethylmethylacrylamide) by controlled radical polymerizations and their thermal phase transition behavior. *J. Polym. Sci. A Polym. Chem.* **2008***, 46*, 60-69.

54. Maeda, Y.; Nakamura, T.; Ikeda, I. Changes in the hydration states of poly (N-n-propylmethacrylamide) and poly (N-isopropylmethacrylamide) during their phase transitions in water observed by FTIR spectroscopy. *Macromolecules* **2001***, 34*, 8246-8251.

55. Djokpé, E.; Vogt, W. N-Isopropylacrylamide and N-Isopropylmethacryl-amide: Cloud Points of Mixtures and Copolymers. *Macromol. Chem. Phys.* **2001***, 202*, 750-757.

56. Han, S.; Hagiwara, M.; Ishizone, T. Synthesis of thermally sensitive water-soluble polymethacrylates by living anionic polymerizations of oligo (ethylene glycol) methyl ether methacrylates. *Macromolecules* **2003***, 36*, 8312-8319.

57. Ishizone, T.; Seki, A.; Hagiwara, M.; Han, S.; Yokoyama, H.; Oyane, A.; Deffieux, A.; Carlotti, S. Anionic polymerizations of oligo (ethylene glycol) alkyl ether methacrylates: effect of side chain length and ω-alkyl group of side chain on cloud point in water. *Macromolecules* **2008***, 41*, 2963-2967.

58. Furyk, S.; Zhang, Y.; Ortiz-Acosta, D.; Cremer, P. S.; Bergbreiter, D. E. Effects of end group polarity and molecular weight on the lower critical solution temperature of poly (N-isopropylacrylamide). *J. Polym. Sci. A Polym. Chem.* **2006***, 44*, 1492-1501.

59. Xia, Y.; Yin, X.; Burke, N. A.; Stöver, H. D. Thermal response of narrow-disperse poly (N-isopropylacrylamide) prepared by atom transfer radical polymerization. *Macromolecules* **2005***, 38*, 5937-5943.

60. Xia, Y.; Burke, N. A.; Stöver, H. D. End group effect on the thermal response of narrow-disperse poly (N-isopropylacrylamide) prepared by atom transfer radical polymerization. *Macromolecules* **2006***, 39*, 2275-2283.

61. Eeckman, F.; Amighi, K.; Moës, A. J. Effect of some physiological and non-physiological compounds on the phase transition temperature of thermoresponsive polymers intended for oral controlled-drug delivery. *Int. J. Pharm.* **2001***, 222*, 259-270.

62. Kapsabelis, S.; Prestidge, C. A. Adsorption of ethyl (hydroxyethyl) cellulose onto silica particles: the role of surface chemistry and temperature. *J. Colloid Interface Sci.* **2000***, 228*, 297-305.

63. Pásztor, E.; Makó, Á; Csóka, G.; Fenyvesi, Z.; Benko, R.; Prosszer, M.; Marton, S.; Antal, I.; Klebovich, I. New formulation of in situ gelling Metolose-based liquid suppository. *Drug Dev. Ind. Pharm.* **2011***, 37*, 1-7.

64. Csóka, G.; Gelencsér, A.; Makó, A.; Marton, S.; Zelkó, R.; Klebovich, I.; Antal, I. Potential application of Metolose® in a thermoresponsive transdermal therapeutic system. *Int. J. Pharm.* **2007***, 338*, 15-20.

65. Sarkar, N. Thermal gelation properties of methyl and hydroxypropyl methylcellulose. *J. Appl. Polym. Sci.* **1979***, 24*, 1073-1087.

66. Kunugi, S.; Yoshida, D.; Kiminami, H. Effects of pressure on the behavior of (hydroxypropyl) cellulose in aqueous solution. *Colloid Polym. Sci.* **2001***, 279*, 1139-1143.

67. Touitou, E.; Donbrow, M. Influence of additives on (hydroxyethyl) methylcellulose properties: relation between gelation temperature change, compressed matrix integrity and drug release profile. *Int. J. Pharm.* **1982***, 11*, 131-148.

68. Clasen, C.; Kulicke, W. Determination of viscoelastic and rheo-optical material functions of water-soluble cellulose derivatives. *Prog. Polym. Sci.* **2001***, 26*, 1839-1919.

69. Pérez, S.; Bertoft, E. The molecular structures of starch components and their contribution to the architecture of starch granules: A comprehensive review. *Starch/Stärke* **2010***, 62*, 389-420.

70. Lindeboom, N.; Chang, P. R.; Tyler, R. T. Analytical, biochemical and physicochemical aspects of starch granule size, with emphasis on small granule starches: a review. *Starch/Stärke* **2004***, 56*, 89-99.

71. Ju, B.; Yan, D.; Zhang, S. Micelles self-assembled from thermoresponsive 2-hydroxy-3-butoxypropyl starches for drug delivery. *Carbohydr. Polym.* **2012***, 87*, 1404-1409.

72. Ju, B.; Cao, S.; Zhang, S. Effect of additives on the cloud point temperature of 2-Hydroxy-3-isopropoxypropyl starch solutions. *J. Phys. Chem. B* **2013***, 117*, 11830-11835.

73. Ju, B.; Zhang, C.; Zhang, S. Thermoresponsive starch derivates with widely tuned LCSTs by introducing short oligo (ethylene glycol) spacers. *Carbohydr. Polym.* **2014***, 108*, 307-312.

74. Simi, C.; Abraham, T. E. Hydrophobic grafted and cross-linked starch nanoparticles for drug delivery. *Bioprocess Biosyst. Eng.* **2007***, 30*, 173-180.

75. Putaux, J.; Molina-Boisseau, S.; Momaur, T.; Dufresne, A. Platelet nanocrystals resulting from the disruption of waxy maize starch granules by acid hydrolysis. *Biomacromolecules* **2003***, 4*, 1198-1202.

76. Ma, X.; Jian, R.; Chang, P. R.; Yu, J. Fabrication and characterization of citric acid-modified starch nanoparticles/plasticized-starch composites. *Biomacromolecules* **2008***, 9*, 3314-3320.

77. Wildi, R. H.; Van Egdob, E.; Bloembergen, S. USA Patent US 20110042841 A1, 2007.

78. Chakraborty, S.; Sahoo, B.; Teraoka, I.; Gross, R. A. Solution properties of starch nanoparticles in water and DMSO as studied by dynamic light scattering. *Carbohydr. Polym.* **2005***, 60*, 475-481.

79. Karski, M. Thermoresponsive starch nanoparticles. **2015**.

80. Funke, U.; Lindhauer, M. G. Effect of reaction conditions and alkyl chain lengths on the properties of hydroxyalkyl starch ethers. *Starch/Stärke* **2001***, 53*, 547-554.

81. Li, D. Characterization, Quantification and Modification of Starch Nanoparticles. **2014**.

82. Xu, A.; Seib, P. Determination of the Level and Position of Substitution in Hydroxypropylated Starch by High-Resolution 1 H-NMR Spectroscopy ofAlpha-limit Dextrins. *J. Cereal Sci.* **1997***, 25*, 17-26.

83. Gidley, M. J. Quantification of the structural features of starch polysaccharides by NMR spectroscopy. *Carbohydr. Res.* **1985***, 139*, 85-93.

84. Merkus, H.; Mourits, J.; De Galan, L.; De Jong, W. Substituent distribution in hydroxyethyl starch. *Starch/Stärke* **1977***, 29*, 406-409.

85. Viridén, A.; Wittgren, B.; Andersson, T.; Abrahmsen-Alami, S.; Larsson, A. Influence of substitution pattern on solution behavior of hydroxypropyl methylcellulose. *Biomacromolecules* **2009***, 10*, 522-529.

86. Fitzpatrick, F.; Schagerlöf, H.; Andersson, T.; Richardson, S.; Tjerneld, F.; Wahlund, K.; Wittgren, B. NMR, cloud-point measurements and enzymatic depolymerization: complementary tools to investigate substituent patterns in modified celluloses. *Biomacromolecules* **2006***, 7*, 2909-2917.

87. Cheng, H.; Shen, L.; Wu, C. LLS and FTIR studies on the hysteresis in association and dissociation of poly (N-isopropylacrylamide) chains in water. *Macromolecules* **2006***, 39*, 2325-2329.

88. Du, H.; Wickramasinghe, R.; Qian, X. Effects of salt on the lower critical solution temperature of poly (N-isopropylacrylamide). *J. Phys. Chem. B* **2010***, 114*, 16594-16604.

89. Atmos, R. Modification and Characterization of Starch Nanoparticles. **2013**.

90. Blumenstein, J. J.; Ukachukwu, V. C.; Mohan, R. S.; Whalen, D. L. Effects of para-substituents on the mechanisms of solvolysis of styrene oxides. *J. Org. Chem.* **1993***, 58*, 924-932.

91. Tizzotti, M. J.; Sweedman, M. C.; Tang, D.; Schaefer, C.; Gilbert, R. G. New 1H NMR procedure for the characterization of native and modified food-grade starches. *J. Agric. Food Chem.* **2011***, 59*, 6913-6919.